Study on Development of Integrated Urban Inundation Model Incorporating Drainage Systems

By

LEE Seungsoo

2013

Abstract

Urban inundation disasters that are due to climate change and torrential rainfall have been some of the most common natural disasters worldwide, generally stemming from a lack of sewer system capacity as well as overflow due to levee failure. Urban inundation has especially been reported to lead to extensive property damage and casualties due to the concentration of people and properties in highly urbanized areas. The urban inundation that has occurred due to local heavy rainfall during a short period of time reinforces the need for accurate models to predict and to prevent the inundation disasters. However, the urban area environment is highly heterogeneous in terms of land use, drainage systems, hydraulic structures, and other factors that influence water cycle processes. In addition to these complex urban-area components, a well-recognized obstacle to the development of an accurate model exists as a result of insufficient experimental data for validating inundation models as most studies about urban inundation have been devoted to model sensitivity analysis (Hunter et al., 2007). Therefore, obtaining experimental data for developing an urban inundation model based on the inundation mechanism is very important.

The sewer system is one of the most important components in urban inundation analysis. The inlet discharge through storm drains also could be a key factor because the discharge should be input data of the sewer system and output data of overland flow, according to the dual drainage concept. Generally, orifice and weir formulas that have different coefficients have been used to determine the inlet and overflow discharge through storm drains. However, the coefficients used in the formulas vary depending on various researchers. In this study, experiments were completed in order to determine the coefficients, and they tested applicability with a numerical simulation that used grid- and square-type storm drain covers.

Rapid urbanization has led to a complicated sewer system and landscape of building structures. The complicated hydraulic characteristic of a sewer system reveals many complex phenomena, such as blown-off manhole covers, sewer pipe rupture, and decreased drain capacity.

Because a major loss in a pipe is friction, it is possible to neglect energy losses while designing sewer systems that feature free surface flow, but under the pressurized condition, the energy losses may exceed the friction losses and reduce system capacity significantly; thus, considering the energy losses is needed.

Basically, a one-dimensional model is used to simulate a sewer system that involves manholes and junctions with pipe configuration for calculating time and capacity efficiency, although the head losses that result from manhole and pipe configuration are not one-dimensional phenomena. Therefore, it is necessary to develop a model that can reflect the head losses, depending on the pipe configuration and manhole shapes. In order to develop the simulation model, the fundamental laboratory experiments were conducted so as to estimate the effects of head loss depending on different manhole shapes and pipe configurations with no benching and no invert. First, straight case experiments were conducted in order to evaluate the head loss for circular- and square-type manhole shapes, and then, adjunction case experiments were conducted for the same type of manhole shapes used in straight cases. However, this was done with a different adjoining angle of the lateral pipe to confirm the head loss effects in both the unsteady and steady conditions. Finally, a numerical simulation model was developed and validated to confirm the model's applicability in using head loss coefficients obtained from laboratory experiments.

Finally, other experiment cases were carried out using the laboratory scale experimental setup to develop an integrated model, which consists of a two-dimensional inundation model on the ground surface and a one-dimensional sewer system; a sub-model (which exchanges storm water between the ground surface and the sewer system through the storm drain boxes) combines those two models. The experimental setup can measure a stable piezometric head of a sewer pipe and inundation depth stemming from a lack of sewer pipe capacity. The 1D sewer pipe model can reproduce change in the piezometric head according to the ascending and descending of the downstream water level, and the model is validated under the various experimental conditions, such as steady and unsteady conditions, for the development of an integrated urban inundation model.

Key Words: urban inundation, orifice and weir coefficient, manhole head losses, integrated urban inundation model.

Acknowledgements

I would like to express my sincere gratitude to my supervisor, Professor Hajime Nakagawa of Disaster Prevention Research Institute (DPRI), Kyoto University, who gave me invaluable guidance, suggestions, and encouragement while I carried my research. His insightful perspective broadened my educational horizons and helped my move beyond simply reproducing research results.

I am deeply thankful to Professor Kenji Kawaike of DPRI at Kyoto University, who introduced me to the captivating world of urban inundation studies. His patience, support, and academic guidance are greatly appreciated.

I would like to thank Prof. Hao Zhang, who is assistant professor of DPRI at Kyoto University, for his keen insight, comments, and recommendations during our laboratory seminars. Even when I was thoroughly confused, he guided me in the right direction.

I am deeply grateful to my dissertation reviewer, Professor Keiichi Toda of Kyoto University, for his valuable comments and suggestions for refining the dissertation.

I want to express my heartfelt gratitude to Mr. Ueda who made the experimental flumes that allowed me to finish my experiments on time, and to Ms. Sugimura and Ms. Himuro who helped me with administrative management. Were it not for their help, I could not have focused on my research.

Thanks to all of my colleagues with whom I studied while obtaining my PhD: Dr. Dongkeun Lee, Dr. Hiroshi Teraguchi, Dr. Hideaki Mizutani, Dr. Ripendra Awal, Dr. Badri Baktha Shresta, Dr. Ram Krishna Regmi, Dr. Pedro Luiz Borges Chaffe, Mr. Pierre Henri Bazin, Mr. Yeonjoong Kim, Mr. Amir Reza Mansoori, Mr. Atsushi Shimizu, Mr. Soshi Yoneda, Mr. Shiro Nakanishi, Mr. Tomouki Ide, Mr. Taichi Tachikawa, Mr. Namgyun Kim, Mr. Dongwoo Ko, Mr. Pawan Bhattarai, etc. Thank you for being there when questions or doubts arose. Your advice and support have meant a lot to me and helped me complete my dissertation.

I thank all of my professors and friends at the Research Center for Fluvial and Coastal Disaster, Disaster Prevention Research Institute of Kyoto University, for making my academic

experience rich and memorable. I would like to thank Mr. Fujihara, Mr. Yoshida, and the entire staffs of Ujigawa Open Laboratory, Disaster Prevention Research Institute of Kyoto University for their support in routine administrative processes and experiments.

I am also greatly indebted to my previous supervisor Professor Kwansue Jung, Chungnam National University, Republic of Korea, for sparking my interest in water resources. I am also greatly appreciative of Dr. Giha Lee, who introduced me to Kyoto University and helped me prepare for the Kyoto University entrance examination.

I gratefully acknowledge the financial support of the Monbukagakusho (Ministry of Education, Culture, Sports, Science and Technology, Japan).

I wish to express my gratitude to my family, especially mother for her ceaseless supports, and my wife's family for their encouragement and prayers throughout the course of my study. They always made me feel that I was doing something special.

Last but not least, I am sincerely grateful to my wife, Junghwa, for her persistent love, continuous support, enormous patience, and for accepting me as I am, Thanks also to Ahyon our little princess.

Table of contents

CHAPTER 1

INTRODUCTION

1.1 General

Although Athens is best known as both the capital of ancient Greece and the birthplace of Western civilization, its modern urban area has rapidly increased since the Industrial Revolution. An explosive increase in urban area also means rapid population growth and from the view point of water resources, it causes a great deal of problems such as lack of drinking water supply and pollution from untreated human excreta. As a result, sanitary facilities are needed such as, water supply facilities and sewer systems in order to prevent an infectious disease or waterborne epidemic. The improvement in land use due to urbanization has resulted in an expansion of impermeable areas, which will increase runoff by decreasing infiltration rate, evapotranspiration, and permeable areas. These phenomena increase the necessary for a sewer system.

Urban inundation due to the heavy rainfall and climate change is an inevitable problem for many cities around the world and constitutes a severe threat to residential life, property and infrastructure. The problems arising from urban inundation range from minor ones, such as water entering the basements of a few houses or buildings, to major incidents, where many parts of urban areas are flooded for long times (Mark et al., 2004).

Generally lack of sewer system capacity causes the urban inundation (Figure 1.1 and Figure 1.2). For instance, if urban surface runoff is smaller than the design capacity of the sewer system it can be drained into sewer pipes. On the other hand, if surface runoff exceeds the design capacity, water overflows from sewer pipes through manholes, storm drains, or outlet pumping stations onto the ground surface (Hsu et al., 2000). Aronica and Lanza (2005) stated that the response of the drainage systems to rain events in the urban environment is characterized by two main components, the first being the surface runoff on natural slopes collected and routed by the natural water-courses. The second component consists of the artificial drainage system, which collects rainwater from the inlets where drainage occurs through the pipes of the sewer network. “Sewerage” refers to the infrastructure that conveys sewage. It encompasses components such as receiving drains, manholes, pumping stations, storm overflows, and screening chambers of the sanitary sewer. Sewerage ends at the entry to a sewage treatment plant or at the point of discharge into the environment (Funk and Wagnall,

Figure 1.1 Urban inundation, capital city of Kerala

Figure 1.2 Overflow from sewer pipe to ground in Seoul, capital city of Korea

(source 1 : http://www.flickr.com/photos/indiawaterportal/3223419498/sizes/o/in/photostream/)
(source 2 : http://www.newsjeju.net/news/photo/201107/59361_41704_3829.jpg)

1960).

The surface runoff rate and volume in urban areas increase due to increased impervious areas such as rooftops, parking lots, and roads. Artificial facilities such as drainage systems, roads, intersections and buildings change overland flow direction (Hsu et al., 2000). As a result, overland flow phenomena and flow patterns have different mechanisms in urban areas than in rural areas.

Urban inundation can limit or completely obstruct the functioning of traffic systems and has indirect consequences such as loss of business and economic opportunities. Not only possible social consequences, but also the expected total direct and indirect loss of a great deal of money are related to the physical properties of the inundation, namely, inundation depth, inundation areas, and duration. Therefore, it is very important to consider the rapidly developing morphology of urban catchments and assess the effects of urban development on urban hydrology. Addressing urban water management issues in an efficient manner requires special adaptation of hydrodynamic modeling techniques to comprehensively study urban hydrological processes (Mignot et al., 2006; Li et al., 2009). Currently, most cities in an urbanized area generally experience from small to large problems mainly due to insufficient capacity in their sewer systems during heavy rainfall (Mark et al., 2004). König et al. (2002) categorized the damages caused by urban inundation as follows:

- Direct damage — typically material damage caused by water or flowing water
- Indirect damage — e.g, traffic disruptions, administrative and labor costs, production

losses, spreading of diseases, etc.

- Social consequences — negative long-term effects of a more psychological character, such as decrease of property values in frequently flooded areas and delayed economic development.

Simulated inundation results, in terms of extent and duration of flows, velocities and water surface elevations, can be used in such applications as flood plain mapping, planning and design of infrastructure, operation of collection and conveyance systems, evacuation plains, mitigation of urban flooding and assessment of augmentation alternatives. Therefore many researchers have been making an effort to develop and improve the urban inundation analysis model. The dual drainage concept (Smith, 1993; Djordjević et al., 1999; Nasello and Tuciarelli 2005) has been introduced to describe the bidirectional flow interactions between the ground surface and underground sewer system flows as shown in Figure 1.3. Hitherto, much of the attention of flood inundation researchers has concentrated on benchmarking model codes against two-dimensional hydraulic models including DIVAST, DIVASTTVD, TUFLOW, JFLOW, TRENT and FISFLOOD-FP (Hunter et al., 2008), simulating the flooding potential associated with the failure of a number of inlets in the system (Aronica & Lanza, 2005), assessing the sensitivity of simulations to the effects of spatial resolution (Yu & Lane, 2006a), discretization of the domain's topography (Mignot et al., 2006; Fewtrell et al., 2008), developing new modeling

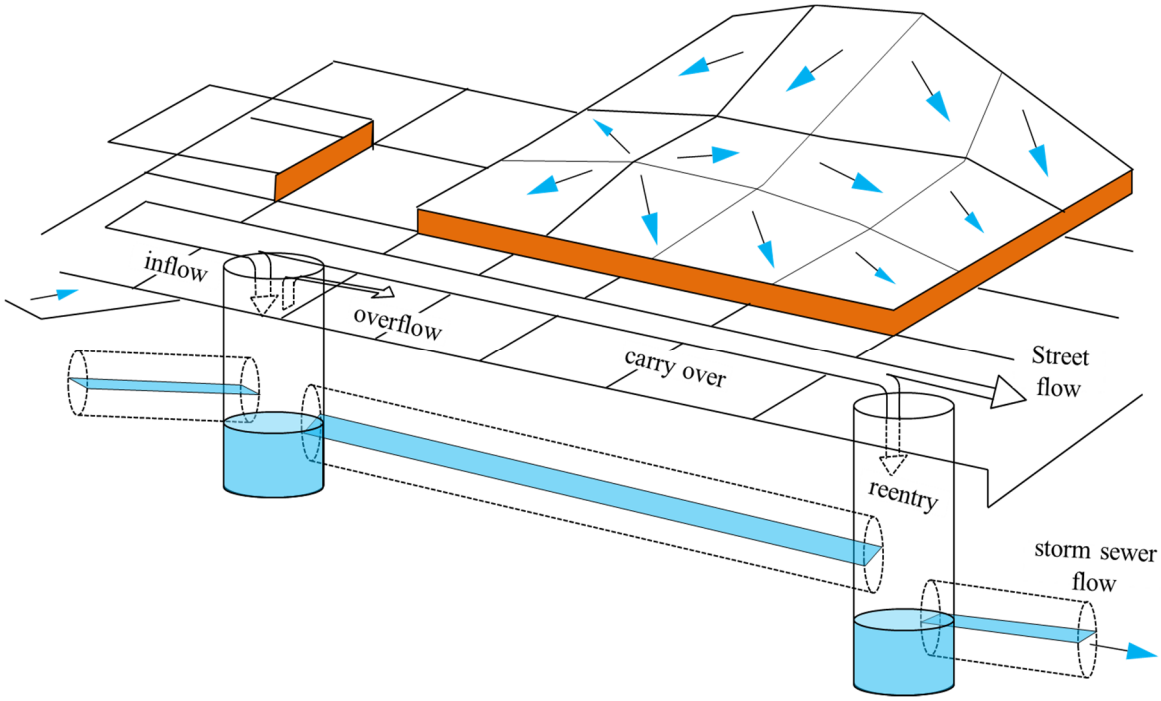

Figure 1.3 Concept of dual drainage, Smith (1993)

tools that manage both surface and sewer flows using the dual drainage concept (Mark et al., 2004; Schmitt et al., 2004), developing methods that incorporate topographic information at the sub-grid scale (Yu and Lane, 2006b; Hilary and James, 2007), and providing a method for the representation of urban areas in a large-scale model using the concept of urban porosity (Sandra et al., 2008).

However, there is a well-recognized lack of experimental data to validate and compare the performance of flood inundation models because most studies of urban inundation are devoted only to model sensitivity analysis (Hunter et al., 2007). Moreover, inundation extent data in urban areas are very rare because it is difficult to obtain high-resolution imagery that occurs simultaneously with the flood peak. Although this is also an issue in rural areas, it is particularly critical in urban areas that tend to inundate only during periods of very high flow or due to some unexpected failure in the drainage system (Neal et al., 2009). Therefore, it is of considerable importance to carry out fundamental experiments and obtain the validation data in order to develop more reasonable and enhanced urban inundation models.

1.2 Literature Review

1.2.1 Background

The development of effective and efficient designs requires a comprehensive understanding of inundation in urban areas and complex drainage and overland flow systems. Traditional one-dimensional models are used to simulate flow in river channels and gravity collection networks but are inadequate for simulating phenomenon such as significant runoff and exchange discharge between the sewer system and ground surface that occurs during extreme events. Coupling of a one-dimensional model for sewerage flow and two-dimensional model for overland flow has begun to be used with the increasing availability of high-quality digital terrain models (DTMs) and the increased power of desktop computers as well as the need for more realistic simulation of flooding.

Models simulate the performance of collection systems and natural channels under a variety of storm events, antecedent conditions, physical upgrades, and future changes in land use (Barnard et al., 2007). Results of these models in terms of extent and duration of flows, velocities and water surface elevations are used in:

- flood plain mapping

- planning and design of infrastructure
- operation of collection and conveyance systems
- evacuation plans
- mitigation of urban flooding
- assessment of augmentation alternatives

Generally urban inundation can be divided into two categories; the first is an internal inundation caused by insufficient drainage capacity at the sewer system and the second is an external inundation caused by extrinsic factors such as the breaking of an embankment, overflow from a river, and so on. Recent urban flooding events in the world have revealed deficiencies in existing storm-water infrastructure and management practices.

In rural areas, the overland flow component of hydrologic and hydraulic models can be appropriately simulated by a two-dimensional model (Wasantha Lal, 1998). However, urban inundation has different mechanisms in comparison to rural areas because most urban inundations should be considered with a sewer system involving a number of storm drains, adjunction parts and very complex interactions between the outlets of sewer pipes and river water depth; therefore the urban watershed is characterized by two components such as the storm sewer-flow component and the surcharge-induced inundation component (Hsu et al., 2000; Mark et al., 2004;). It means that the sewer system is one of the most important factors in urban flood inundation analysis. However, insufficient research has been conducted to understand fully the complex mechanism of sewer systems based on both experiments and simulations.

As mentioned above, the primary factors to analyze and predict urban inundation can be divided into three parts: a) calculation of inlet discharge through the storm drain, b) analysis of the sewer network according to different manholes shapes, and c) pipe configurations and discharge interactions among ground surface, sewer system, and river flow.

1.2.2 Previous related studies

During the last few decades, the primary target of inundation analysis shifted from rural sites to urban areas because of the dramatic increase in urbanization. Typical research on rural site inundation only focused on measuring inundation discharge from rivers due to overtopping or breaking the embankment, calculating maximum inundation depth and analyzing propagation of flooding velocity; sewer system analysis such as drain discharge through the storm drain, effects

of pipe configuration, and interaction phenomena between ground surface and sewer system, was not carried out sufficiently. This research focuses on development of an integrated urban inundation model incorporating drainage systems with laboratory experiments and simulations.

1.2.2.1 Inlet discharge coefficient

Johnson (2000) conducted experiments to measure discharge coefficient scale effects for weirs using various flat-topped and sharp-crested weirs. In his paper, he mentioned that the general form equation of the weir is widely accepted and is commonly used although this equation is not as theoretically correct as the broad-crested weir equation. The unsteady flow pattern of a rectangular orifice was presented using a large-size orifice tank to minimize scale effects by Chanson et al. (2002). They mentioned that the flow changes from a submerged flow to a free-surface overflow for $H_t/b_0 \approx 0.43$ to 0.51. Hydraulic description of the bottom rack intake was provided for a more in-depth analysis.

A novel approach to determine the discharge coefficient of a rack structure was presented using a specific porosity. Burnella et al. (2003) determined the discharge coefficient of the general orifice formula using only a porosity concept of racks. Therefore some coefficients showed somewhat non-physical values bigger than 1.0. Aronica et al. (2005) concluded that micro-topography effects have the potential to produce local flooding with significant water depth and velocity in zones of flow concentration, and that local topography may significantly affect the behavior of the urban drainage system as a whole. However, they simply compared two groups of simulation results. One of those is a virtual hydraulic connection with the subsurface drainage network and the other one includes no connection between the surface and sewer system. They did not address how drainage water could be treated according to time. James et al. (2011) conducted proto type experiments in order to calculate discharge through the bottom slot and suggested empirical formula to determine the slot length.

1.2.2.2 Manhole head losses

Masalek (1984) focused on the effect of junction geometry on head losses in the pressurized flow region regarding manhole shapes and the ratio of the manhole size to the pipe diameter. It was found that the head-loss coefficient decreased with the decreasing manhole width.

Johnston and Volker (1990) presented the results of a detailed experimental hydraulic model study of the hydraulic interactions in two common junction box configurations using a three-

pipe and a two-pipe configuration. Both configurations demonstrate that the influence of Froude number and box submergence are not major, but nevertheless are important in some flow conditions. Pederwen and Mark (1990) outlined a submerged jet theory for the flow in manholes with straight through flow. They mentioned that the entrance head loss has been related to the kinetic energy transformation associated with the entrainment / detrainment in the jet, and the exit head loss is calculated as a Carnot loss in connection with the vena contracta in the exit pipe. Zhao et al. (2006) conducted laboratory investigation on pressurized flow in combining sewer junctions. The study confirmed the existence of three flow regimes in sewer junctions with a steep outgoing pipe. Wang et al. (1998) conducted a laboratory investigation of a manhole and pipe-line system for the head loss coefficients regarding a variety of outlet-flow Reynolds numbers, surcharge levels, pipe sizes, flow configurations, and inlet-flow rates. They developed empirical formulas to estimate head-loss coefficients. The results showed that head loss is insensitive to the amount of surcharge, but depends heavily on the flow configuration, relative flow rate, and the change of pipe diameter within the pipelines. Merlein (2000) developed a mathematical model that calculates the influence of manholes with and without cover plate in a submerged sewer. She concluded that the cover plate can reduce a loss coefficient at manholes and the reduction of head losses causes a reduction of water levels at manholes further upstream. Experiments were performed to consider the behavior of supercritical flow in sewer junction manholes by Juan et al. (2012). They carried out physical prototype-scale model experiments using three approach flow configurations.

- Manhole entry flow through main pipeline only (direct flow)
- Manhole entry flow through lateral pipeline only
- Manhole entry flow through both entry and lateral branches (junction flow)

They found three types of standing-wave conditions, which are able to choke the exit pipe according to the dominated flow discharge.

Maciej (2007) carried out three kinds of experiments to focus on determination of the loss coefficient K_s using straight-through and angled manholes configurations, depending on varied relative depth during surcharge. The obtained results are somewhat different from the equation recommended in the literature, especially distinct for the angled configuration.

1.2.2.3 Interaction of exchange discharge

Figure 1.4 shows the concept of urban inundation and drainage process, in which many hydrologic and hydraulic factors should be considered such as rainfall intensity, overland runoff flow, infiltration, sewer system and its interaction with river flow, etc. Therefore it is very important that these phenomena should be dealt with comprehensively in urban inundation analysis.

Hsu et al. (2000) conducted an integrated simulation with the SWMM (Storm Water Management Model) and 2D diffusive overland flow model, and pointed out that the urban watershed is characterized by two components, the storm sewer flow component and the surcharge-induced inundation component. However, the two components could not deal with detailed information such as inundation zones and depths caused by pressurized water. Duchesne et al. (2001) demonstrated the efficiency of real-time control (RTC) in comparison with USEPA EXTRAN. Although global predictive control (GPC) provides an effective strategy to perform real-time management of sewers and could compute flow rates and water levels, this model did not consider an exchange discharge between ground surface and sewer pipe. Hsu et al. (2002) simulated inundation in the urban area coupling a 2D non-inertia overland flow model with a stormwater management model, in which overland flow was calculated by the EXTRAN block of SWMM. In this research, exchange capacity was decided by designed discharge. Akiyama et al. (2008) developed a dynamic network model for free-surface-pressurized flows based on the flux difference splitting scheme combined with the Preissmann slot to simulate flow in a closed conduit. The model could predict the prone inundation area but there was no consideration of the discharge exchange between overland flow and the sewer system. Leandro

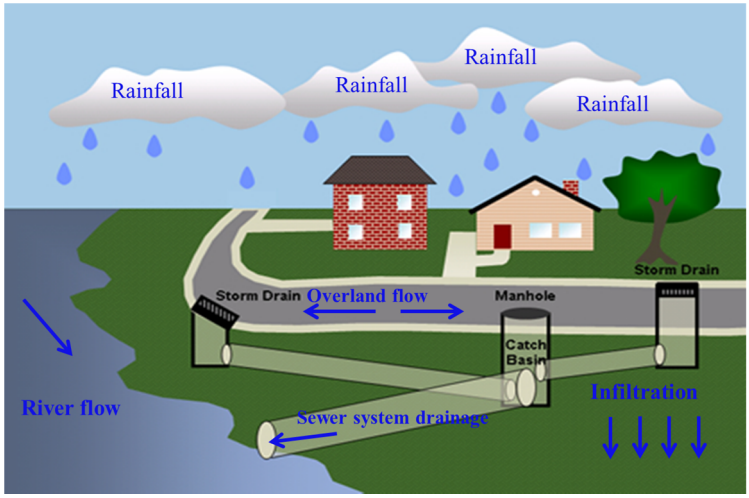

Figure 1.4 Drainage process concept of urban area

(source : http://www.concordnc.gov/departments/stormwater-services/stormwater-pollution/where-does-it-go)

et al. (2009) carried out comparison of a one-dimensional (1D) sewer model coupled with a 1D surface network model and a 1D sewer model coupled with a two-dimensional (2D) surface model. The surface pathways, linking elements sewer/surface, and inclusion of virtual manholes are defined as key factors for setting up a more accurate 1D/1D model.

Li et al. (2009) developed a methodology to simulate inundation processes comprehensively by dynamically coupling 1D and 2D hydrodynamic models. This method could be used to estimate the potential inundation risks of a designed drainage system by allowing the simultaneous solution of the processes of rainfall and runoff and urban drainage. However, the calculation method of exchange discharge was not stated.

Cantone and Schmidt (2011) developed an Illinois urban hydrologic model (IUHM) that can analyze and predict the hydrologic response of a highly urbanized catchment even without detailed input data using the geomorphologic instantaneous unit hydrograph concept. They emphasized that urban catchments are significantly different than natural watersheds, but there are similarities that allow features of the pioneering geomorphologic instantaneous unit hydrograph concept. Application of IUHM to a real catchment highlights the model's ability to predict the hydrologic response of the catchment.

Amaguchi et al. (2012) developed a vector-based distributed storm event runoff model for urban runoff analysis based on landscape GIS delineation that faithfully describes the complicated urban land use features in detail. The model was set up and evaluated for a small catchment in Tokyo incorporating runoff, infiltration sewer system, river element, and outside catchment. Simulated water levels could reproduce the observed data, but only a general model formulation was used with no calibration; standard parameter values were used.

1.3 Objectives of the Research

The aim of this research is to study the interaction between the ground surface and sewer system involving a storm drain box in order to develop an integrated urban inundation model. In this context, three kinds of research have been conducted through laboratory experiments and numerical simulation. The main objectives of this research are described as follows.

1. To suggest a calculation method of inlet discharge through the storm drain based on flow pattern on the ground surface.
2. To develop and validate a numerical model of a one-dimensional sewer system according to manhole shapes and pipe configurations under surcharge condition.

3. To experimentally validate the suggested calculation method of inlet discharge through the storm drain and interaction between sewer pipe and ground surface using a laboratory-scaled experimental facility.
4. To analyze the discharge exchange mechanism and head loss effect depending on manhole shape and pipe configuration at manhole

1.4 Outlines of the Thesis

The present thesis consisting of five chapters is organized as follows.

Chapter 1 describes the important topics concerning urban inundation that may negatively affect human life and presents brief background, objectives, and literature review of prior this research.

Chapter 2 presents the experimental investigation cases and simulation results, which suggest the method to calculate inlet discharge through the storm drain depending on the relation between flow depth and width of the storm drain cover.

In chapter 3, a second experimental procedure and analysis results to develop a one-dimensional (1D) model that can consider the head loss effects depending on different manhole shapes and pipe configuration are described. The purposes of the experiments are to analyze head loss effects according to manhole shape and pipe configuration, and to obtain validation data for developing a 1D sewerage model that can consider head loss effect and pipe configuration.

Chapter 4 presents the final experimental procedure and analysis methods carried out to validate applicability of the method suggested in chapter 2, and to confirm the behavior of the exchange discharge and inundation process among the ground surface, storm drain, and sewer pipe.

Finally, in chapter 5, the main findings and conclusions about the characteristics of the urban inundation process and the main factors that should be considered in an urban inundation simulation are summarized. In addition, various remaining issues are identified and recommendations for future research are described.

CHAPTER 2

STUDY ON INLET DISCHARGE THROUGH STORM DRAINS

2.1 Introduction

Urban inundation resulting from climate change is a serious problem for many cities around the world. Therefore, it is important to accurately simulate urban hydrological processes and efficiently predict the potential risks of urban floods for the improvement of drainage designs and implementation of emergency actions (Li et al., 2009). In order to solve these types of problems, two-dimensional numerical simulation models of flood inundation in urban environments have become more popular in the last few years (Cea et al., 2010). However, the urban environment is highly heterogeneous in terms of land use, drainage systems, and other factors influencing the processes of the water cycle, including rainfall, surface runoff, infiltration and movement of water in the sub-soils, interaction between surface water and groundwater, interaction between the drainage network and groundwater, and evapotranspiration (Campana et al., 2001). In addition to these complex interactions, there is a well-recognized lack of experimental data to validate and compare the performance of flood inundation models, because most studies of urban flooding have been devoted to model sensitivity analysis (Hunter et al., 2007).

There are two main reasons for urban inundation. The first is a lack of sewer system capacity and the second is an insufficiency of storm drains. For instance, if the flow rate in a sewer pipe exceeds maximum capacity of the pipe, the surface runoff flow will not drain into the sewer system through the storm drain and overflow may occur. On the other hand, if the flow rate does not exceed the maximum capacity, the surface flow can be captured and drained through the storm drain. Generally, it is somewhat difficult to imagine that there may be an inundation in the latter, but it is possible. Although the designed capacity of a sewer system is enough to carry flooding discharge, if the discharge cannot be drained through the storm drains, ground surface inundation may occur (Hsu et al., 2000). Local failures are also indeed observed as a consequence of precipitation events with even lower intensities than the designed rainfall capacity, when inlets flow due to rainfall in greater quantity than the design capacity can handle (Aronica and Lanza, 2005). Therefore, it should be emphasized that estimating an inlet

discharge through the storm drains is as important as analyzing the sewer network or designing the maximum discharge according to the scenario. The sewer system is one of the most important factors in urban flood inundation models and the inlet discharge through the storm drains is also very important input data for in planning a sewer system.

Many previous researchers who performed urban inundation research used the weir and orifice formula when they calculated inlet discharge through storm drains. These formulas could be divided as submerged (orifice) and non-submerged (weir) cases, respectively. There are several forms of the weir and orifice discharge equation. Equation (2.1) and (2.2) show the general form of weir equations.

$$\mathrm{Q} = \frac{2}{3} C_{dw} L \sqrt{2g} (H_t)^{\frac{3}{2}} \tag{2.1}$$

where

$$H_t = \left(h + \frac{V^2}{2g} \right) \tag{2.2}$$

in which, Q is the discharge, C_{dw} is the discharge coefficient for the weir, L is the length of the weir, H_t is the total head, h is the piezometric head over the weir, V is the average velocity of the flow at the gauging location, and g is the acceleration of gravity. Equation (2.3) shows the general form of an orifice equation.

$$Q = C_{do} A \sqrt{2gh} \tag{2.3}$$

where Q is the discharge, C_{do} is the discharge coefficient for orifice, A is the orifice cross-section area and h is the piezometric head over the orifice. Equation (2.4) shows the discharge coefficient.

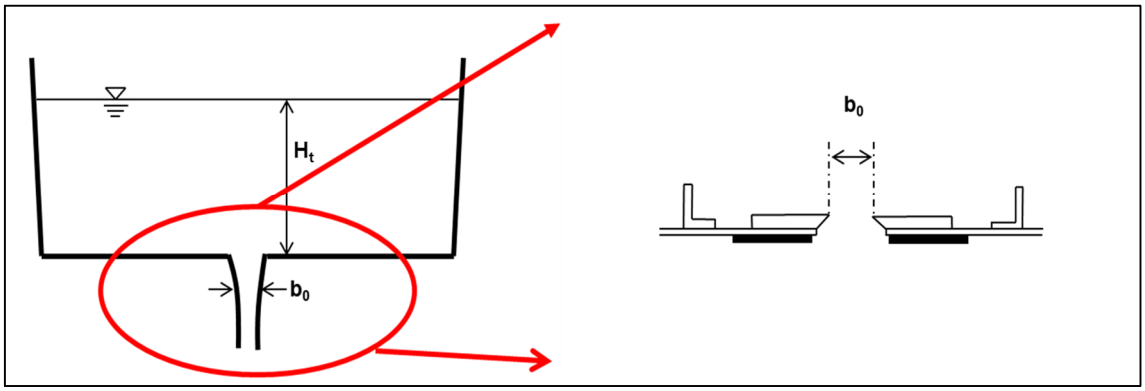

Figure 2.1 Sketch of the experiment and definition, Chanson et al (2002)

$$C_{do} = C_c \times C_v \quad (2.4)$$

where the velocity coefficient C_v account for the energy losses and C_c is the contraction coefficient.

Both equations are widely accepted and commonly used. However it is occasionally very difficult to apply suitable coefficient values for each formula because the different values of weir and orifice coefficients were suggested by each researcher. It was usually assumed that the velocity head term was zero in the equation (2.2). Also, it is not simple to decide upon and apply a suitable formula under several conditions. Therefore, if we can determine suitable coefficients and standards to select appropriate formulas that can consider velocity head from the experimental data, it could be an appropriate-criterion and extensively used for more reasonable urban inundation analysis.

Chanson et al. (2002) suggested the relations to distinguish the weir and orifice flow patterns, which were verified on their experiment examining the unsteady two-dimensional orifice flow as $H_t / b_0 \approx 0.43 \sim 0.51$ as shown in Figure 2.1. In this relation, H_t is the total head (water depth + velocity head) and b_0 is orifice thickness (small dimension). If H_t / b_0 is bigger than 0.51, the water flow shows an orifice flow pattern with free surface, and if H_t / b_0 is smaller than 0.43, the water flow shows a weir flow pattern without free surface. However, a transition flow pattern exists when H_t / b_0 ranges from 0.51 to 0.43.

In this chapter, laboratory experiments to measure the inlet discharge coefficients of weir and orifice through the storm drain are carried out using different storm drain cover shapes and hydraulic conditions. First, storm drain covers are divided into square and grid types and then the influence of both shapes is analyzed. Secondly, it is assumed that H_t / b_0 is 0.5 as a criterion to divide a weir and an orifice flow and then, in order to consider the velocity head, the front total head of storm drain is assumed to be the total head of the storm drain based on the Bernoulli's equation, because it is very difficult to measure a velocity head with dynamic fluctuation near the storm drain caused by interaction between captured discharge and passing discharge. Finally, application of the relation suggested by this assumption is evaluated by comparing the experimental data and simulation results, with new weir and orifice coefficients suggested based on the experimental data.

2.2 Description of Experimental Set-up

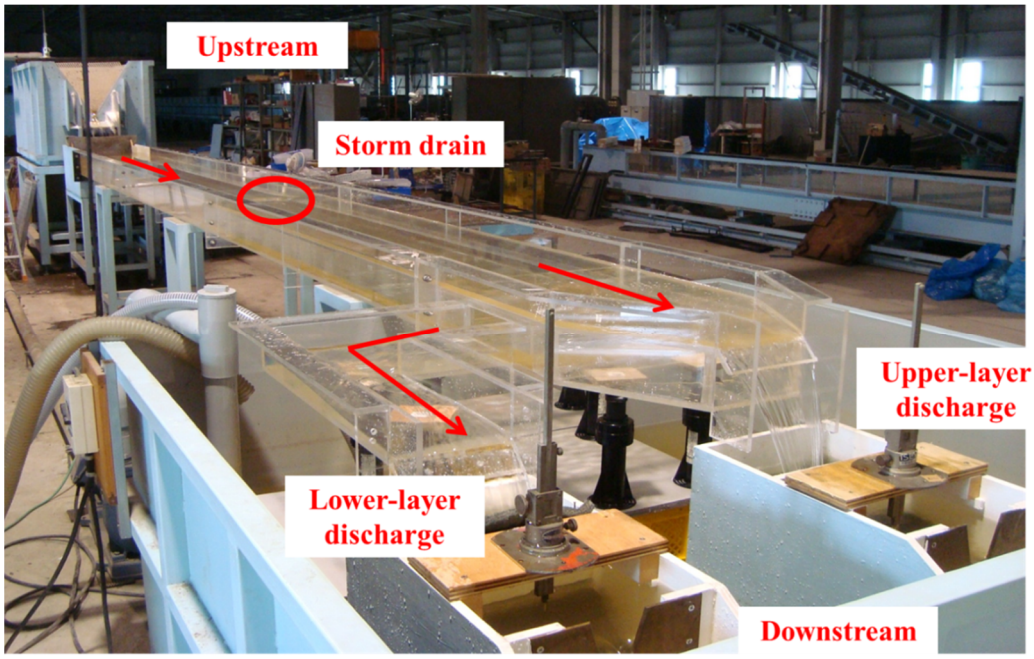

Figure 2.2 Experiment flume setup

Table 2.1 Ratio between real scale and experimental scale

Index	Ratio
Length	1/10
Velocity	1/3.16
Discharge	1/316
Roughness coefficient	1/1.48

The experiments were carried out in a flume located at the Ujigawa Open Laboratory (UOL) of the Disaster Prevention Research Institute (DPRI), Kyoto University, Kyoto, Japan. A scale model was constructed in order to determine the weir and orifice coefficients that can be applied for urban inundation simulation in chapter 4. Figure 2.2 and Figure 2.3 show the experimental setup, which consists of three parts: the upper layer, the lower layer, and the storm drain. Figure 2.4 shows two storm drain cover shapes used in this experiment. The thickness of the grid is 1mm. The width and length of both storm drain covers, Figure 2.4 (a) and Figure 2.4 (b), are 0.1m×0.05m. The experimental scale is assumed to be 1/10 and Table 2.1 shows the ratios between the real scale and the experimental scale based on the similarity law of Froude. The upper layer has a flat inundation basin 6m long and 0.5m wide, on which there is a storm drain of 0.1m×0.05m size at the center of the flume with zero slope.

Johnson (2000) stated that the gauging point should be located sufficiently far upstream of the weir to avoid the area of water surface draw-down, yet it should be close enough to neglect the

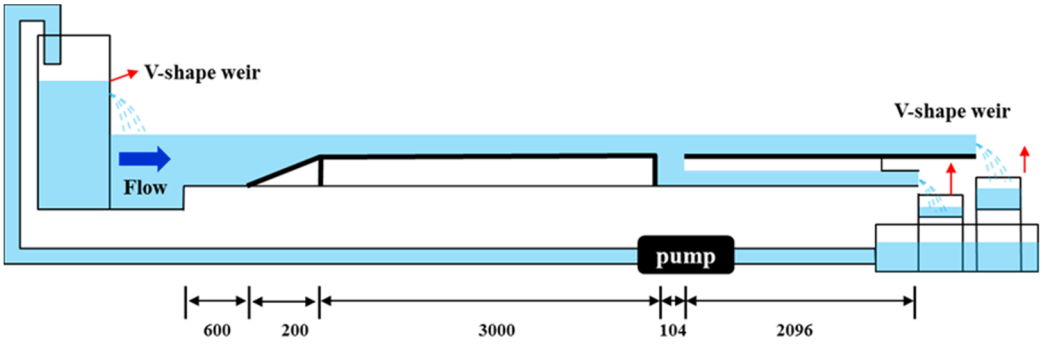

(a) Side view of whole flume

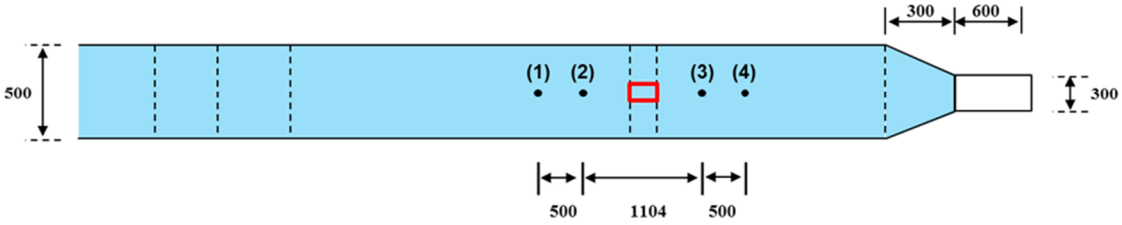

(b) Plan view of upper layer

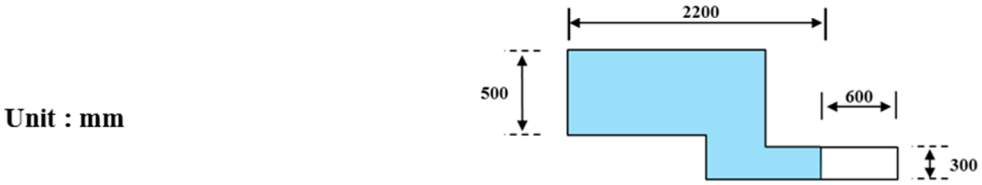

(c) Plan view of lower layer

Figure 2.3 Schematic of flume

energy loss between the gauging point and the structure. He conducted experiments to analyze the various types of weir coefficient by measuring water depth considering the gauge point at a distance equal to three times of the maximum total head from the weir's leading edge.

Velocity and water depths are obtained in strategic places, as shown in Figure 2.3; black points (no.(1) ~ no.(4)) mean the measuring points of the velocity and water depth and the obtained data are used to validate applicability of the simulation model. The lower layer begins under the storm drain cover and has a flat basin 2.2m long, 0.5m wide, and 0.12m tall and drained discharge flow through the lower layer measured by the V-shape weir at the downstream. In addition, overland flow discharge is measured by V-shape weir to compare total

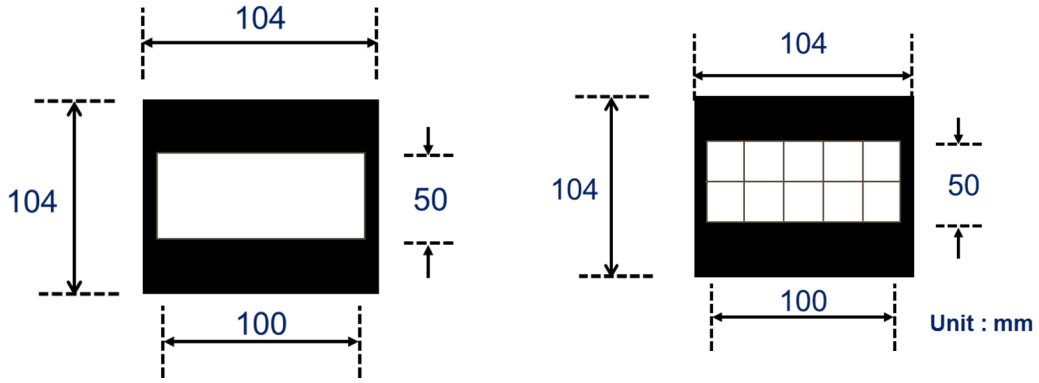

Figure 2.4 Shape of the storm drain cover

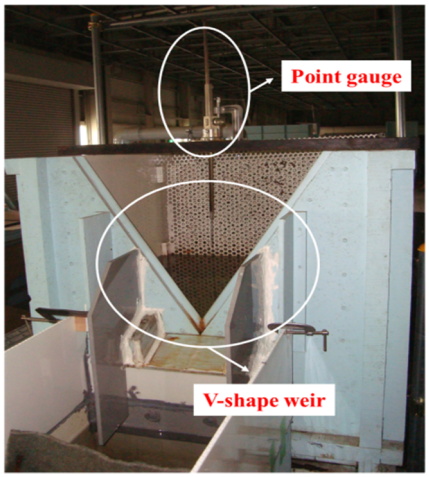

Figure 2.5 Point gauge and V-shape weir at upstream tank

outlet discharge with input discharge.

The storm drain is located at the center line of the channel and approximately 3.8m away from the upstream. The flow source has a constant head and is controlled by a circulating pump valve. The input discharge is also measured using a V-shape weir and point gauge (Figure 2.5) from the constant head reservoir upstream.

2.3 Experimental Conditions

In total, 12 experimental cases were selected to fulfill the weir and orifice flow pattern. The following hydraulic parameters used for the experiments are summarized in Table 1.2. All experiments were carried out under steady flow condition.

Table 2.2 Experimental Hydraulic conditions

Case		Input discharge Q (l/s)	Mean Velocity v (m/s)	Water depth h (cm)	Froude number, Fr	slope
Square type cover	1	0.82	0.38	1.30	1.06	0
	2	1.66	0.44	1.88	1.03	0
	3	2.50	0.46	2.36	0.63	0
	4	3.23	0.48	2.74	0.93	0
	5	3.96	0.47	3.16	0.84	0
	6	4.58	0.45	3.54	0.76	0
Grid type cover	7	1.09	0.40	1.54	1.03	0
	8	2.06	0.44	2.15	0.96	0
	9	3.04	0.42	2.71	0.81	0
	10	3.68	0.45	3.10	0.82	0
	11	4.32	0.44	3.52	0.75	0
	12	4.99	0.43	3.90	0.70	0

The main purposes of the experiment are as follows:

- to measure stable inlet discharge;
- to analyze the influence of different storm drain cover shape on inlet discharge;
- to obtain and suggest the suitable weir and orifice coefficients.

2.4 Measurement Techniques

2.4.1 Discharge measurement

The inflow discharge was supplied by a circulation pump and should be calculated by a point gauge and V-shape weir upstream after steady state conditions are achieved, just as the inlet discharge are calculated downstream using a different V-shape weir. Two types of different empirical H-Q relation are necessary to measure the inflow and inlet discharge, because each of the V-shape weirs (upstream and downstream) has different properties (size and angle). The following procedures were adopted to develop the empirical relations:

(a) Select the arbitrary input discharge near the zero

(b) Supply it to the downstream V-shape weir and maintain until it creates steady flow conditions

(c) Measure the water depth and fill with water using a basket for 10 seconds

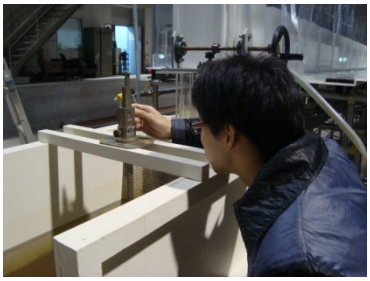
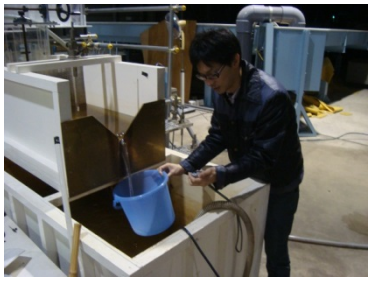


(a) Measuring the water depth (b) Filling with water (c) Weighting the water weight

Figure 2.6 The processes to make the empirical H-Q relations

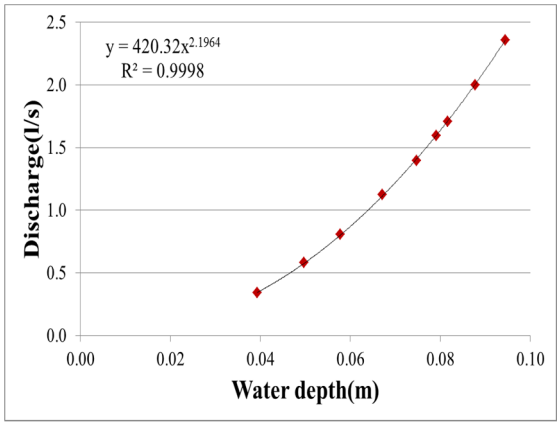

(a) Upstream weir

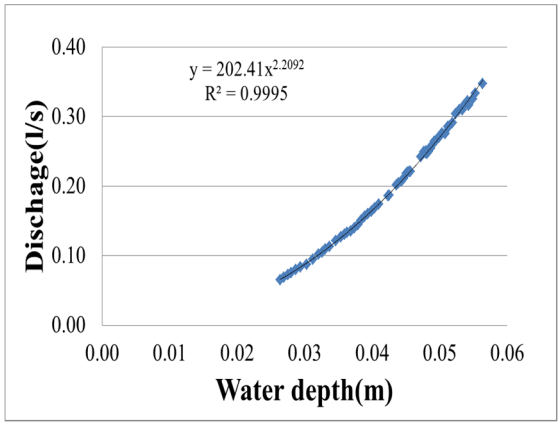

(b) Downstream weir

Figure 2.7 Empirical H-Q relations

(d) Measure the weight of the water in the basket

(e) Record the water depth and water weight

(f) Slightly increase the input discharge and repeat the processes from (a) to (f)

However, this method can only be applied to downstream weirs because upstream weir has relatively large capacity. Therefore, the empirical relation of the upstream weir can be obtained using the downstream weir. Figure 2.6 shows the working processes to obtain the H-Q relations and Figure 2.7 shows the obtained empirical H-Q relations.

2.5 Experimental Procedure

Basically, the experimental procedure followed the same steps for all cases as described in the following paragraphs. Storm water stored in the downstream reservoir is pumped up to the

upstream end and added as the inflow discharge from the upstream. Two types of storm drain covers (square and grid) are used to determine the discharge coefficients.

The experimental procedure is relatively straightforward. The variables for each storm drain cover shape are input discharges. A series of discharges is established to determine each discharge coefficient, as shown in Table 1.2. The initially closed control valve is opened and kept open until the increased flow results in constant discharge and a steady state condition is established. The input and inlet discharge are measured at each point gauge upstream and downstream. After measuring the discharge, water depths at strategic places are measured by point gauge and the mean velocities are calculated using the continuity equation. The total head of the strategic point (2) in Figure 2.3 is assumed as a total head on the storm drain in order to avoid the area of water surface draw-down, as mentioned by Johnson (2000). In the square type cover, water discharges were controlled from approximately 0.8*l/s* to 4.6*l/s*, and in the grid type cover were controlled from approximately 1.1*l/s* to 5.0*l/s* by the circulating pump valve.

2.6 Experimental Results

Experimental studies are important in estimating the applicability of each formula and to confirm division of the flow pattern between weir and orifice flow near the storm drain. In this section, the experimental observation and results are presented and discussed. Several observations regarding the storm drain were made regarding the change of upstream discharge and storm drain cover shape. The effects of each type of storm drain cover and each coefficient of the applicable formula are investigated.

2.6.1 Flow pattern

The weir and orifice flow pattern can be distinguished by the existence of free surface on a storm drain. For example, if the water depth near the storm drain is too shallow to create free surface on the storm drain cover, there will not be a free surface on the storm drain and the water may drop like a cascade into the storm drain box. After that, if the water depth increases in sufficient quantity to reach both sides of the storm drain, the flow pattern can be changed to an orifice flow pattern with free surface on the storm drain.

Similarly, in this section, at low upstream discharges the trajectory of the water around the storm drain was observed to be similar with regards to weir flow, because there was no free surface on the storm drain. For this reason, it looked like the orifice flow when upstream

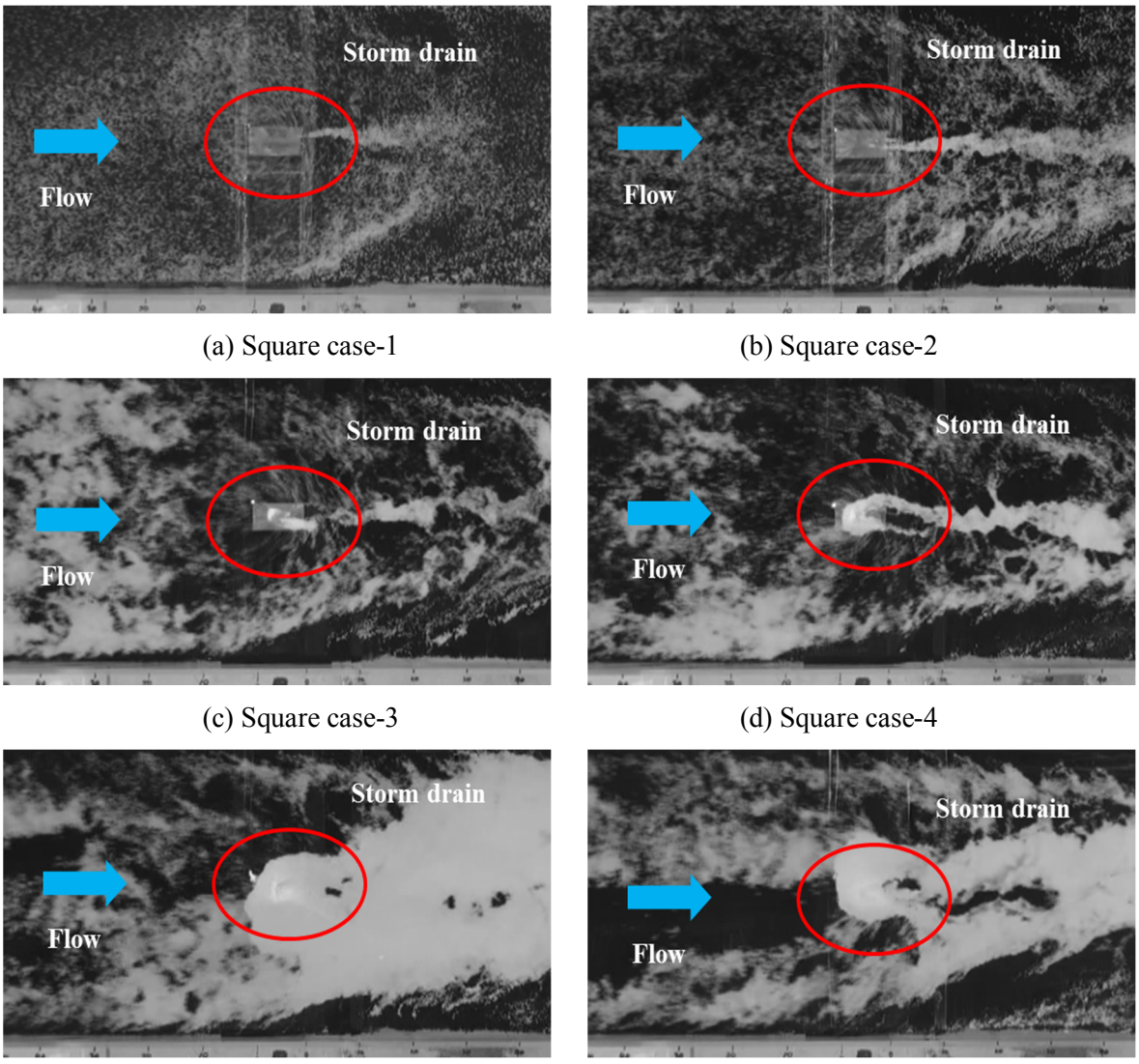

(a) Square case-1 (b) Square case-2

(c) Square case-3 (d) Square case-4

(e) Square case-5 (f) Square case-6

Figure 2.8 Surface flow visualization of square cases

discharge was increased, as shown in Figure 2.8. In order to confirm the existence of free surface on the storm drain, white powder was used to increase visibility. Figure 2.8 (a) and (b) show that there is no free surface; it starts to develop in Figure 2.8 (c). Finally, the free surface is clearly observed in Figure 2.8 (d) and (e). With the change of surface on the storm drain, this observation implies that the formula could be divided into the equation (2.1) and (2.3) as both equations could be applied when calculating the inlet discharge through the storm drain; further details will be discussed in section 2.7.

2.6.2 Inlet discharge and discharge coefficients

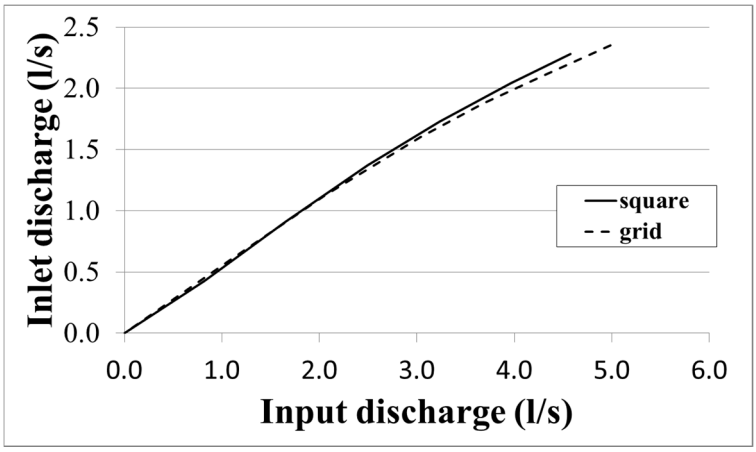

Figure 2.9 Comparison of inlet discharge

In the experiments performed in these studies, an inundation process of drainage flow was made to occur by controlling the circulation pump valve. Inlet discharge was measured using a downstream V-shape weir using the empirical H-Q relation suggested in section 2.4. Figure 2.9 shows measured inlet discharge, which could be used to analyze each discharge coefficient.

The result of dimensional analysis assuming a high Reynolds number shows the negligible effect of fluid viscosity. Therefore, the weir and the orifice formula discharge coefficients are directly determined by equation (2.5) and (2.6).

$$C_{dw} = \frac{Q_{exp}}{\frac{2}{3}L\sqrt{2g}(H_t)^{3/2}} \tag{2.5}$$

$$C_{do} = \frac{Q_{exp}}{A\sqrt{2gh}} \tag{2.6}$$

The H_t of equation (2.5) is a total head at the strategic point (2) in Figure 2.3, but we can

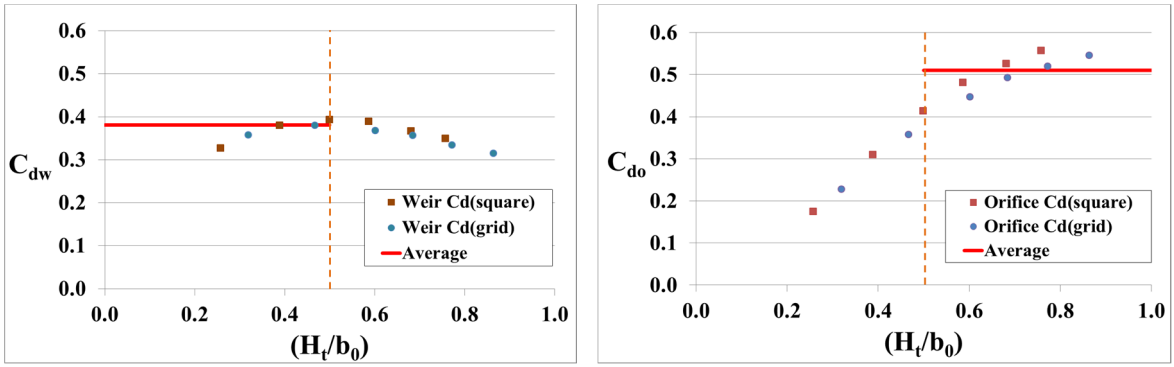

(a) Weir coefficients (b) Orifice coefficients

Figure 2.10 Calculated each coefficient

assume it to be a total head on the storm drain by the Bernoulli's equation.

Figure 2.10 (a) presents the experimental results in a constant form with equation (2.5) and the data are well represented. It is difficult to detect the constant coefficient C_{dw} from the graph, but the effect of increasing the total head is slightly increased to the $H_t / b_0 = 0.5$ and decreased, and the influence was very small between square and grid shape. Therefore, the weir coefficient for both shapes is determined to be 0.381.

Figure 2.10 (b) presents the experimental results in a constant form with equation (2.6). It is also difficult to decide the constant coefficient C_{do} from the graph, so the simplified average value of the orifice discharge coefficient is calculated as 0.51.

2.7 Numerical Modeling

2.7.1 Introduction

A numerical simulation model using continuity and momentum equations is used to estimate each coefficient obtained from the laboratory experiments. The model consisting of a 2D horizontal depth average flow model for the flow of two layers and an inlet discharge model to calculate inflow discharge from the upper layer to the lower layer estimates an applicability of obtained coefficient and suggested criteria (H_t / b_0 =0.5).

2.7.2 Two-dimensional upper-layer flow model

2.7.2.1 Governing equation

A two-dimensional (2D) flow model with a momentum equation and continuity equation is used to analyze upper-layer flow. The governing equations used here are as follows:

Continuity equation:

$$\frac{\partial h}{\partial t} + \frac{\partial M}{\partial x} + \frac{\partial M}{\partial y} = -q_{low} \tag{2.7}$$

Momentum equation:

$$\frac{\partial M}{\partial t} + \frac{\partial (uM)}{\partial x} + \frac{\partial (vM)}{\partial y} = -gh\frac{\partial H}{\partial x} - \frac{gn^2 M\sqrt{u^2+v^2}}{h^{4/3}} \tag{2.8}$$

$$\frac{\partial N}{\partial t} + \frac{\partial (uN)}{\partial x} + \frac{\partial (vN)}{\partial y} = -gh\frac{\partial H}{\partial y} - \frac{gn^2 N\sqrt{u^2+v^2}}{h^{4/3}} \tag{2.9}$$

where h is water depth, H is water level, u, v are x, y directional velocity, M (=uh), N (=vh) are x, y directional flow flux, q_{low} is inflow discharge from the upper-layer to lower-layer per unit area (if its value is negative, that means surcharge flow discharge) and is only calculated on the storm drain grid, g is gravity acceleration, and n is Manning's roughness coefficient (n=0.012 is adopted in this study). Computational meshes are a rectangular shape (x=10cm, y=10cm) and FDM is adopted.

2.7.2.2 Discretization methods

Figure 2.11 (a) shows an arrangement of each parameters *M, N* and *h* on the mesh. The leap-frog method, which alternately calculates water depth and flux, is used to analyze water flow as shown in Figure 2.11 (b).

Continuity equation

$$\frac{h_{i+1/2,j+1/2}^{n+3}-h_{i+1/2,j+1/2}^{n+1}}{2\Delta t}+\frac{M_{i+1,j+1/2}^{n+2}-M_{i,j+1/2}^{n+2}}{\Delta x}+\frac{N_{i+1/2,j+1}^{n+2}-N_{i+1/2,j}^{n+2}}{\Delta y}=q_{low}{}_{i+1/2,j+1/2}^{n+2} \qquad (2.10)$$

Momentum equation

X-direction

$$\frac{M_{i,j+1/2}^{n+2}-M_{i,j+1/2}^{n}}{2\Delta t}+\frac{u_{i+1/2,j+1/2}^{n}\left(\frac{M_{i+1,j+1/2}^{n}+M_{i,j+1/2}^{n}}{2}\right)+\left|u_{i+1/2,j+1/2}^{n}\right|\left(\frac{M_{i,j+1/2}^{n}-M_{i+1,j+1/2}^{n}}{2}\right)}{\Delta x}$$

$$-\frac{u_{i-1/2,j+1/2}^{n}\left(\frac{M_{i,j+1/2}^{n}+M_{i-1,j+1/2}^{n}}{2}\right)+\left|u_{i-1/2,j+1/2}^{n}\right|\left(\frac{M_{i-1,j+1/2}^{n}-M_{i,j+1/2}^{n}}{2}\right)}{\Delta x}$$

$$+\frac{v_{i,j+1}^{n}\left(\frac{M_{i,j+3/2}^{n}+M_{i,j+1/2}^{n}}{2}\right)+\left|v_{i,j+1}^{n}\right|\left(\frac{M_{i,j+1/2}^{n}-M_{i,j+3/2}^{n}}{2}\right)}{\Delta y} \qquad (2.11)$$

$$-\frac{v_{i,j}^{n}\left(\frac{M_{i,j+1/2}^{n}+M_{i,j-1/2}^{n}}{2}\right)+\left|v_{i,j}^{n}\right|\left(\frac{M_{i,j-1/2}^{n}-M_{i,j+1/2}^{n}}{2}\right)}{\Delta y}$$

$$=-g\frac{h_{i+1/2,j+1/2}^{n+1}+h_{i-1/2,j+1/2}^{n+1}}{2}\left(\frac{H_{i+1/2,j+1/2}^{n+1}-H_{i-1/2,j+1/2}^{n+1}}{\Delta x}\right)$$

$$-g\frac{n_{i,j+1/2}^2\left(\frac{M_{i,j+1/2}^{n+2}+M_{i,j+1/2}^n}{2}\right)\sqrt{\left(u_{i,j+1/2}^n\right)^2+\left(\tilde{v}_{i,j+1/2}^n\right)^2}}{\left(\frac{h_{i+1/2,j+1/2}^{n+1}+h_{i-1/2,j+1/2}^{n+1}}{2}\right)^{4/3}}$$

Y-direction

$$\frac{N_{i+1/2,j}^{n+2}-N_{i+1/2,j}^n}{2\Delta t}+\frac{u_{i+1,j}^n\left(\frac{N_{i+3/2,j}^n+N_{i+1/2,j}^n}{2}\right)+\left|u_{i+1,j}^n\right|\left(\frac{N_{i+1/2,j}^n-N_{i+3/2,j}^n}{2}\right)}{\Delta x}-$$

$$\frac{u_{i,j}^n\left(\frac{N_{i+1/2,j}^n+N_{i-1/2,j}^n}{2}\right)+\left|u_{i,j}^n\right|\left(\frac{N_{i-1/2,j}^n-N_{i+1/2,j}^n}{2}\right)}{\Delta x}+$$

$$\frac{v_{i+1/2,j+1/2}^n\left(\frac{N_{i+1/2,j+1}^n+N_{i+1/2,j}^n}{2}\right)+\left|v_{i+1/2,j+1/2}^n\right|\left(\frac{N_{i+1/2,j}^n-N_{i+1/2,j+1}^n}{2}\right)}{\Delta y}- \qquad (2.12)$$

$$\frac{v_{i+1/2,j-1/2}^n\left(\frac{N_{i+1/2,j}^n+N_{i+1/2,j-1}^n}{2}\right)+\left|v_{i+1/2,j-1/2}^n\right|\left(\frac{N_{i+1/2,j-1}^n-N_{i+1/2,j}^n}{2}\right)}{\Delta y}$$

$$=-g\frac{h_{i+1/2,j+1/2}^{n+1}+h_{i+1/2,j-1/2}^{n+1}}{2}\left(\frac{H_{i+1/2,j+1/2}^{n+1}-H_{i+1/2,j-1/2}^{n+1}}{\Delta y}\right)-g\frac{n_{i,j+1/2}^2\left(\frac{N_{i+1/2,j}^{n+2}+N_{i+1/2,j}^n}{2}\right)\sqrt{\left(\tilde{u}_{i+1/2,j}^{n+1}\right)^2+\left(v_{i+1/2,j}^n\right)^2}}{\left(\frac{h_{i+1/2,j+1/2}^{n+1}+h_{i+1/2,j-1/2}^{n+1}}{2}\right)^{4/3}}$$

where,

$$u_{i,j+1/2}^n=\frac{2M_{i,j+1/2}^n}{h_{i+1/2,j+1/2}^{n+1}-h_{i-1/2,j+1/2}^{n+1}},\quad v_{i+1/2,j}^n=\frac{2N_{i+1/2,j}^n}{h_{i+1/2,j+1/2}^{n+1}-h_{i+1/2,j-1/2}^{n+1}}$$

$$\tilde{u}_{i+1/2,j}^n=\frac{u_{i,j+1/2}^n+u_{i+1,j+1/2}^n+u_{i,j-1/2}^n+u_{i+1,j-1/2}^n}{4}$$

$$\tilde{v}_{i,j+1/2}^n=\frac{v_{i+1/2,j}^n+v_{i-1/2,j}^n+v_{i+1/2,j+1}^n+v_{i,j+1}^n}{4}$$

$$u_{i+1/2,j+1/2}^n=\frac{u_{i,j+1/2}^n+u_{i+1,j+1/2}^n}{2},\quad u_{i-1/2,j-1/2}^n=\frac{u_{i-1,j+1/2}^n+u_{i,j+1/2}^n}{2}$$

$$v_{i,j+1}^n=\frac{v_{i+1/2,j+1}^n+v_{i-1/2,j+1}^n}{2},\quad v_{i,j}^n=\frac{v_{i+1/2,j}^n+v_{i-1/2,j}^n}{2}$$

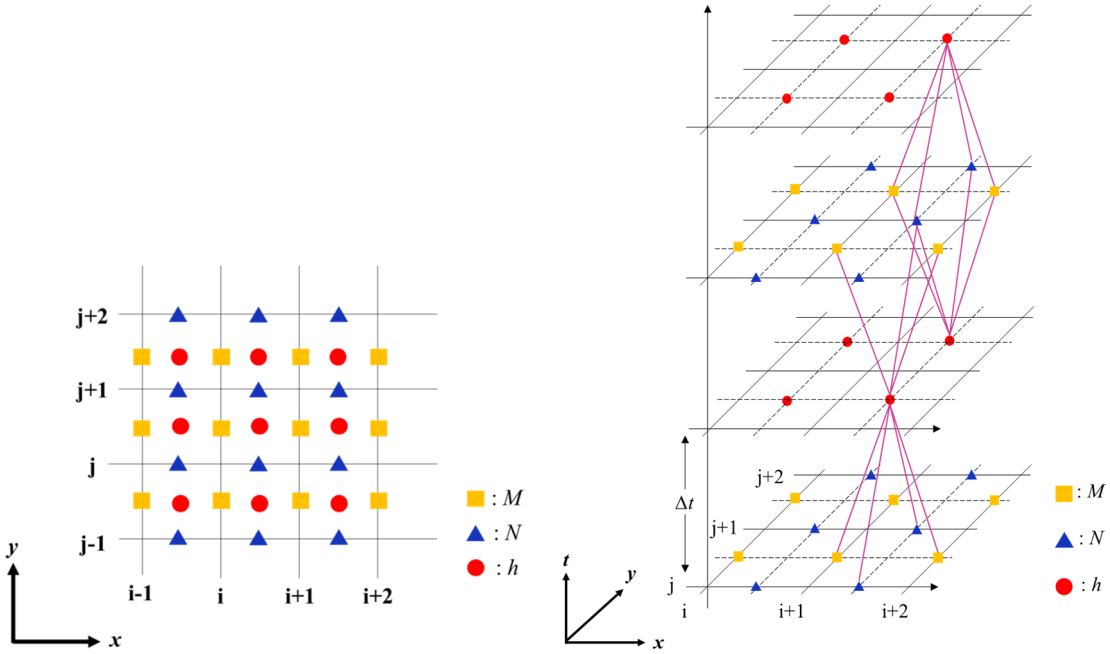

(a) Unknown quantity on grid (b) Calculation process of leap-frog method

Figure 2.11 Variable arrangement and numerical calculation process

$$u_{i+1,j}^{n} = \frac{u_{i+1,j+1/2}^{n} + u_{i+1,j-1/2}^{n}}{2}, \quad u_{i,j}^{n} = \frac{u_{i,j+1/2}^{n} + u_{i,j-1/2}^{n}}{2}$$

$$v_{i+1/2,j+1/2}^{n} = \frac{v_{i+1/2,j}^{n} + v_{i+1/2,j+1}^{n}}{2}, \quad v_{i+1/2,-1/2\,j}^{n} = \frac{v_{i+1/2,j}^{n} + v_{i+1/2,j-1/2}^{n}}{2}$$

2.7.3 Two-dimensional lower-layer flow model

Equation (2.7), (2.8) and equation (2.9), which are used in the 2D upper layer flow model, are also used for the 2D lower layer flow model. Inlet discharge q_{low} is used as input data for the lower layer. Equation (2.13) shows the continuity equation used for 2D lower-layer flow model.

$$\frac{\partial h}{\partial t} + \frac{\partial M}{\partial x} + \frac{\partial N}{\partial y} = q_{low} \tag{2.13}$$

Computational meshes are also a rectangular shape (x=10cm, y=10cm) and FDM is adopted.

2.7.4 Treatment of the cutting-edge of the water

If the water is not continuous, the ground surface flow is calculated as shown in Figure 2.12

and the equations (2.14), (2.15) are used to calculate and treat the flux instead of the governing equation.

Complete overflow case

The water depth, which is the water elevation of the lower grid minus the ground elevation of the higher grid is used to calculate the flux *M* between the adjoining two grids using equation (2.14).

$$M = \mu_1 h_l \sqrt{2gh_l} \tag{2.14}$$

where M is the flux, h_l $(= H_l - z_l)$ is the water depth, H_l is water elevation on lower grid, z_l is ground elevation of higher grid, μ_1 is discharge coefficient taken as 0.35 in this study.

Waterfall case

If the water depth of the lower grid does not reach the higher grid elevation between the adjoining two grids, the water depth of the higher grid is used to calculate the flux using equation (2.15).

$$M = \mu_2 h_h \sqrt{gh_h} \tag{2.15}$$

where M is the flux, , h_h is the water depth on the higher grid, and μ_2 is the discharge coefficient (0.544 in this study). Water depth lower than 0.001m is ignored.

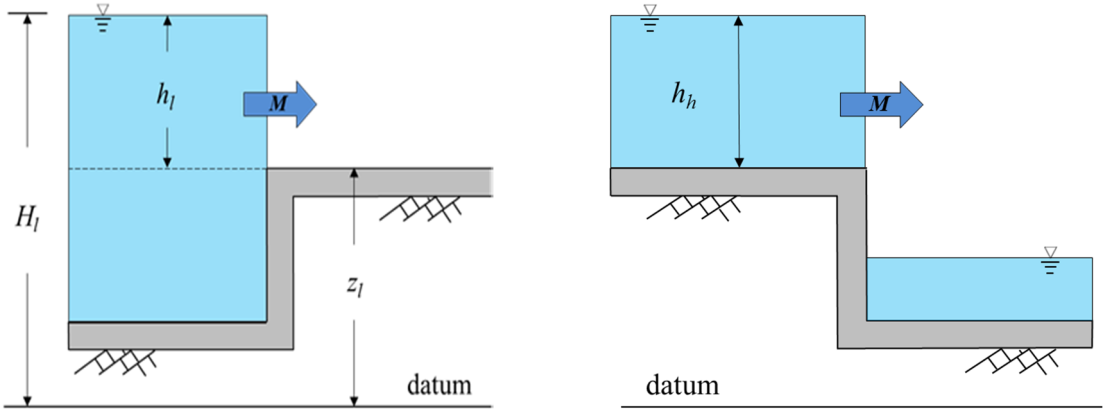

(a) anadromous case (overflow flow) (b) waterfall case

Figure 2.12 Treatment of cutting-edge on surface

2.7.5 Boundary conditions

It is necessary to define two kinds of boundary conditions, namely, upstream and downstream boundaries should be given to fully apply the model. In this study, input discharge of each case is used to set upstream boundary conditions, and Equation (2.15) is used to treat the downstream ends of both the upper layer and the lower layer as downstream boundary conditions. In order to apply Equation (2.15) as an outlet boundary condition, one grid is extended, and then the water depth of the last grid is set as zero.

Table 2.3 Modified discharge coefficient

	Taken from experiments	Modified
C_{dw}	0.378	0.48
C_{do}	0.510	0.57

2.7.6 Inlet discharge from ground surface to lower-layer

Storm water on the ground surface computational mesh with the storm drain is drained into the lower layer. That drained discharge is estimated by Equation (2.16) and Equation (2.17). The important point here is that the water depth h is used instead of total water head H_t for the simulation, because it is very difficult to measure the velocity head on the storm drain due to interference around it. Additionally, in the experiment the H_t of the strategic point (2) is assumed equal to H_t on the storm drain, considering negligible energy loss between the two points. Besides, the use of the water depth h helps the simulation model avoid numerical instability. Therefore, all experimental analysis uses total head but the total head is assumed to be the water depth in the simulation. The discharge coefficients of weir and orifice are taken as obtained from the experiment results and the storm water is assumed to be immediately drain into the lower layer. The drainage discharge is estimated using the following formula.

In the case of $h/b_0 \leq 0.5$ (Non-submerged case)

$$q_{low} = \frac{2}{3} C_{dw} L \sqrt{2g} (h)^{2/3} \tag{2.16}$$

In the case of $h/b_0 > 0.5$ (Submerged case)

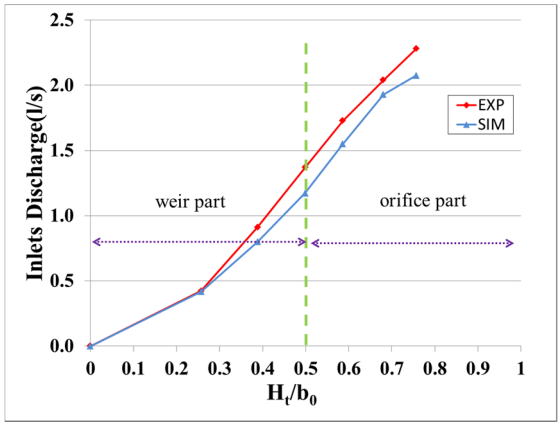

(a) Comparison result of square cases

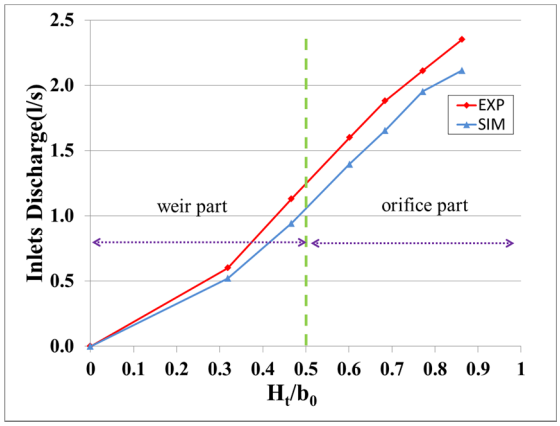

(b) Comparison result of grid cases

Figure 2.13 Comparison of experiments and simulation data using original coefficient

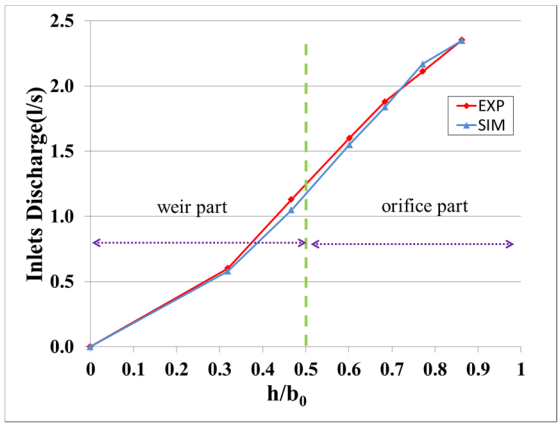

(a) Modified simulation result of square cases

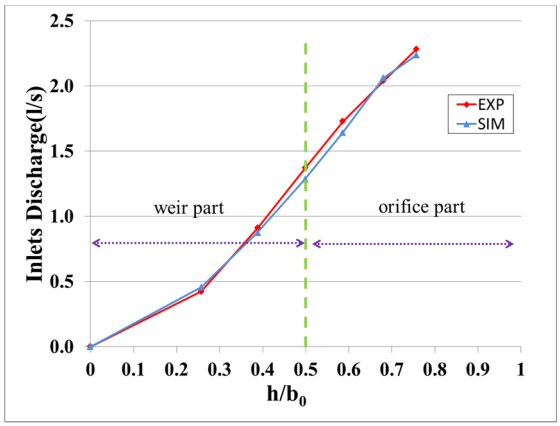

(b) Modified simulation result of grid cases

Figure 2.14 Comparison of experiments and simulation data using modified coefficient

$$q_{low} = C_{do} A \sqrt{2gh} \tag{2.17}$$

where h is the water depth on the storm drain mesh.

2.7.7 Model verification

Figure 2.13 presents a comparison of the experimental and simulated results of inlet discharge through the storm drain using original coefficients obtained from experiments in the weir and orifice formulas. However, the simulated results are approximately 1.5~14% less than the experimental results because water depths were used instead of total head in the simulation. Since the total head is always higher than the water head, it could be concluded that each coefficient was calculated as slightly less than the experimental results. Hence, a trial and error

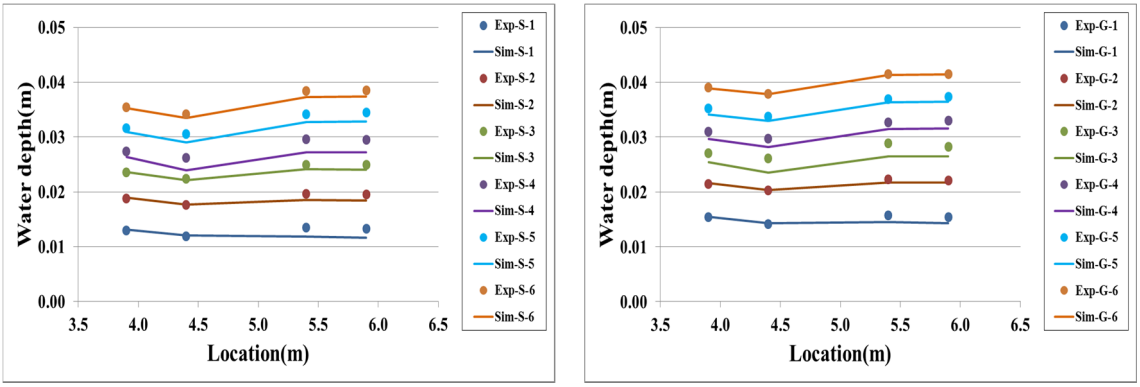

(a) Square cases (b) Grid cases

Figure 2.15 Comparison of water depth

method was applied in order to revise suitable coefficients and then suitable values were determined. Table 2.3 shows these values, which were determined by a trial and error method. The weir coefficient changed from 0.378 to 0.48 and the orifice coefficient changed from 0.51 to 0.57. Figure 2.14 (a) and (b) show corrected simulation results of the square case and grid case, respectively.

These simulated results, using modified discharge coefficients, show good agreement with the experimental results. The experimental and simulation results were compared. Figure 2.15 illustrates the water depth in the 4 locations mentioned in Section 2 obtained by the laboratory measurements and from the numerical model. Changed coefficients are used in this simulation.

It can be observed that for the center line water depth, at the upstream and downstream of the storm drain, the differences are less than 1mm.

An interesting factor to note here is that there is no significant difference between the square type and grid type coefficients. Generally, different shapes have different coefficients when discharge is calculated by the weir or the orifice formula. The reason why they have the same value of the coefficients may be due to the fact that the grid space is too wide to represent its shape property.

From those results, in steady state cases, the interaction model and the corrected discharge coefficients were used to calculate modified inlet discharges, which were then used to reproduce water surface profile and the profiles of water depth are then validated with the experimental results.

2.8 Summary

In this chapter, in order to determine the storm water interaction and new discharge coefficient, which was based on the real experiment between the ground surface and lower layer, experiments were carried out and compared with simulation results using the square and grid type storm drain cover under the steady flow condition. The relation, which was suggested by Chanson et al. (2002), was applied and validated to determine each weir and orifice coefficient for the submerged and non-submerged cases. The weir discharge coefficient, which was obtained through experiment data, was initially 0.381, and orifice coefficient was 0.51. Although that relation, which was suggested by Chanson et al. (2002), showed acceptable trends, the simulated results were approximately 1.5 ~ 14% less than the experimental results when the original coefficients obtained from the experiments were used. Therefore, each coefficient was modified by a trial and error method considering velocity heads. The final discharge coefficients were decided as C_{dw} = 0.48 and C_{do}= 0.57. The inlet discharges and the profiles of water depth using modified coefficients show good agreement with experimental results. The reason each coefficient was different is based on the fact that the water depth was used instead of total head in the simulation.

The flow pattern can be categorized by the relations between smaller width of storm drain (b_0) and water depth (h) according to the change in water depth.

Generally, different shapes should have different coefficients when discharge is calculated by Equation (2.1) or the Equation (2.3). However an interesting fact observed here is that the same values for the coefficient of discharge for square and grid type covers were obtained. The reason why they have same values is due to the fact that each grid space is too wide to represent its shape property.

Therefore, in the next study, it will be necessary to apply these coefficients and determine not only inlet discharge, but also overflow discharge from sewer systems for a more accurate urban inundation simulation.

CHAPTER 3

INTERATION EFFECT OF STORM WATER BETWEEN MANHOLE AND PIPES

3.1 Introduction

Rapid urbanization has caused various social problems. With increasing urbanization, drainage, and water quality requirements, sanitary sewer and storm water systems have been drastically complicating. The hydraulic characteristic of a drainage system often reveals many complex phenomena, such as back water effects from outlet boundary or hydraulic structures, confluence interactions at manholes, and interchanges between pressurized pressure flow and free surface flow conditions. Additionally, it may cause serious problems, such as inundation caused by a lack of sewer pipe capacity, blown-off manhole covers, and sewer pipe rupture and soil erosion (Zhao et al., 2006). Normally, sewer systems are designed to carry free-surface flow

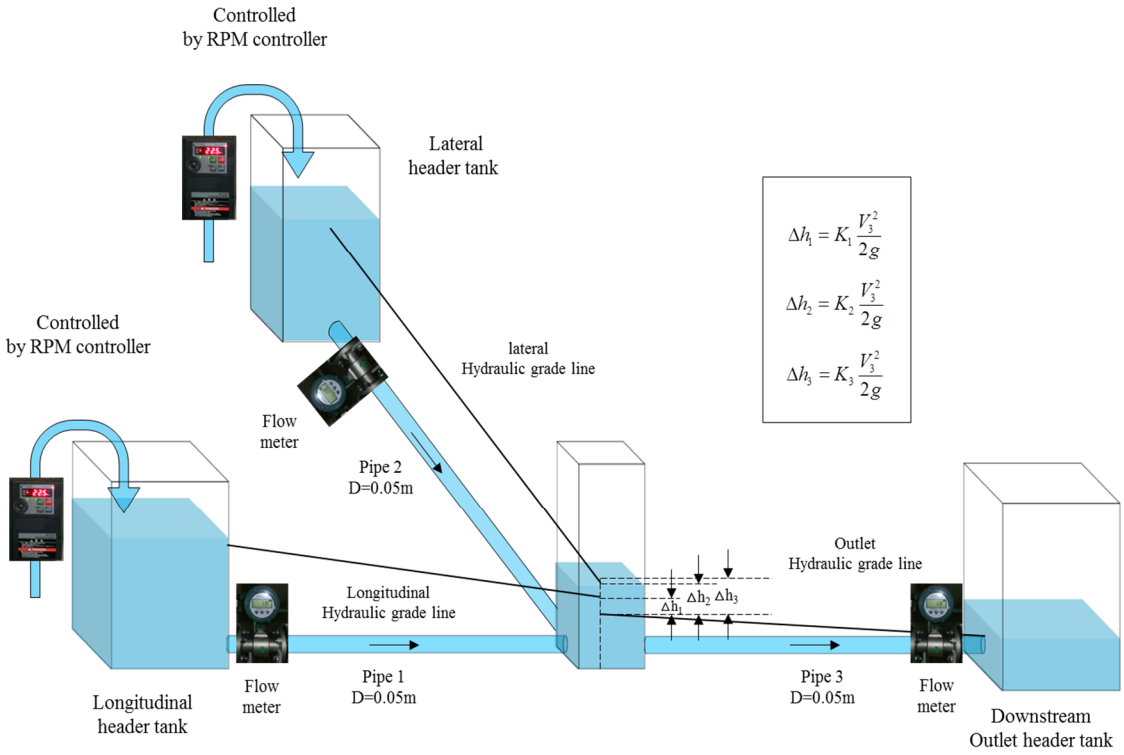

Figure 3.1 Plan view of experimental setup

where the energy losses are neglected for simplicity. The friction head losses are major losses in pipes, and they can be predicted with relative accuracy using the Darcy-Weisbach equation (Johnston et al., 1990). However, the minor losses caused by junctions, sewer inlets, house connections, and other appurtenances in many pressurized sewer systems exceed the friction losses and reduce system capacity significantly (Marsalek, 1984). Recently, pressurized flow is occurring more frequently in sewer systems due to the growth of urbanization, increased impermeable layers, complex sewer pipe configurations and increased rainfall frequency due to climate change. Although the hydraulic characteristics of sewer flow in a single pipe are understood reasonably well, limited research has been carried out on sewer junctions depending on pipe configurations or adjoining angles.

The determination of pressure changes across the junction box requires ascertaining the vertical distance between the inlet and outlet hydraulic grade lines (HGLs) at the manhole, as shown in Figure 3.1. Sangster et al. (1958) define the longitudinal and lateral loss coefficients to be

$$K_1 = \frac{\Delta h_1}{V_3^2/2g} \tag{3.1}$$

$$K_2 = \frac{\Delta h_2}{V_3^2/2g} \tag{3.2}$$

$$K_w = \frac{\Delta h_3}{V_3^2/2g} \tag{3.3}$$

where K_1 is the longitudinal head loss coefficient, K_2 is the lateral head loss coefficient, K_w is the free surface head loss coefficient, Δh_1 is a pressure head change in the longitudinal pipe, Δh_2 is a pressure head change in the lateral pipe, Δh_w is the distance between the water surface and the downstream HGL intersection point at the branch point in the manhole, g is the acceleration due to gravity, and V_3 is a mean velocity in the outlet pipe. They suggested empirical relationships to decide the head loss coefficients. After that, many similar studies were carried out to improve and modify a measurement technique according to various circumstances near the manholes.

Marsalek (1984) measured the effect of different types of manhole benching as well as the manhole head losses for a system with a 90° bend or a "T" junction. A submerged jet theory for the flow in straight through manholes was presented by Pedersen and Mark (1990) to determine the head losses in manholes. Wang et al. (1998) conducted laboratory experiments to determine the head loss coefficients with regard to various pipe configurations and flow rates. Merlein (2000) developed the mathematical model using the Predictor-Corrector method, which could

calculate water depth change under unsteady conditions; however, that model can calculate only the water depth of manhole, as it was assumed that manholes hydraulically behave like surge tanks. Supercritical flow at a sewer junction in a 45° junction manhole was studied by Del Giudice and Hager (2001), and a 90° junction was investigated by Gisonni and Hager (2002). Zhao et al. (2004) carried out a model study for a 25.8° combining junction with two inflows and one outflow. Zhao et al. (2006) conducted experiments to improve understanding on flow regimes in sewer junctions.

Head losses at sewer junctions are affected by flow rate, junction geometry, adjoining angles and the change in pipe diameter between the inflow and outflow lines. To better understand these complicated hydraulic features and accurately simulate flows in a complicated sewer system, an unsteady flow model based on the solution of the full hydrodynamic equations is needed to consider the head loss phenomena.

Therefore, in this chapter, fundamental laboratory experiments to estimate the head losses are carried out under the various circumstances with no benching and no invert. First of all, straight cases are conducted in order to evaluate the head losses depending on manhole shape between circular and square type, and then T-shape case experiments are conducted using similar manhole shapes, as previous and different adjoining angles confirm the effect under unsteady conditions as well as steady conditions. Finally, the numerical simulation model is developed and tested to confirm applicability based on the experimental data from laboratory experiments.

3.2 Description of Experimental Setup

The experiments were carried out in a flume located at the Ujigawa Open Laboratory (UOL) of the Disaster Prevention Research Institute (DPRI), Kyoto University, Kyoto, Japan. Figure 3.1 and 3.2 show a schematic and photo of the experimental facility. The experimental setup is designed to estimate head losses between manhole and pipes regarding different manhole shapes and pipe configurations. There are two upstream input discharge tanks of 0.3m×0.5m×1.0m and one downstream water tank of 0.3m×0.5m×1.5m with a movable gate to adjust the downstream water level. Each tank is connected to a manhole by the transparent acrylic pipes of 4m long and 0.05m diameter with zero slope. Three flow meters were installed, in which the two meters are just in front of the longitudinal and lateral header tank, and the third one is just before the downstream outlet header tank, as shown in Figure 3.1. The input discharge can be supplied to each upstream tank through the independent circulation pumps, respectively. Each pump can be accurately controlled by the RPM controller. A total of eight piezometer tubes are

used to read the water head at the bottom of the pipe. Out of that, four of them were set at intervals of 1.0m, and the rest four are set at intervals of 0.1m to read a water head carefully near the manhole, as shown in Figure 3.3. Figure 3.4 and Figure 3.5 show the manhole shapes and pipe configurations. There are six kinds of manhole configurations, and they can be divided into two classes. At first, they can be categorized according to the manhole shapes (circular and square) and then classified according to number of pipes, such as two pipe manholes (Figure 3.5 (a) and (b)) and three pipe manhole case (Figure 3.5 (c) ~ (f)). The three pipe manhole cases consist of four types of configurations. The square-shaped manhole (0.15m×0.15m×1.0m), circular-type manhole (Diameter = 0.15m, 1.0m height), and downstream tank are made from a transparent acrylic sheet. The manhole part can be separated to replace the different manhole shapes or pipe configurations by moving or disconnecting the lateral pipe 2, as shown in Figure 3.1. This experiment setup was built with the consideration of space and working time efficiency. Figure 3.8 shows the level meter, which is used to adjust pipe slope, and it was readjusted after replacing different manhole shapes.

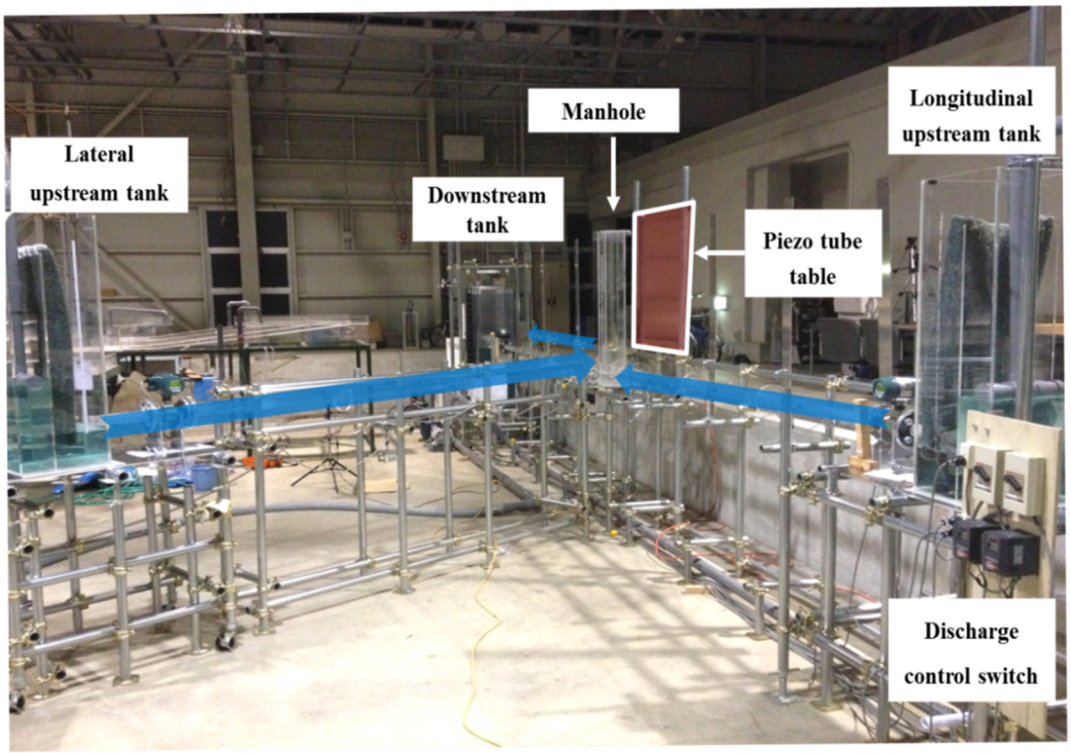

Figure 3.2 Photo of experimental setup

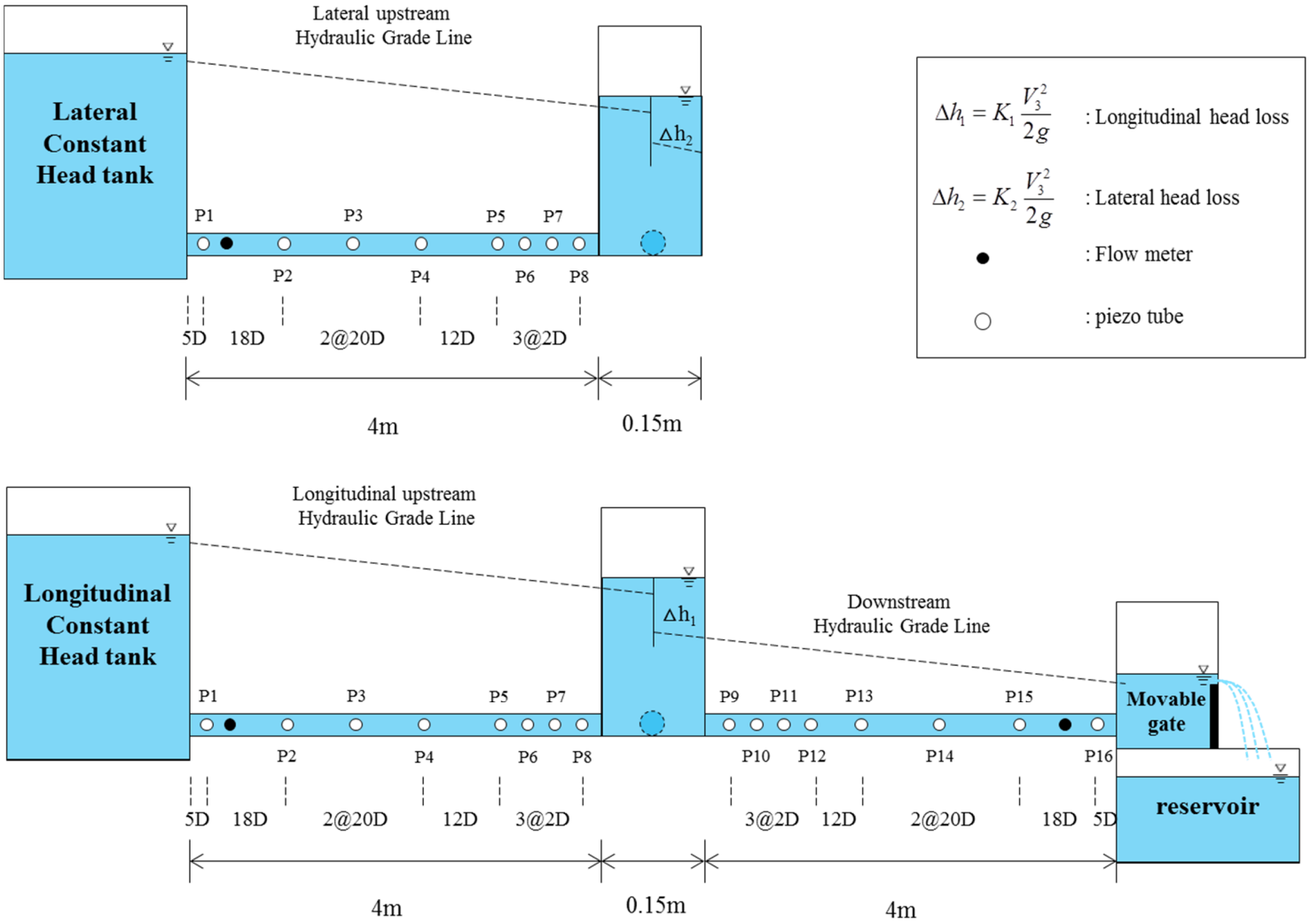

Figure 3.3 Side view of experimental setup

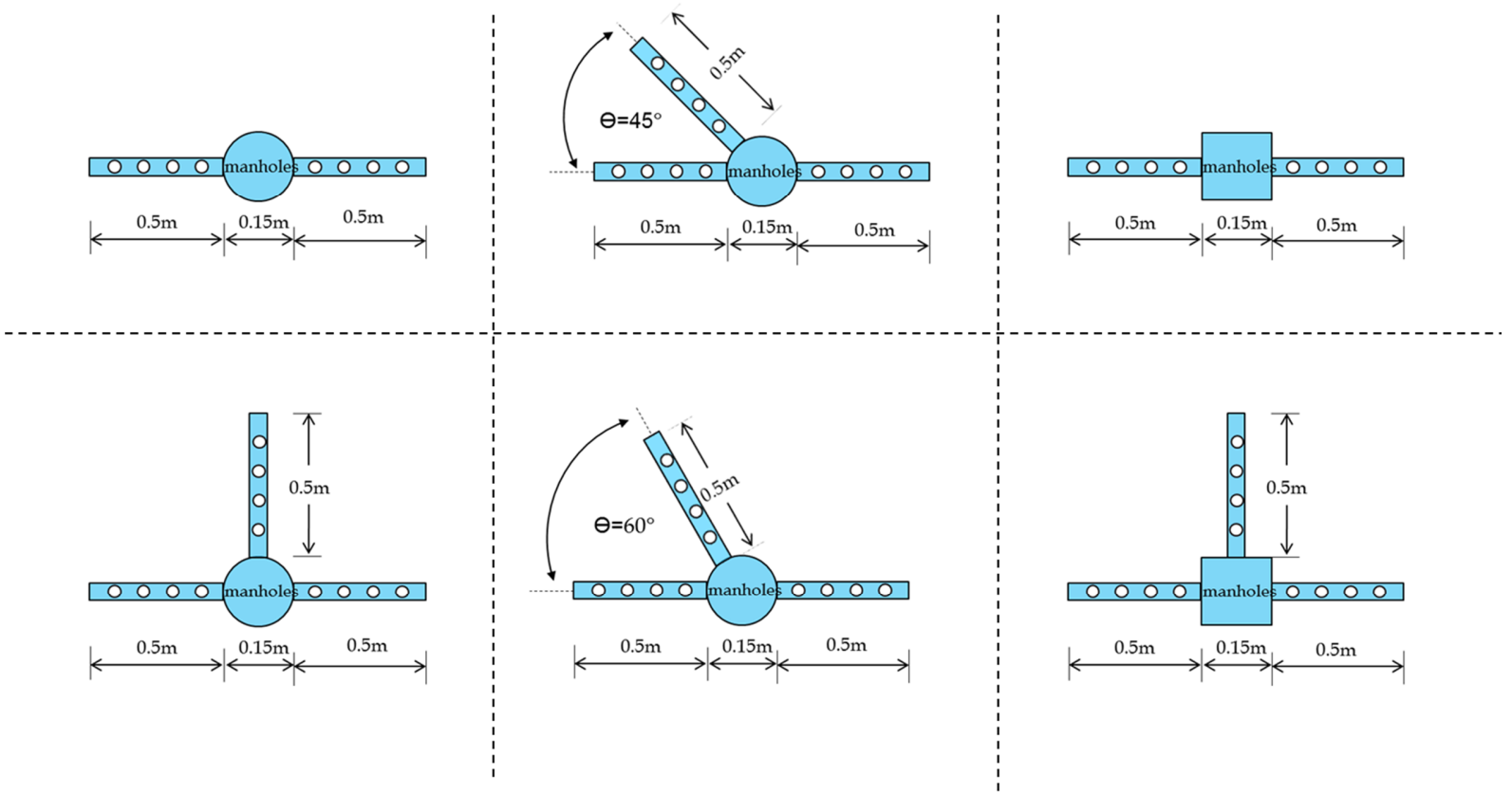

Figure 3.4 Each manhole shapes and pipe configuration

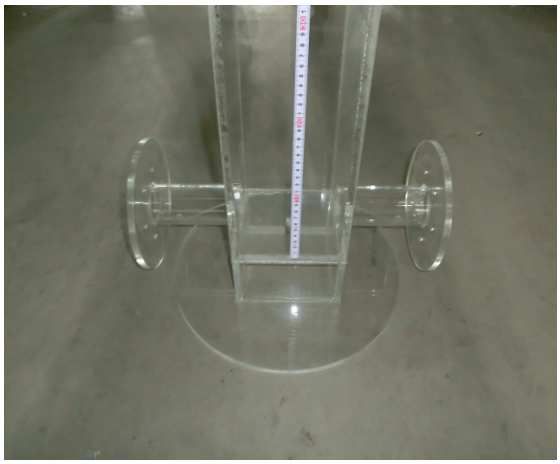

(a) Square shape manhole with 2 pipes

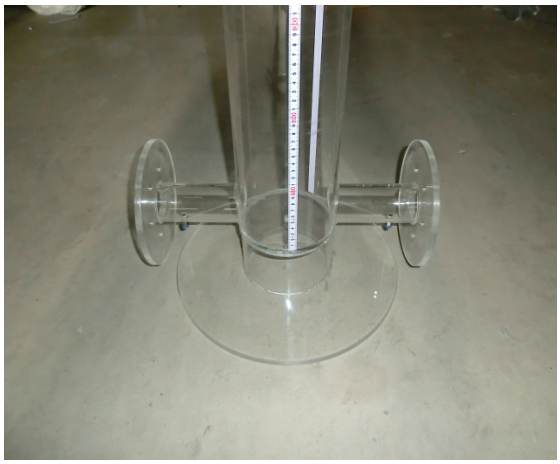

(b) Circular shape manhole with 2 pipes

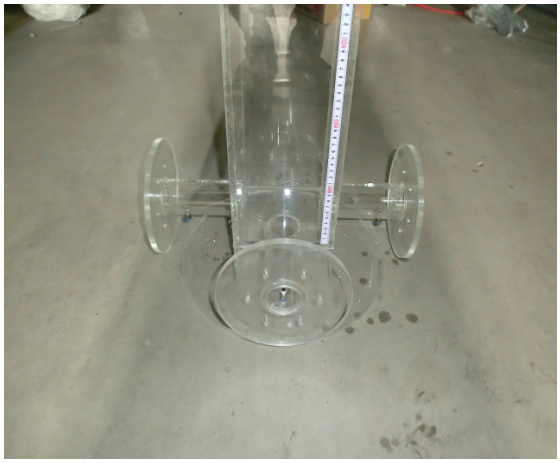

(c) Square shape manhole with 3 pipe (90°)

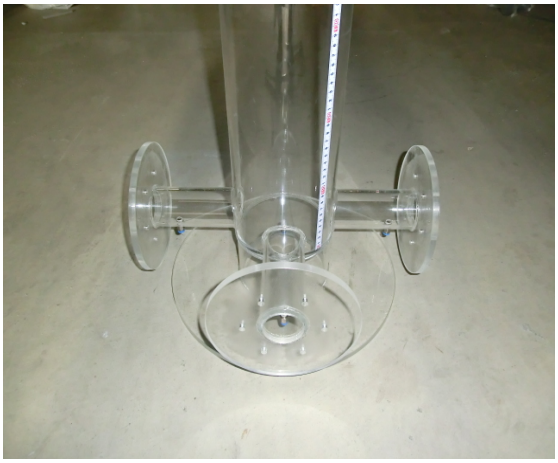

(d) Circular shape manhole with 3 pipe (90°)

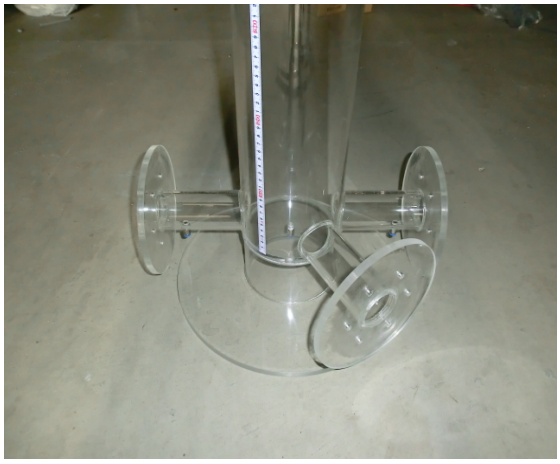

(e) Circular shape manhole with 3 pipe (60°)

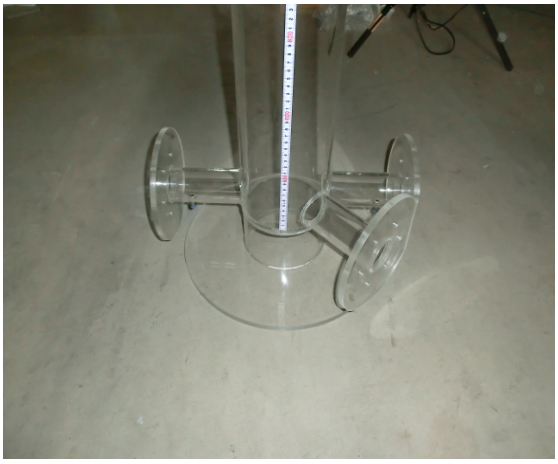

(f) Circular shape manhole with 3 pipe (45°)

Figure 3.5 Photo of each manhole shape

3.3 Experimental Conditions

3.3.1 Two pipes case

In total, 18 cases experiments are carried out to estimate head losses at the manhole using circular- and square-type manholes with no benching and no invert under the steady state condition. Each circular and square case has nine cases, and the experimental case starts from an approximate 3.0*l/s* inflow discharge at the upstream with the fixed downstream water level at the downstream tank, and the input discharge is gradually decreased by approximately 0.3*l/s* per case, respectively. The selected hydraulic conditions and detail hydraulic parameters are summarized in Table 3.1. The elevation of the bottom of the pipe can be used as a datum to measure the water level since there is no slope.

After execution of the experiments under the steady state condition, unsteady condition experiments are carried out in order to estimate the applicability of obtained manhole head loss coefficients. Unsteady experiments can be conducted by changing the water level of the downstream tank. At first, the downstream water level is maintained with a movable gate at

Table 3.1 Steady cases of 2 pipes

Number	Upstream discharge(*l/s*)	Mean Velocity(*m/s*)	Froude Number	Downstream water level(*m*)
C-S*-1	3.03	1.54	2.20	0.026
C-S-2	2.71	1.38	1.97	0.026
C-S-3	2.42	1.23	1.76	0.026
C-S-4	2.11	1.07	1.53	0.028
C-S-5	1.80	0.92	1.31	0.028
C-S-6	1.51	0.77	1.10	0.026
C-S-7	1.29	0.66	0.94	0.024
C-S-8	0.91	0.46	0.66	0.019
C-S-9	0.87	0.29	0.41	0.013
S-S*-1	3.04	1.55	2.21	0.026
S-S-2	2.66	1.35	1.93	0.025
S-S-3	2.40	1.22	1.74	0.026
S-S-4	2.06	1.05	1.50	0.027
S-S-5	1.85	0.94	1.34	0.026
S-S-6	1.52	0.77	1.10	0.039
S-S-7	1.18	0.6	0.86	0.022
S-S-8	0.92	0.47	0.67	0.028
S-S-9	0.49	0.25	0.36	0.010

*C-S – Circular type - Steady condition, *S-S - Square type - Steady condition

Table 3.2 Unsteady cases of 2 pipes

Number	Upstream discharge (*l/s*)	Downstream water level (*m*)
C-U*	2.13	0.06→0.50→0.05
S-U*	2.13	0.06→0.50→0.05

*C-U – Circular type - Unsteady condition, *S-U – Square type – Unsteady condition

downstream, and the water level is increased to reach an elevation of 0.5*m* and then decreased to 0.06*m* with a constantly changing velocity of the downstream water level. The same hydraulic conditions are used in both cases of the circular and square manholes, and more detailed information of the unsteady condition experiments has been summarized in Table 3.2.

3.3.2 Three pipes case

Firstly, three pipes cases can be simply categorized in four items: the Square-90°, Circle-90°, Circle-60°, and Circle-45° under steady conditions. Secondly, three pipes cases also can be divided according to the manhole shape as circular and square cases in 90° cases. Both 90° cases are used to compare the effects of the manhole shapes. All of the circular cases are used to confirm the effect of pipe configurations, according to the changes in input discharge ratios (longitudinal / lateral flow).

For each set of experiments, initially, the longitudinal discharge is set as 3.0 *l/s* with a lateral input discharge of zero, and then the lateral input discharge is increased by 0.3 *l/s* until the

Table 3.3 Steady study cases of three pipes (Circle-90°)

Number	Discharge(*l*/s) (Longitudinal)	Discharge(*l*/s) (Lateral)	Mean Velocity (*m*/s)	Froude Number	Downstream water level(*m*)
C-S-90°-1	3.04	0.00	1.55	2.21	0.023
C-S-90°-2	2.68	0.34	1.54	2.20	0.023
C-S-90°-3	2.44	0.63	1.56	2.23	0.023
C-S-90°-4	2.11	0.91	1.54	2.20	0.023
C-S-90°-5	1.82	1.23	1.55	2.22	0.023
C-S-90°-6	1.53	1.54	1.56	2.23	0.023
C-S-90°-7	1.22	1.84	1.56	2.23	0.023
C-S-90°-8	0.87	2.10	1.51	2.16	0.023
C-S-90°-9	0.62	2.44	1.56	2.23	0.023
C-S-90°-10	0.33	2.67	1.53	2.18	0.023
C-S-90°-11	0.00	2.97	1.51	2.16	0.023

Table 3.4 Steady study cases of three pipes (Square-90°)

Number	Discharge(*l/s*) (Longitudinal)	Discharge(*l/s*) (Lateral)	Mean Velocity (*m/s*)	Froude Number	Downstream water level(*m*)
S-S-90°-1	3.06	0.00	1.56	2.23	0.026
S-S-90°-2	2.69	0.31	1.53	2.18	0.026
S-S-90°-3	2.42	0.62	1.55	2.21	0.026
S-S-90°-4	2.09	1.02	1.58	2.26	0.026
S-S-90°-5	1.75	1.24	1.52	2.18	0.026
S-S-90°-6	1.55	1.57	1.59	2.27	0.026
S-S-90°-7	1.19	1.83	1.54	2.20	0.026
S-S-90°-8	0.90	2.15	1.55	2.22	0.026
S-S-90°-9	0.58	2.41	1.52	2.18	0.026
S-S-90°-10	0.39	2.71	1.58	2.26	0.026
S-S-90°-11	0.00	3.01	1.53	2.19	0.026

Table 3.5 Steady study cases of three pipes (Circle-60°)

Number	Discharge(*l/s*) (Longitudinal)	Discharge(*l/s*) (Lateral)	Mean Velocity (*m/s*)	Froude Number	Downstream water level(*m*)
C-S-60°-1	3.03	0.00	1.54	2.20	0.026
C-S-60°-2	2.70	0.40	1.58	2.26	0.026
C-S-60°-3	2.43	0.63	1.56	2.23	0.026
C-S-60°-4	2.10	0.90	1.53	2.18	0.026
C-S-60°-5	1.84	1.20	1.55	2.21	0.026
C-S-60°-6	1.51	1.48	1.52	2.18	0.026
C-S-60°-7	1.23	1.87	1.58	2.26	0.026
C-S-60°-8	0.88	2.14	1.54	2.20	0.026
C-S-60°-9	0.61	2.41	1.54	2.20	0.026
C-S-60°-10	0.34	2.72	1.56	2.23	0.026
C-S-60°-11	0.00	3.05	1.55	2.22	0.026

longitudinal input discharge becomes zero. This means that the total discharge always remains constant as 3 *l/s*. The detailed steady experimental conditions are summarized from Table 3.3 to Table 3.6.

Table 3.6 Steady study cases of three pipes (Circle-45°)

Number	Discharge(*l/s*) (Longitudinal)	Discharge(*l/s*) (Lateral)	Mean Velocity (*m/s*)	Froude Number	Downstream water level(*m*)
C-S-45°-1	3.01	0.00	1.53	4.80	0.067
C-S-45°-2	2.67	0.42	1.57	5.05	0.067
C-S-45°-3	2.43	0.63	1.56	4.96	0.067
C-S-45°-4	2.12	0.91	1.54	4.86	0.067
C-S-45°-5	1.82	1.23	1.55	4.92	0.067
C-S-45°-6	1.51	1.53	1.55	4.89	0.067
C-S-45°-7	1.20	1.83	1.54	4.86	0.067
C-S-45°-8	0.90	2.10	1.53	4.76	0.067
C-S-45°-9	0.64	2.39	1.54	4.56	0.067
C-S-45°-10	0.40	2.71	1.58	5.12	0.067
C-S-45°-11	0.00	3.01	1.53	4.80	0.067

Table 3.7 Unsteady study cases of three pipes

Number	P1 input Discharge(*l/s*)	P2 input Discharge(*l/s*)	Downstream water level(*m*)
S-U-90°	1.0	1.0	0.103→0.400→0.096
C-U-90°	1.0	1.0	0.105→0.408→0.107
C-U-60°	1.0	1.0	0.100→0.400→0.099
C-U-45°	1.0	1.0	0.092→0.400→0.097

Finally, four cases of unsteady experiments are carried out to obtain the validation data for the numerical analysis model and to test the applicability of the obtained head loss coefficients from the former experiments. Both input discharges are maintained as 1.0*l/s*, and the downstream water levels are controlled by the downstream movable gate, as shown in Table 3.7.

3.4 Major Apparatus for Experiments

Several pieces of equipment were used to conduct the experiments, such as Magnetic Flowmeters to measure the inflow and outflow discharge, the RPM controller to control the inflow discharge, and a Level meter to set the pipe slope. In addition, seven video cameras are used to record the variation of the piezometric heads in the pipes and tanks, according to time under the unsteady-state condition.

3.4.1 Magnetic Flowmeter

To measure the inflow discharge from the upstream header tank and the outlet discharge to the downstream tank, the Magnetic Flowmeters were used as shown in Figure 3.6. The standard accuracy is 0.35% of reading.

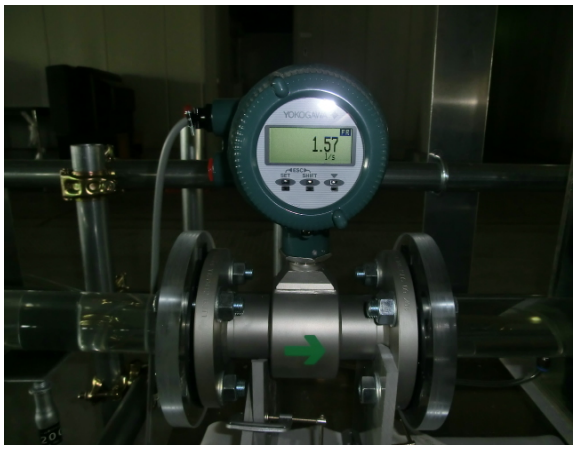

Figure 3.6 Photo of Magnetic Flowmeter

3.4.2 RPM controller

This controller (inverter) is used for controlling speeds of three-phase induction motors, in general. Upper levers mean main power switches of both upstream water tanks, and lower black boxes mean the RPM controller, as shown in Figure 3.7. The red number shows a hertz (Hz), and it can be adjusted by tripping a switch, and constant inflow discharge can be supplied to the upstream tank.

Figure 3.7 RPM controller of circulation pump

3.4.3 Level meter for measuring slope

The experimental setup is designed to exchange the manhole shapes, and the lateral pipe should move according to the pipe configuration to adjust the lateral pipe angle. Although this design concept can greatly save not only the use of space, but also the construction cost, it may cause a disturbance of the experimental facility, such as a distortion of the linearized pipe arrangement, an elevation change of the lateral part, a slope change near the manhole part, etc. Therefore, it is necessary to regularly recheck and readjust the pipe slope, as well as the adjoining angle of the lateral pipe part for every experimental case. For this process, the level meter is used with the scale bar as shown in Figure 3.8.

Figure 3.8 Photo of level meter

3.4.4 Video camera for recording piozometric head

There are 28 measuring points (24 points of piezometric head, two points of upstream tank, a downstream tank, and a manhole) in which the piezometric head and water level should be recorded. However, it is impossible to read all points at once, especially because time variation data are needed under the unsteady condition. Therefore, seven HD video cameras (HDR-CX590V) were used to measure the change of the piezometric heads in the pipes according to time variation and downstream water depth change, and experimental data were imported through the video analysis. More details on the experimental technique will be explained in the next section.

3.5 Experimental Procedure

3.5.1 Steady cases

The specified inflow discharge is supplied according to each case and waits until the flow condition becomes steady-state. The waiting time necessary is at least 30 minutes. After that, all measurement points are read with the naked eye, and the measurements are recorded. Figures 3.9 and 3.10 show a connection part between the pipe and the piezometric tube, and the piezometric tube panel where all piezometric tubes are getting together with scale bar. However, the water levels of each tank and manhole are measured by the scale bar, which is attached outside of each tank. The number of experiments that have been carried out under steady-state conditions is 62. They are composed of two pipe cases (18 cases) and three pipe cases (44 cases). All processes are repeated until every experimental case is finished, along with the already mentioned steps.

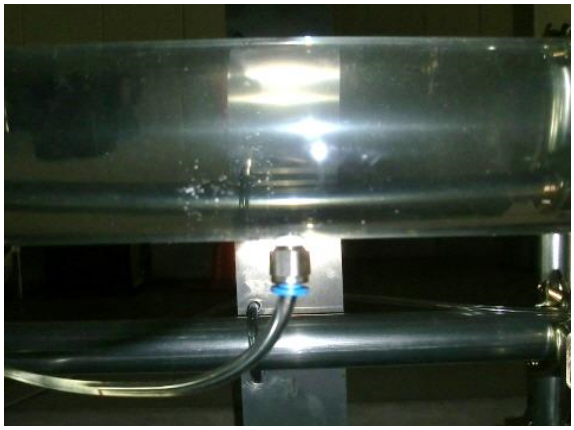

Figure 3.9 Connection part of piezometric tube

Figure 3.10 Panel of piezometric tubes

3.5.2 Unsteady cases

The experiments under the unsteady-state condition are relatively complicated in comparison with the steady-state condition. First, seven cameras are set in front of upstream tanks, manhole, downstream, and piezometric tubes panel, and then the specified discharge is supplied to the designated upstream tank with an adjustment of the downstream water level by controlling a movable gate to set an appointed level. A stopwatch is started, and then all of the video cameras are turned on in order of precedence while recording the time by the stopwatch. Finally, the downstream water level is changed by controlling the movable gate at a speed of 0.5mm/sec.

3.6 Results and Analyses

The objectives of this study are to recognize the hydraulic characteristics at the manhole depending on change of various conditions and to obtain validation data to verify the newly developed numerical simulation model. Head loss coefficients of different types are obtained depending on manhole shapes (circular and square type) and pipe configurations (square-90°, circular-90°, circular-60°, and circular-45°).

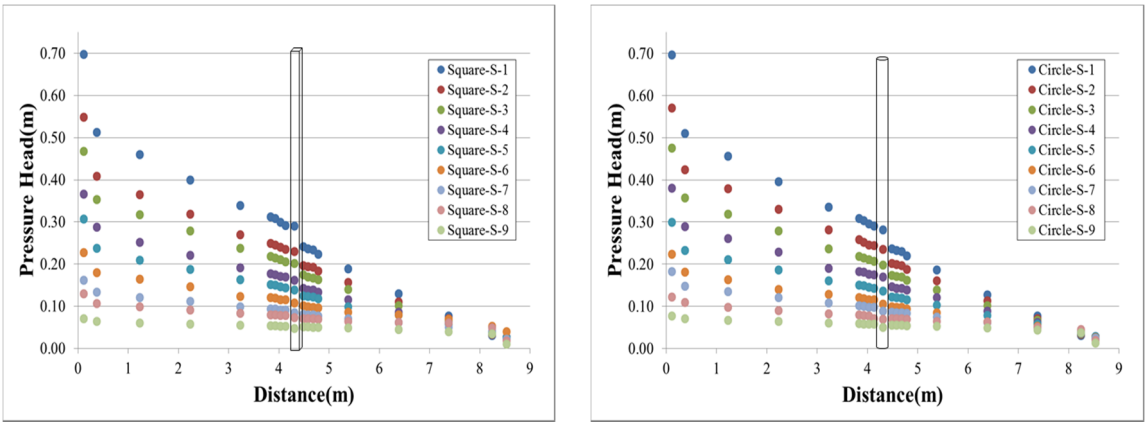

(a) Square shape manhole (b) Circular shape manhole

Figure 3.11 Pressure head change profile at manhole in 2 pipes (straight) case

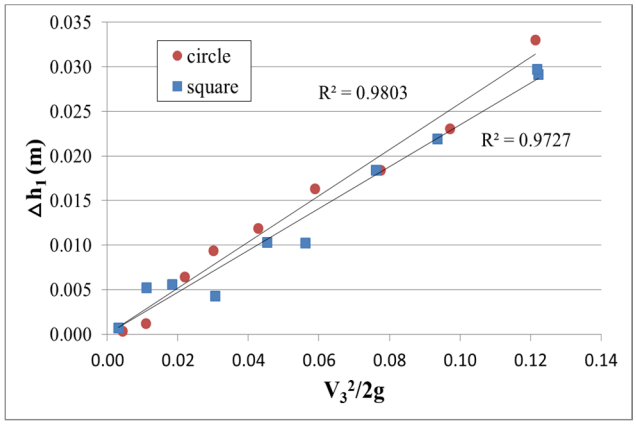

Figure 3.12 Comparison of head loss coefficients depending on manhole shape

3.6.1 Head loss coefficients in two pipes cases

Wang et al. (1998) constructed a physical model of a manhole/pipeline system for head-loss measurements and conducted laboratory experiments to determine the head losses at sewer pipe junctions (manholes) under pressurized conditions. They suggested an empirical formula, which

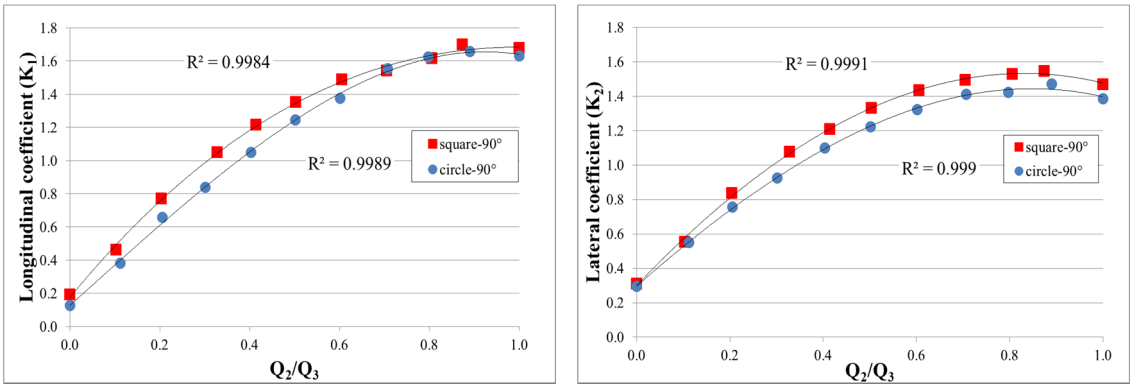

Figure 3.13 Comparison of head loss coefficients depending on manhole shape at 90° cases

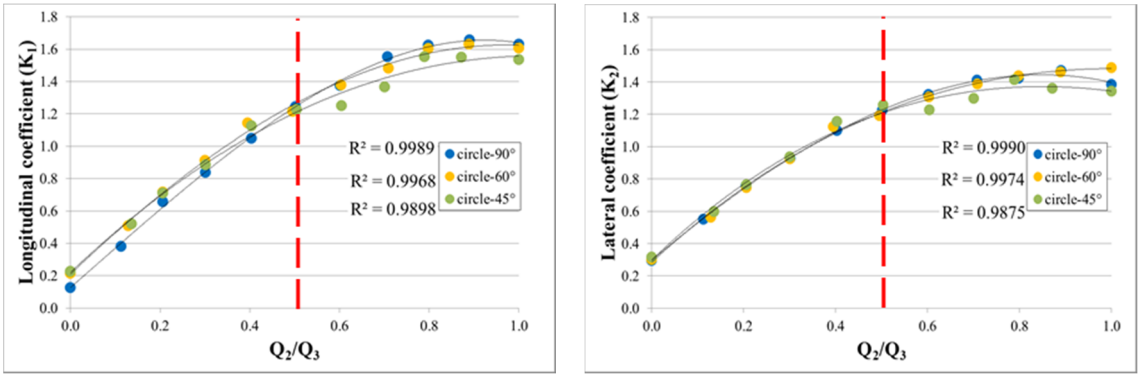

Figure 3.14 Comparison of head loss coefficients depending on adjoining angles in circular shape manhole

can estimate head-loss coefficients, and they mentioned that head loss is insensitive to the amount of pressurized discharge, but it depends heavily on the configuration of the flow, the relative flow rate, and the change of the pipe diameter.

To measure the head loss coefficients depending on different manhole shapes, the two pipes case experiments are conducted under steady-state cases using circular and square manhole shapes, and the results of the pressure head changes are shown in Figure 3.11. As appears out of these graphs, it is clear that pressure head losses occurred at the manhole, and it can be calculated by Equation (3.1). The obtained head loss coefficients are 0.259 and 0.235 for square- and circular-type manholes, respectively. Figure 3.12 shows the comparison of the relationship between velocity head and pressure head in both cases.

3.6.2 Head losses coefficients in three-pipes cases

Table 3.8 Curve fitting coefficients generated from three-pipes configuration cases

Index	Description of case studies	Head loss coefficient	A	B	C	D	R^2
1	Square-90°	K_1	0.2822	-2.0728	3.2995	0.1752	0.9984
		K_2	-0.1659	-1.5095	2.8519	0.3007	0.9991
2	Circle-90°	K_1	-1.0301	0.1108	2.4314	0.1272	0.9989
		K_2	-0.4321	-0.8652	2.3981	0.2968	0.9990
3	Circle-60°	K_1	-0.2857	-0.9484	2.6486	0.2095	0.9989
		K_2	-0.4321	-0.8652	2.981	0.2968	0.9990
4	Circle-45°	K_1	0.0483	-1.3412	2.6283	0.2205	0.9898
		K_2	0.2814	-1.9681	2.7331	0.2973	0.9875

In accordance with the convention, the results of the three-pipes studies were drawn in a graph (Figure 3.13) where the loss coefficients were plotted versus the lateral inlet to the outlet flow as a ratio of (Q_2/Q_3). From the comparison of the square shape-90° and the circular-90°, it is concluded that head loss of square shape is a little higher than the circular shape, and the difference of the longitudinal coefficients (K_1) between the square- and circular-type manholes is decreasing with increasing Q_2/Q_3 in the 90° cases, as shown in Figure 3.13. Also, the difference of the lateral coefficient (K_2) between the two shapes is increasing along with the increasing Q_2/Q_3 as opposed to the longitudinal coefficient (K_1). It means that the lateral input discharge disturbs the longitudinal flow, and it causes increasing head losses at the manhole, and the effect is stronger at the square-shaped manhole than at the circular-shaped one. Figure 3.14 shows a comparison of longitudinal and lateral head loss coefficients through all circular cases. As it is shown in the graphs, although the increasing tendency of both the longitudinal and lateral coefficients show a similar trend with almost the same value in three different adjoining angle, as they start to be divided into different patterns from $Q_2/Q_3 = 0.5$. This means that the relation, $Q_2/Q_3 = 0.5$, could be a criterion in which to define a characteristic of manhole head losses.

Johnston and Volker (1990) presented the results of a detailed experimental hydraulic model study of the hydraulic interactions in two common junction box configurations using a three-pipe and the two-pipe configuration. The experiments data of both cases were expressed by the form of Equation (3.4) using the least-squares-fitted method.

$$K_1 \text{ or } K_2 = A\left(\frac{Q_2}{Q_3}\right)^3 + B\left(\frac{Q_2}{Q_3}\right)^2 + C\left(\frac{Q_2}{Q_3}\right) + D \tag{3.4}$$

The dimensionless coefficients A, B, C and D, as well as the correlation coefficient, are listed in Table 3.8. Resultant functions of K_1 and K_2 are shown in Figures 3.13 and 3.14. This obtained data set will be used to calculate the head losses at the manhole in comparison with the experimental data, and the simulation results are presented in the next section.

3.7 Sewer Network Model with Manhole

3.7.1 Introduction

In urban inundation simulation, it is very important to comprehensively understand the behavior of storm water in the sewer networks because very complex phenomena are related with the overflow and drainage process. Generally, governing equations of open flow and fully pressurized flow in the pipes are different. Equation (3.5) and Equation (3.6) are used to explain the open flow, and Equation (3.7) and Equation (3.8) are used to analyze pressurized flow.

Open flow

$$\frac{\partial h}{\partial t} + \mathrm{v}\frac{\partial h}{\partial x} + \frac{A}{B}\frac{\partial v}{\partial x} = 0 \tag{3.5}$$

$$g\frac{\partial h}{\partial x} + \frac{\partial v}{\partial t} + v\frac{\partial v}{\partial x} = g(S_0 - S_f) \tag{3.6}$$

Fully surcharge flow

$$\frac{\partial H}{\partial t} + \mathrm{v}\frac{\partial H}{\partial x} + \frac{a^2}{g}\frac{\partial v}{\partial x} = 0 \tag{3.7}$$

$$g\frac{\partial h}{\partial x} + \frac{\partial v}{\partial t} + v\frac{\partial v}{\partial x} = g(S_0 - S_f) \tag{3.8}$$

where v is velocity in x direction, h is water depth, S_0 is slope of pipe, S_f is friction slope of the pipe, g is acceleration due to gravity, A is cross section area, B is water surface width, a is pressure propagation velocity, and H is piezometric head.

Because the flow pattern in the pipe could be an open flow or a fully pressurized flow depending on the hydraulic conditions, it is very difficult to analyze both patterns with the same governing equation and to distinguish between the two patterns. To solve these problems, Preissmann (chaudhry, 1979) developed a slot model that analyzes open flow and pressurized flow regime at once, in which both flow regimes are treated by the same governing equations.

This approach introduces hypothetically a continuous, narrow, piezometric slot attached to

the pipe crown and over the entire length of the pipe as shown in Figure 3.15. The idea is to transform the pressurized pipe flow situation into a conceptual open-channel flow situation by introducing a virtual free surface to the flow. The idea was suggested by Preissmann (Cunge and Wegner, 1964). The hypothetical open-top slot should be narrow so that it would not introduce an appreciable error in the volume of the water. On the contrary, the slot should not be too narrow, with the aim of avoiding the numerical problem associated with a rapidly moving pressure surge. A theoretical basis for determining the width of the slot is to size the width, such that the wave celerity in the slotted sewer is the same as the surge celerity of the compressible water in the actual elastic pipe.

The width (B_s) of the slot pipe is

$$B_s = \frac{gA_0}{a^2} \tag{3.9}$$

where A_0 is the pipe cross section area and a is the pressure propagation velocity. For small pipes, Equation (3.9) may give a too-small slot width, which would cause numerical oscillations. The transition between the partially pressurized flow and the fully pressurized flow is by no means computationally smooth and easy, and assumptions are necessary (Cunge and Mazadou, 1984).

Jun and Yen (1985) suggested that if each sewer in a network is divided into many

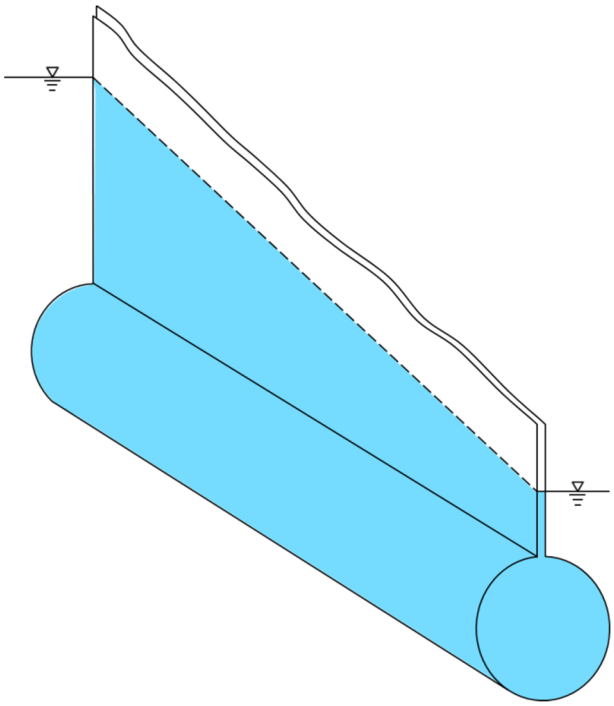

Figure 3.15 Concept of Preissmann slot model (chaudhry, 1979)

computational reaches and a significant part of the flow duration is under surcharge, the standard approach saves computational time. On the other hand, if the transition between the open-channel and pressurized conduit flows occurs frequently; the transitional stability problem is important, and the slot model would be preferred. Nevertheless, a one-dimensional (1D) Preissmann slot model is extensively accepted and used to simulate the sewer network even in the commercial models, such as the Storm Water Management Model (SWMM) and ARC info.

In addition, a pipe/channel network is a set of nodes and links in the topological sense (Djordjević et al., 2004). Although the 1D Preissmann slot model has the advantage of simulating both flow patterns (open flow and pressurized flow) without consideration of transition flow, it is very difficult to consider head losses effectively at connection parts between a manhole and pipes, or among the conjunction parts. The nodes and links concept are applied to consider the head losses effects in this research.

Therefore, a numerical model using the Preissmann slot model concept for pipes as links and the rigid column theory for the manhole a node have been developed with the momentum equation and the energy equation, in which the head losses caused by interaction disturbance between longitudinal flow and lateral flow at the manhole are considered appropriately based on analyzed head loss coefficients from the experiments.

3.7.2 Governing equation for 1D pipe flow

The Preissmann slot concept is used to analyze a one-dimensional unsteady flow in a sewer network with a manhole. The governing equations of pipe flow are as follows:

$$\frac{\partial A}{\partial t} + \frac{\partial Q}{\partial x} = q \tag{3.10}$$

$$\frac{\partial Q}{\partial t} + \frac{\partial (uQ)}{\partial x} = -gA\frac{\partial H_p}{\partial x} - gn^2\frac{|Q|Q}{R^{4/3}A} \tag{3.11}$$

where A is wetted cross section, Q is discharge, q is lateral inflow, u is flow velocity, R is hydraulic radius, H_p is piezometric head ($H_p = z_p + h$), z_p is bottom elevation of pipe, and h is water depth in pipe. The water depth h can be calculated by Equation (3.12).

$$h = \begin{cases} f(A) & : A \le A_0 \\ D + \frac{(A - A_0)}{B_s} & : A > A_0 \end{cases} \tag{3.12}$$

where f is a function that expressing a relation between the flow cross section area and water depth in the pipe, A_0 is the pipe cross section area, D is the pipe diameter and B_s is slot width. In

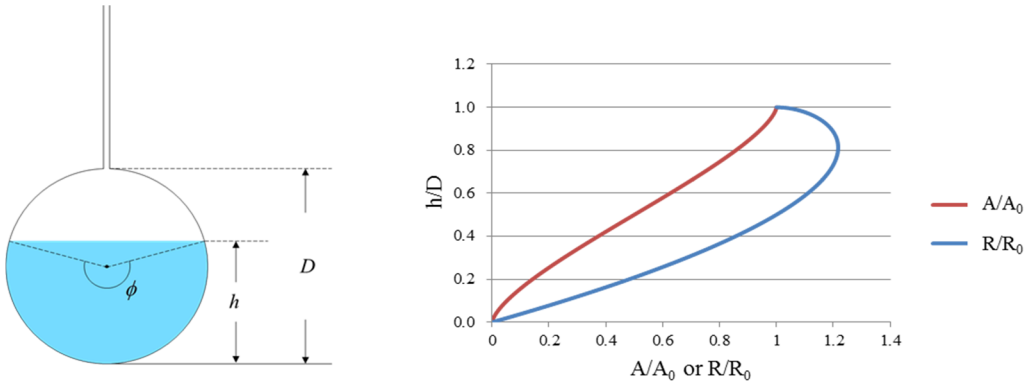

Figure 3.16 Hydraulic characteristic curves of the circular sewer pipe

this research, the shape of the pipe is circular type, and the circular type hydraulic characteristic formulas are considered, as shown in Figure 3.16. The hydraulic characteristics formulas are calculated by Equation (3.13) ~ (3.15).

$$\emptyset = 2cos^{-1}\left(1 - 2\frac{h}{d}\right) \tag{3.13}$$

$$\frac{\mathrm{A}}{\mathrm{A_0}} = \frac{\emptyset - \sin\emptyset}{2\pi} \tag{3.12}$$

$$\frac{R}{R_0} = 1 - \frac{sin\emptyset}{\emptyset} \tag{3.15}$$

Slot width B_s can be calculated by Equation (3.9) with pressure propagation velocity a.

3.7.3 Rigid column theory

Consider a simple pipeline from an open reservoir discharging into the atmosphere through a valve as shown in Figure 3.17. Friction is neglected, so that all points along the pipe are at a head H. The valve is now shut, with the result that after time Δt the velocity in the pipe has been reduced by Δu, and the head at the valve has risen by ΔH. The total force accelerating the flow is $-\rho g A \Delta H$, and the acceleration of the flow is $-du/dt$. According to Newton's second law, Equation (3.17) is obtained through Equation (3.16).

$$-\rho g A_p \Delta H = -\frac{dv}{dt}\rho A_p L \tag{3.16}$$

$$\frac{dv}{dt} = \frac{g}{l}\Delta H \tag{3.17}$$

where ρ is the density of the water, g is gravity acceleration, A_p is the pipe cross-sectional

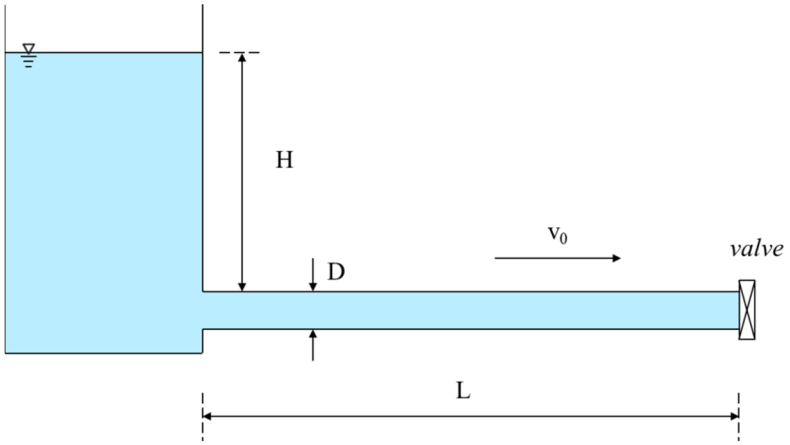

Figure 3.17 Simple pipeline of constant cross-section a terminated by a valve

area, H is the water depth of the tank, v is the water velocity in the pipe, and L is the length of the pipe. If we apply this rigid column theory to sewer networks, head loss term can be reflected as ΔH, and it yields Equation (3.18).

$$\frac{dv}{dt} = \frac{g}{l}(\Delta H - \Delta e) \tag{3.18}$$

where e is head loss between manhole and pipe so that it can be expressed as follows,

$$\Delta e = \begin{cases} K_1 \times \frac{v_1^2}{2g} : Longitudinal\ head\ loss \\ K_2 \times \frac{v_2^2}{2g} : Lateral\ head\ loss \end{cases} \tag{3.19}$$

If pipe cross-sectional area A_p can be multiplied on both sides, and substitutes Δx for L, dynamic equation is obtained (Merlein, 2000).

$$\frac{dQ}{dt} = A_p \frac{g}{\Delta x}(\Delta H - \Delta e) \tag{3.20}$$

The equation (3.20) is used to calculate the head losses between the manhole and the pipes. In addition, the continuity equation of Equation (3.21) is used to calculate the water depth of the manhole.

$$A_m \frac{dh}{dt} = Q + \sum_L^M q_L \tag{3.21}$$

where A_m is the manhole horizontal area, h is the water depth of the manhole, Q is discharge, M is the number of lateral pipes, and q_L is the lateral inflow to the manhole.

3.7.4 Discretization methods

The one dimensional continuity equation and the momentum equation of Equation (3.10) and Equation (3.11) are discretized on the grid, as shown in Figure 3.18, and the leap-frog method is used to computing each parameter, as shown in Figure 3.19.

Continuity equation for pipes

$$\frac{A_{j+1/2}^{n+3}-A_{j+1/2}^{n+1}}{2\Delta t}+\frac{Q_{j+1}^{n+2}-Q_{j}^{n+2}}{\Delta x_j}=q_{j+1/2}^{n+2} \tag{3.22}$$

Momentum equation for pipes

$$\frac{Q_j^{n+2}-Q_j^n}{2\Delta t}+\begin{cases}\frac{u_{j+1/2}^{*}Q_j^{*}-u_{j-1/2}^{*}Q_{j-1}^{*}}{\Delta x_j} & ;\quad u_{j+1/2}^{*}>0,\ u_{j-1/2}^{*}>0\\ \frac{u_{j+1/2}^{*}Q_j^{*}-u_{j-1/2}^{*}Q_j^{*}}{\Delta x_j} & ;\quad u_{j+1/2}^{*}>0,\ u_{j-1/2}^{*}\le 0\\ \frac{u_{j+1/2}^{*}Q_{j+1}^{*}-u_{j-1/2}^{*}Q_{j-1}^{*}}{\Delta x_j} & ;\quad u_{j+1/2}^{*}\le 0,\ u_{j-1/2}^{*}>0\\ \frac{u_{j+1/2}^{*}Q_{j+1}^{*}-u_{j-1/2}^{*}Q_j^{*}}{\Delta x_j} & ;\quad u_{j+1/2}^{*}\le 0,\ u_{j-1/2}^{*}\le 0\end{cases}$$

$$=-\mathrm{g}\frac{A_{j+1/2}^{n+1}+A_{j-1/2}^{n+1}}{2}\frac{H_{j+1/2}^{n+1}-H_{j-1/2}^{n+1}}{\Delta x_j}-gn^2\frac{\left|Q_j^n\right|\frac{Q_j^{n+2}+Q_j^n}{2}}{\left(\frac{R_{j+1/2}^{n+1}+R_{j-1/2}^{n+1}}{2}\right)^{\frac{4}{3}}\left(\frac{A_{j+1/2}^{n+1}+A_{j-1/2}^{n+1}}{2}\right)} \tag{3.23}$$

Treatment of convection term

The time averaged value is used to calculate the non-liner convection terms using a method suggested by Inoue (1986) for numerical stabilization.

$$Q_j^{*}=\frac{Q_j^{n+2}+Q_j^n}{2} \tag{3.24}$$

$$u_j^{*}=\frac{Q_j^{*}}{\frac{A_{j-1/2}+A_{j+1/2}}{2}} \tag{3.25}$$

$$u_{j-1/2}^{*}=\frac{u_{j-1}^{*}+u_j^{*}}{2}=\frac{Q_{j-1}^{*}}{A_{j-3/2}+A_{j-1/2}}+\frac{Q_j^{*}}{A_{j-1/2}+A_{j+1/2}} \tag{3.26}$$

$$u_{j+1/2}^{*}=\frac{u_j^{*}+u_{j+1}^{*}}{2}=\frac{Q_j^{*}}{A_{j-1/2}+A_{j+1/2}}+\frac{Q_{j+1}^{*}}{A_{j+1/2}+A_{j+3/2}} \tag{3.27}$$

Equation (3.19) and Equation (3.20) for calculating head losses depending on manhole shape

and pipe adjoining angle are discretized as in the following.

Dynamic equation for calculating head loss

$$\frac{Q_j^{n+2}-Q_j^n}{2\Delta t} = g\frac{A_{p\ j-1/2}+A_{p\ j+1/2}}{2}\frac{H_{j-1/2}^{n+1}-H_{j+1/2}^{n+1}-\Delta e_{j+1/2}^{n+1}}{\Delta x} \tag{3.28}$$

Continuity equation for manhole

$$\frac{h_{j+1/2}^{n+3}-h_{j+1/2}^{n+1}}{2\Delta t} = \frac{Q_j^{n+2}-Q_{j+1}^{n+2}+\Sigma_L^M q_L^{n+2}}{A_m} \tag{3.29}$$

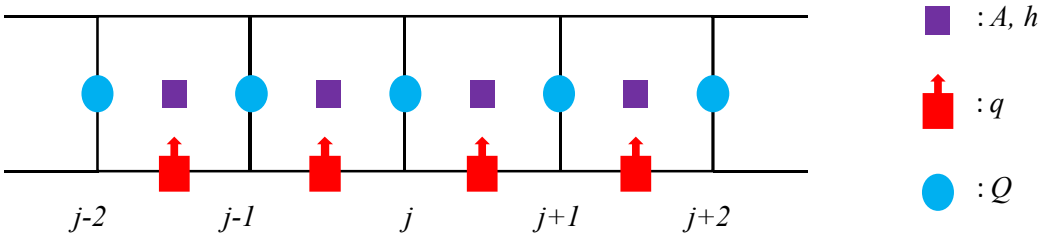

Figure 3.18 Arrangement of each parameter

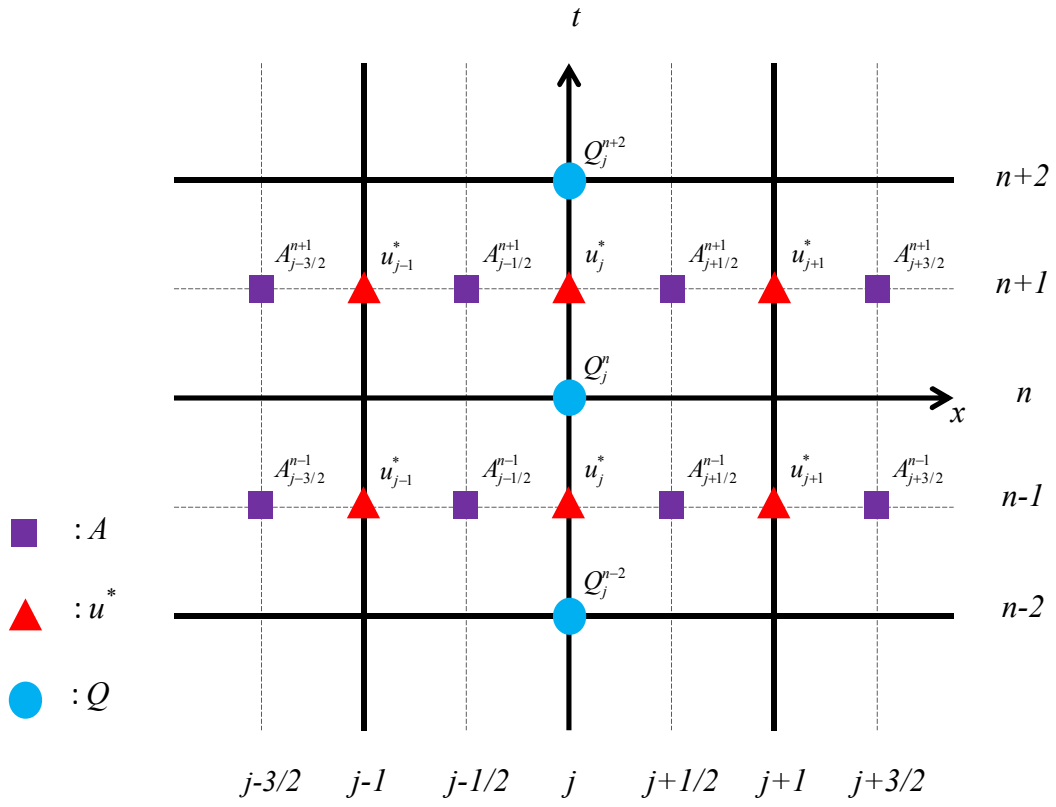

Figure 3.19 Variable arrangement and numerical calculation process

3.7.5 Calculation concept at adjoining section

The longitudinal pipe and the lateral pipe, which are connected to the manhole, can be simulated considering each head loss according to the manhole shapes and adjoining angles in this model. Momentum and dynamic equations are used in order to compute pipe flow and head losses of the connection point at the manhole. Basically, the momentum equation is used to calculate the momentum in each pipe, and the dynamic equation is used to compute the exchange discharge between the manhole and pipes involving head losses. Figure 3.20 shows the calculation concept of the exchange discharge with considering head losses at adjoining points between the manhole and the pipes, and a single grid at the center means the manhole, and the other grids mean the pipe grid, where i is pipe number, j is grid number, and n is time step. Although this model is one-dimensional, the interactions between manhole and pipes can be considered so that head losses can be calculated by Equation (3.20) using the coefficients from Table 3.8. A green line means an application of Equation (3.20), a red line refers to the discharge ratio in order to consider the head loss Δe, and a blue line in Figure 3.20 (d) means the application of Equation (3.21). For instance, $Q_{i,j}^{n+2}$, $Q_{i,j+1}^{n+2}$ and $Q_{i+1,jmax}^{n+2}$ are calculated by Equation (3.20), and $h_{i,j}^{n+3}$ is calculated by Equation (3.21). Other points of the grids are calculated by Equations (3.10) and (3.11). Head loss due to lateral inflow effect is considered through referring to the value of $Q_{i+1,jmax}^{n+2}$ as shown in Figure 3.20 (b).

The interference effect caused by the lateral pipe is reflected by the head loss Δe when the exchange discharge between the longitudinal pipe and the manhole is calculated so that it is possible to consider the head loss effects according to the variation of Q_2/Q_3. In addition, the exchange discharge, $Q_{i+1,jmax}^{n+2}$, which is calculated by the dynamic equation, is used as lateral discharge (q_L) to the longitudinal pipe.

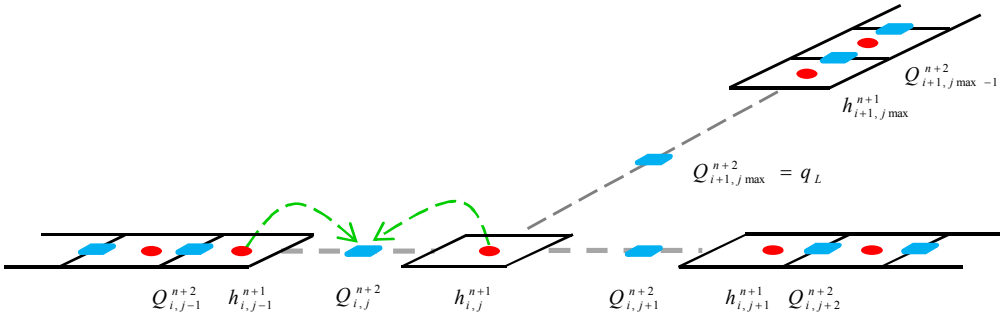

(a) Calculation of longitudinal inflow at manhole using dynamic equation

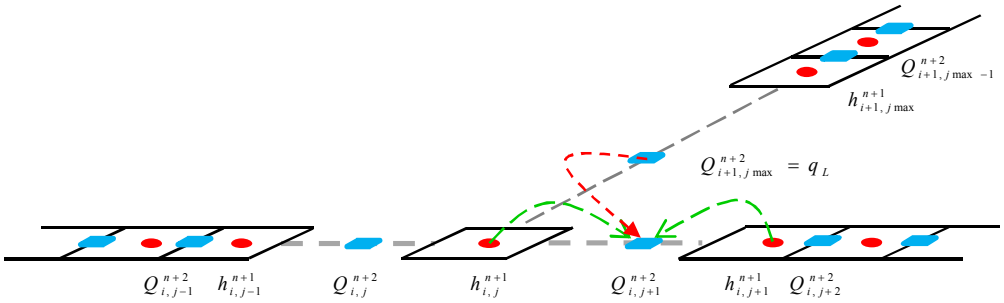

(b) Calculation of longitudinal outflow at manhole using dynamic equation

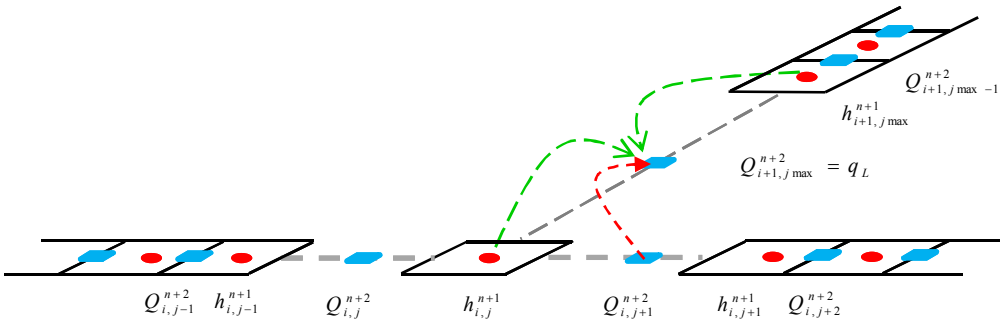

(c) Calculation of lateral outflow at manhole using dynamic equation

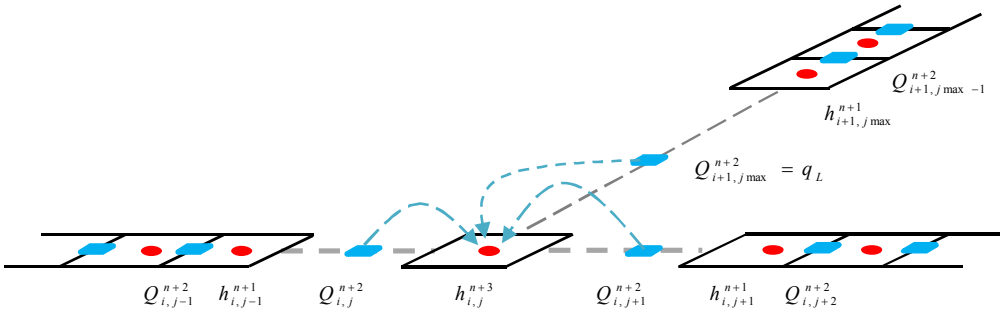

(d) Calculation of water depth at manhole using continuity equation

Figure 3.20 Calculation concept of exchange discharge with considering head losses at adjoining points between manhole and pipes

3.7.6 Treatment of the cutting-edge in pipe

If the water between the neighborhood grids is not continuous in the pipe, the discharge is calculated as shown in Figure 3.21, as per the method described in previous chapter. The equations (3.30) and (3.31) are used to calculate and treat the discharge, instead of the governing equation.

Complete overflow case

If water elevation (H_{ls}) of the lower grid minus ground elevation (z_{ls}) of the higher grid is higher than the ground elevation of the higher grid, water elevation of the lower grid minus ground elevation of the higher grid (h_{ls}) is used to calculate the Q between the adjoining two grids using Equation (3.30).

$$Q = \mu_1 D h_{ls} \sqrt{2 g h_{ls}} \tag{3.30}$$

where Q is discharge, D is a pipe diameter, h_{ls} is water depth ($h_{ls} = H_{ls} - z_{ls}$), H_{ls} is water elevation on the pipe grid, z_{ls} is ground elevation of the same grid, and μ_1 is discharge coefficient; 0.35 is used in this study.

Waterfall case

If the water depth (h_{hs}) of lower grid has not reached the higher grid elevation between the adjoining two grids, the water depth of the higher grid is used to calculate the discharge using

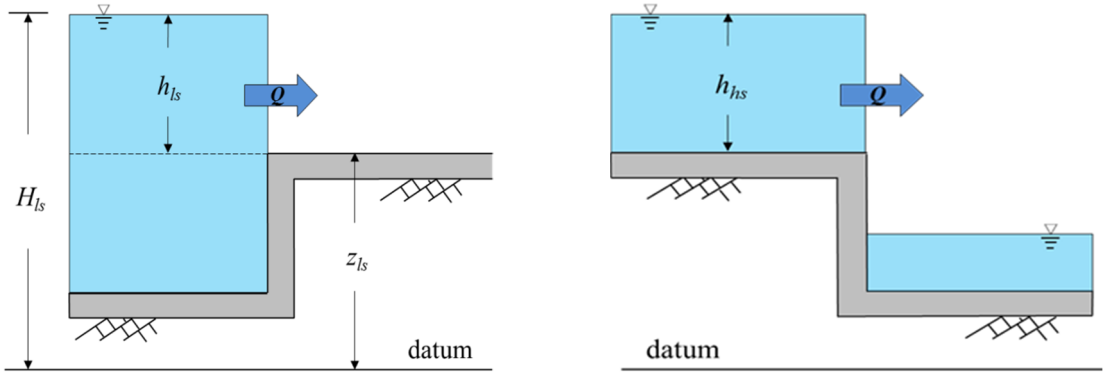

(a) Anadromous case (overflow flow) (b) Waterfall case

Figure 3.21 Treatment of cutting-edge on surface

Equation (3.31).

$$Q = \mu_2 D h_{hs} \sqrt{g h_{hs}} \tag{3.31}$$

where Q is the discharge, , h_{hs} is the water depth on the higher grid, and μ_2 is the discharge coefficient, and 0.544 is used in this study. The water depth, which is lower than 0.001m, is ignored.

3.7.7 Model verification

The numerical model was developed with the interaction of the combination of the 1D momentum equation and the dynamic equation based on the rigid column theory, in which the

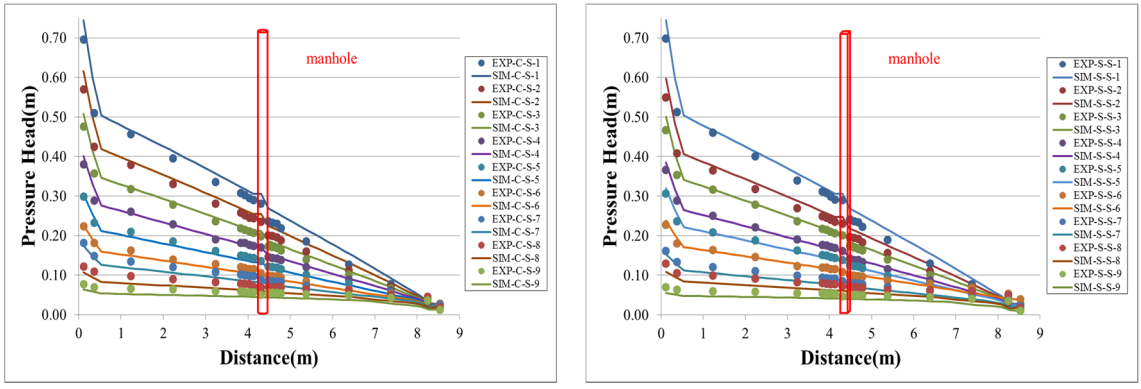

(a) Circular shape manhole (b) Square shape manhole

Figure 3.22 Simulated and experimental pressure head of 2 pipes, steady-state cases

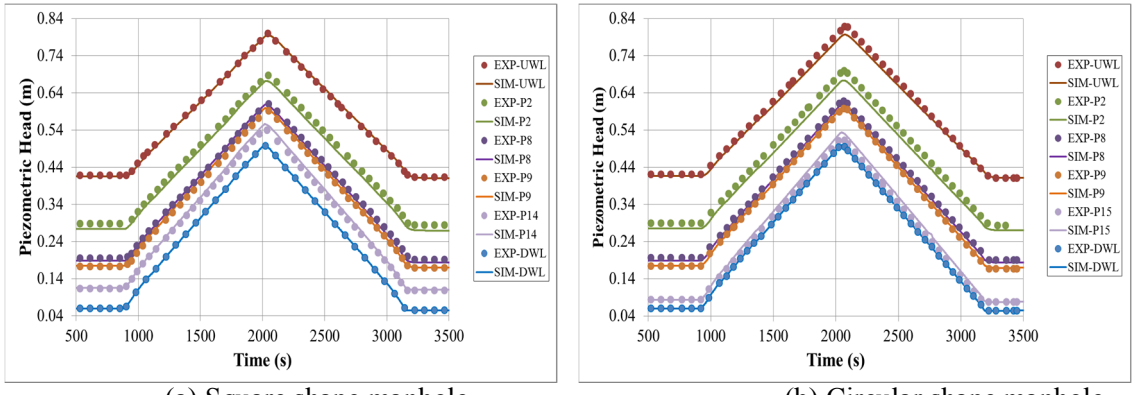

(a) Square shape manhole (b) Circular shape manhole

Figure 3.23 Simulated and experimental pressure head of 2 pipes, unsteady-state cases

(***UWL** : Upstream Water Level, **DWL** : Downstream Water Level)

head losses at the manhole are dealt with in combination of the discharge ratio of the lateral input discharge over the total output discharge at the manhole. In this chapter, the numerical simulation was carried out with a time step of 0.001 second, pressure propagation velocity of 5m/s, Manning coefficient of 0.009, and space steps of 20cm (in pipe) and 15cm (in manhole) in x (longitudinal) directions with various study cases, as shown from Table 3.1 to Table 3.7.

Figure 3.22 shows the simulated and experimental pressure head profiles at different piezometric tubes, according to different manhole shapes under the steady-state condition. It is clear that the pressure head profiles have been changed before and after passing the manhole, as the head losses occurred at the manhole.

Consequently, all simulation results in Figure 3.22 show good agreement with the experimental results even if there are small evidences of mismatching, as in the case of C-S-1 and S-S-1. Johnston and Volker (1990) mentioned that an influence of the Froude number and the manhole submergence are not major, but nevertheless, they are important in some flow conditions. The Froude numbers of C-S-1 and S-S-1 are 2.20 and 2.21, respectively. This indicates that their flow conditions are supercritical flow, and their approaching speed to the manhole is relatively very fast compared with other cases, which causes a fluctuation in the manhole. Actually, the fluctuation has reported a range of $\pm$0.1mm ~ $\pm$20.0mm by Johnston and Volker (1990). Therefore, these simulation results are acceptable if the experimental observation errors caused by the fluctuation are allowed.

Figure 3.23 shows the simulated and experimental pressure head profiles at different piezometric tubes according to the manhole shape difference under the unsteady-state condition. Measurement points; upstream tank; and pipe segments no.2, no. 8, no. 9, no. 14, and no. 15 are all selected to measure the change of the piezometric head according to time variation. In this experiment, an input discharge was selected as 2.13*l/s* in order to improve experimental observation accuracy and reduce fluctuation at the manhole. Unsteady-state condition was made by controlling the downstream movable gate, which may reflect the ascending and descending water level of the river in an actual case. The head loss coefficients obtained through the experimental data analysis are used same as with steady-state experiments, and all simulation results showed good agreement with the experimental data.

Figures 3.24 to 3.27 present the presure head profiles of the numerically calculated and experimentally observed value under the steady-state condition depending on the different manholes' shapes (circluar and square) and the different adjoining angles of 90°, 60°, and 45° between the longitudinal and lateral pipes. The red line experesses the simulated longitudinal pressure head profiles, and the sky blue line expresses the simulated lateral pressure line. The

lines are represented as one-dimensional in the all graphs even though the pipe configurations of three pipes cases can be spatially three-dimensional.

It is observed that the pressure head losses are increased with increasing lateral input discharge until the sixth case, in which the longitudinal and lateral input dishcarge are the same. Then, the lateral pressure head turned the longitudinal pressure head around through all of the three pipes cases under the steady-state condition.

In addition, a growing trend in the gap between the longitudinal pipe segment no. 8 and no. 9 were slowed down after the reversal of the pressure head profiles between the longitudinal and lateral pipes. As a result, the developed model could reproduce such phenomena, and it shows good agreement with the experimental results through all of the three pipes, steady-state experimental cases.

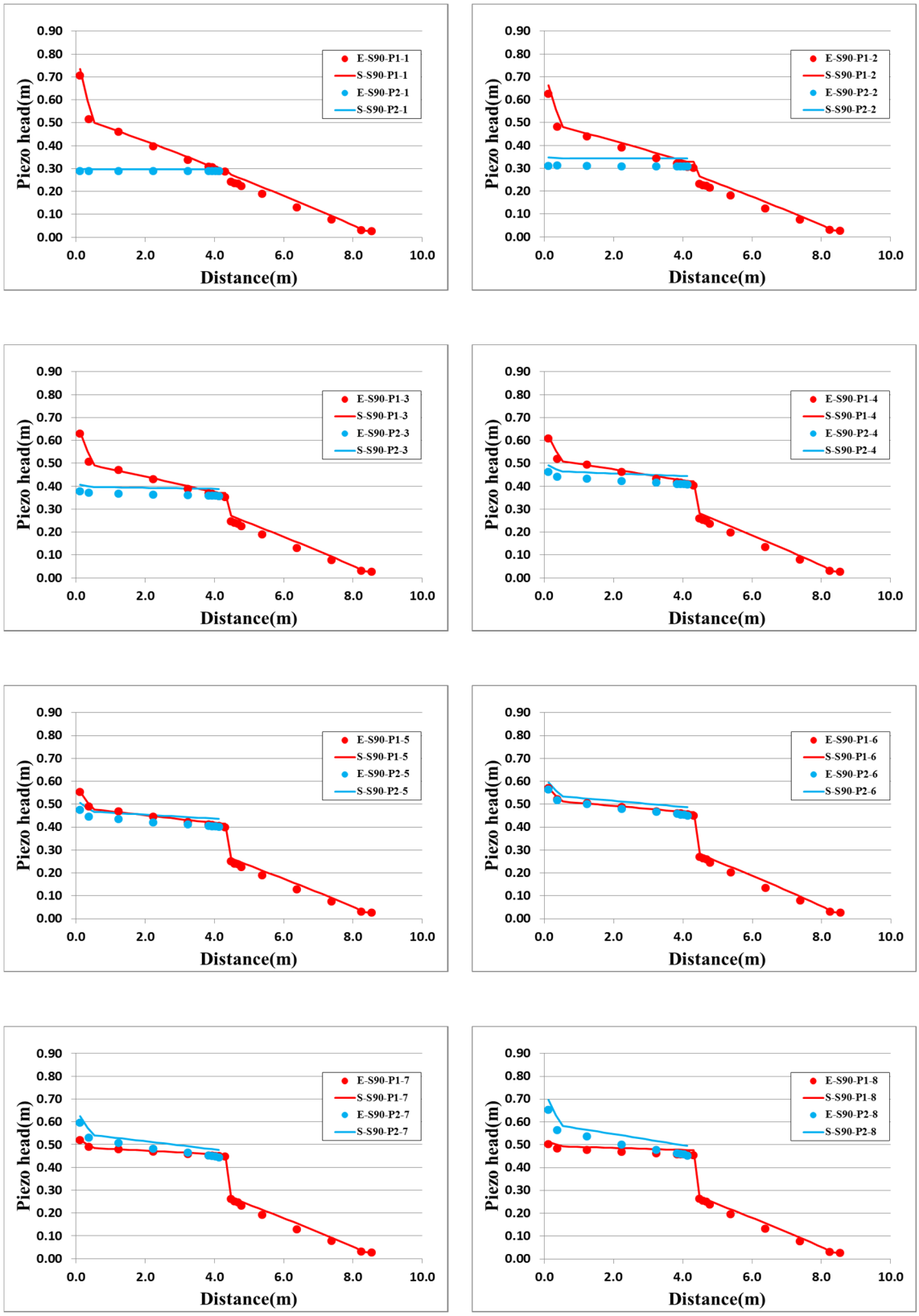

Figure 3.24 Three pipes square cases, steady-state cases (90°)

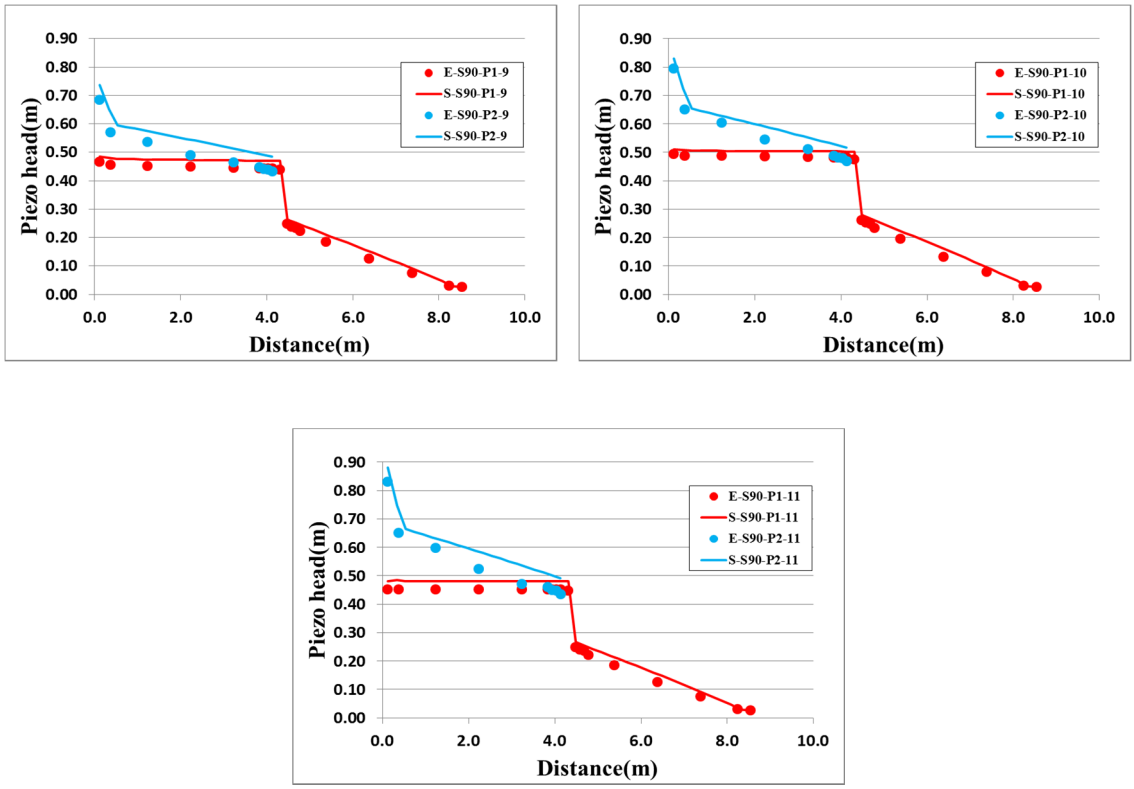

Figure 3.24 Three pipes square cases, steady-state cases (90°) (continue)

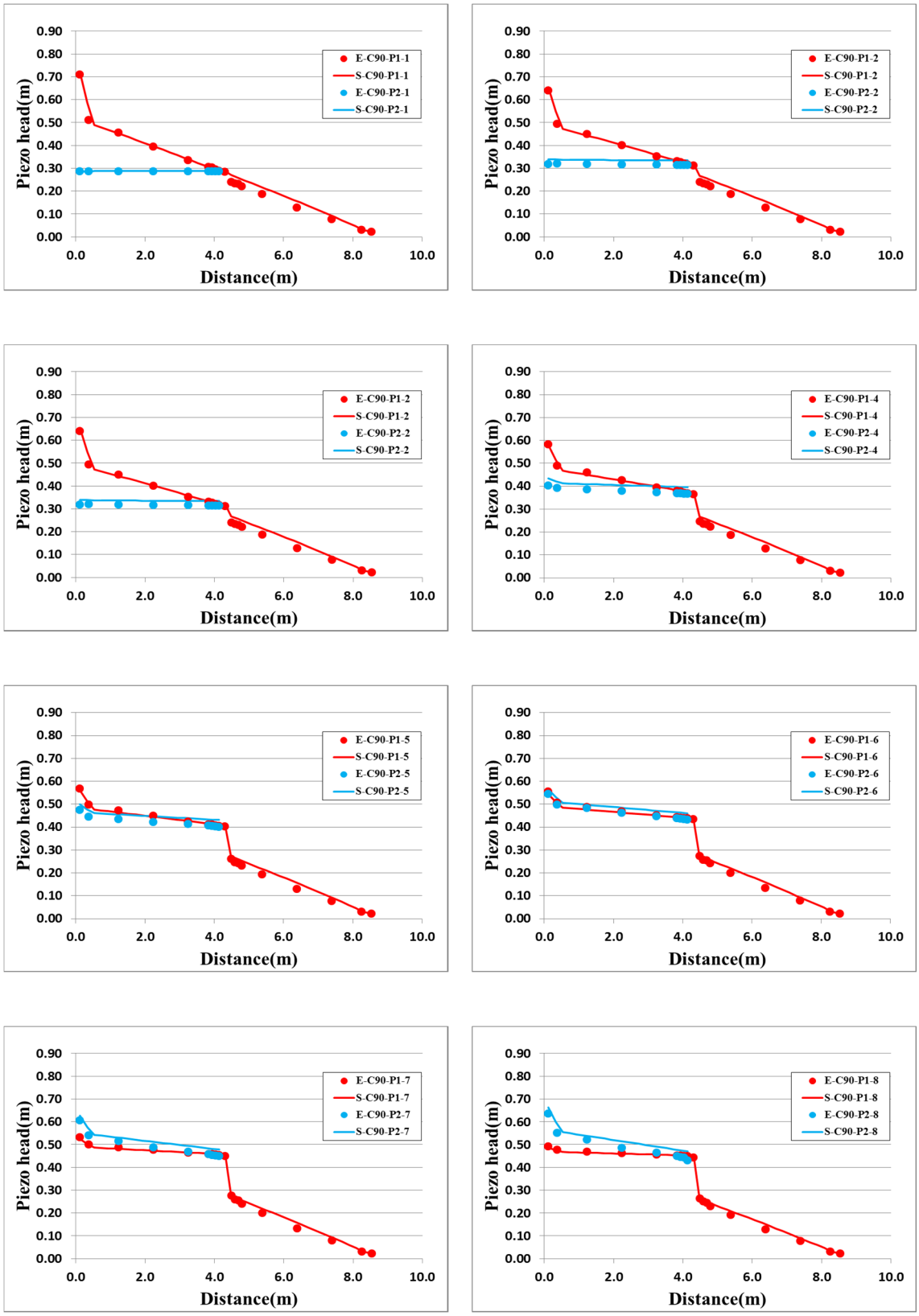

Figure 3.25 Three pipes circle cases, steady-state cases (90°)

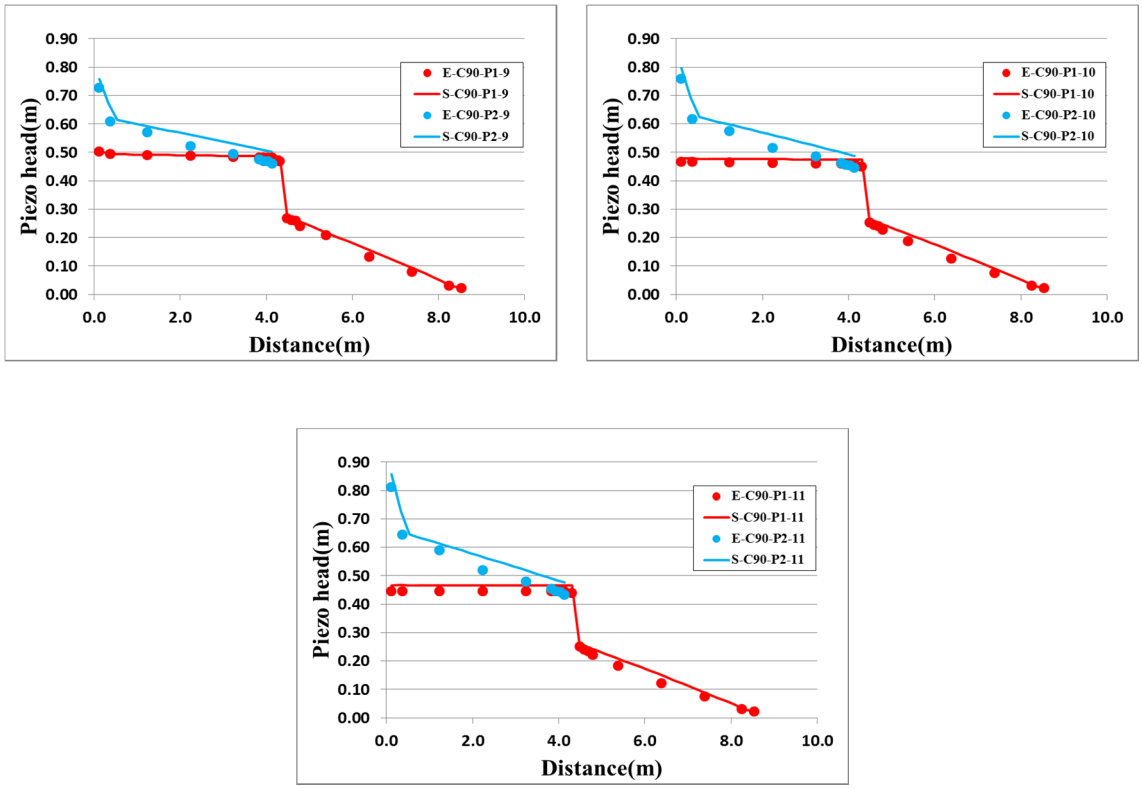

Figure 3.25 Three pipes circle cases, steady-state cases (90°) (continue)

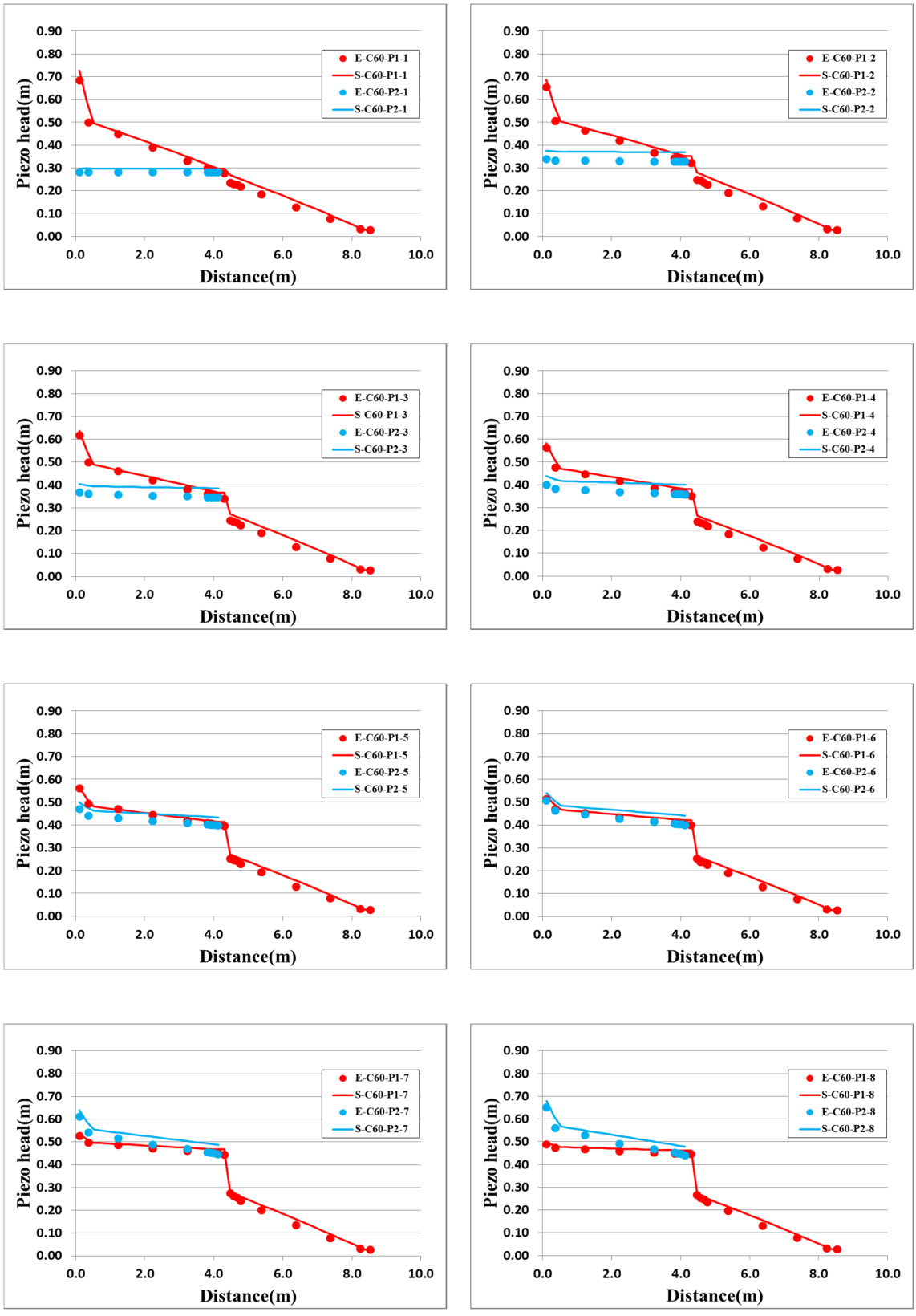

Figure 3.26 Three pipes circle cases, steady-state cases (60°)

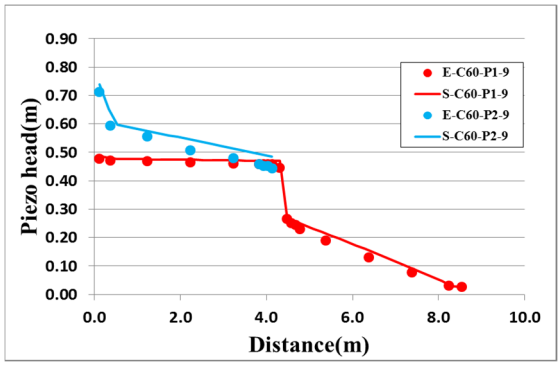

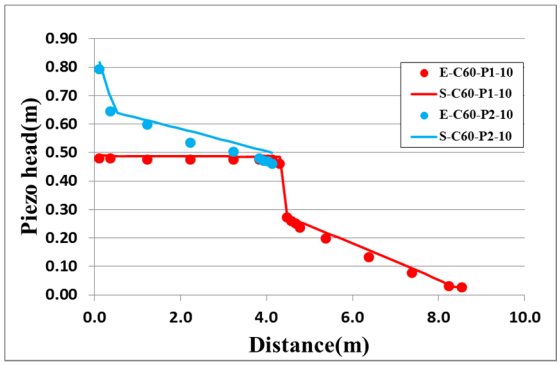

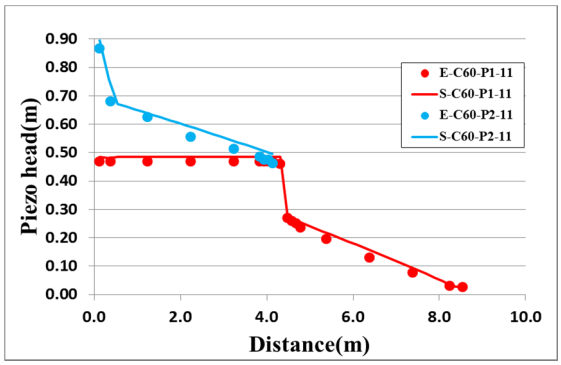

Figure 3.26 Three pipes circle cases, steady-state cases (continue)

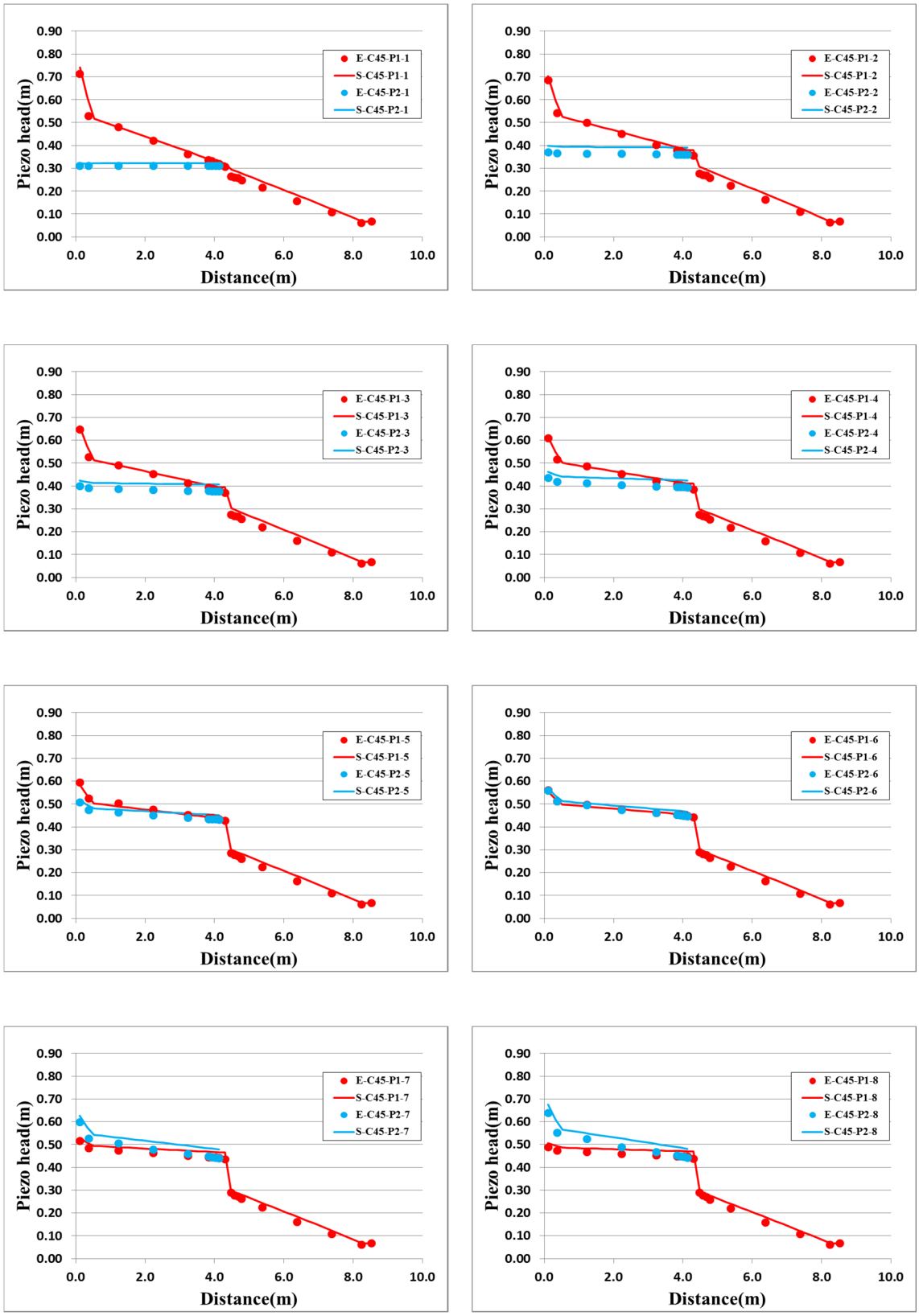

Figure 3.27 Three pipes circle cases, steady-state cases (45°)

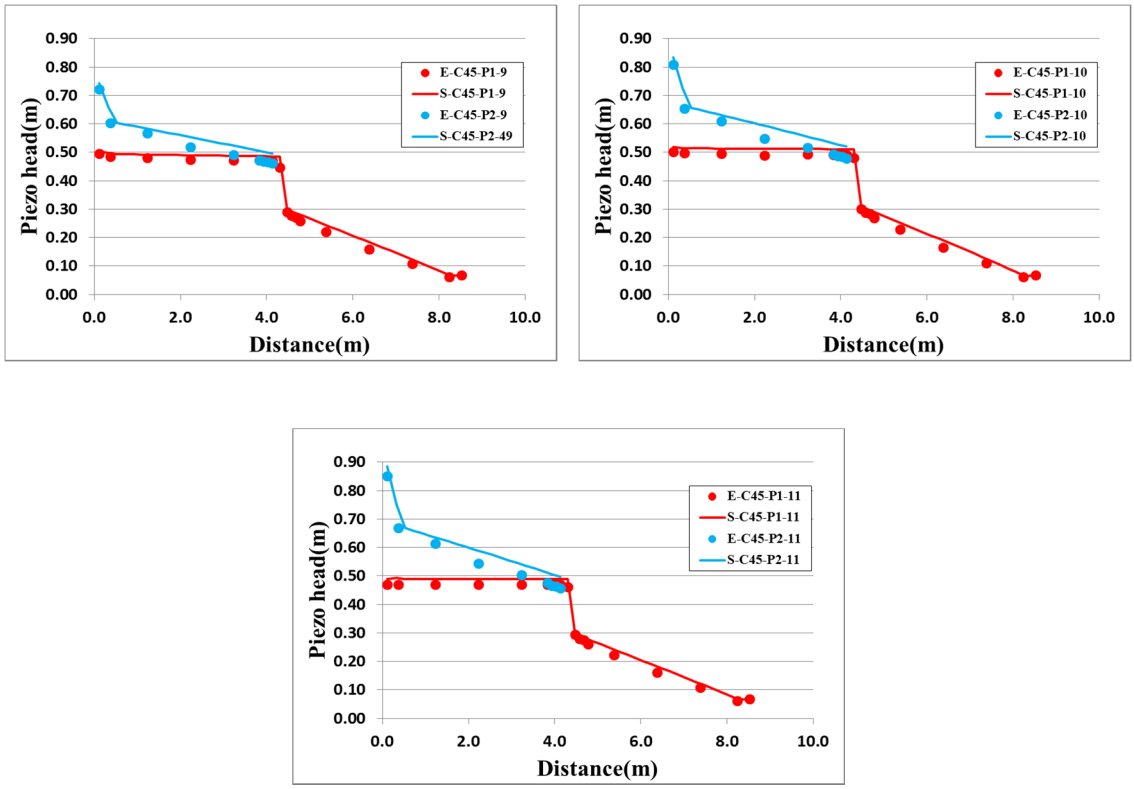

Figure 3.27 Three pipes circle cases, steady-state cases (45°) (continue)

Figures 3.28 to 3.31 present the pressure head profiles of the numerically calculated and experimentally observed values under the unsteady-state condition, depending on the different manhole shapes (circular- and square-type), and the different adjoining angles, same as the steady-state cases.

Each input dishcarge of P1 (longitudinal pipe) and P2 (lateral pipe) are 1.0*l/s* through all cases of the three-pipe experiments under the unsteady-state condition in order to acquire stable experimental data. Longitudinal pipe segments no. 2, no. 4, no. 13, and no. 15 and, lateral pipe segments no. 2 and no. 4 are selected with the manhole point in order to measure the pressure head change according to the change of the downsteam water level. As a result, the developed model could reproduce such phenomena, and it shows good agreement with the experimental results through all three-pipes, steady-state experimental cases. The downstream water level was changed from about 0.1m to 0.4m to 0.1m during about 1600 seconds. The numerically calculated results are well matched with the experimental results through all of the three-pipe cases under the unsteady-state condition.

Figure 3.28 Three pipes square cases, unsteady-state cases (90°)

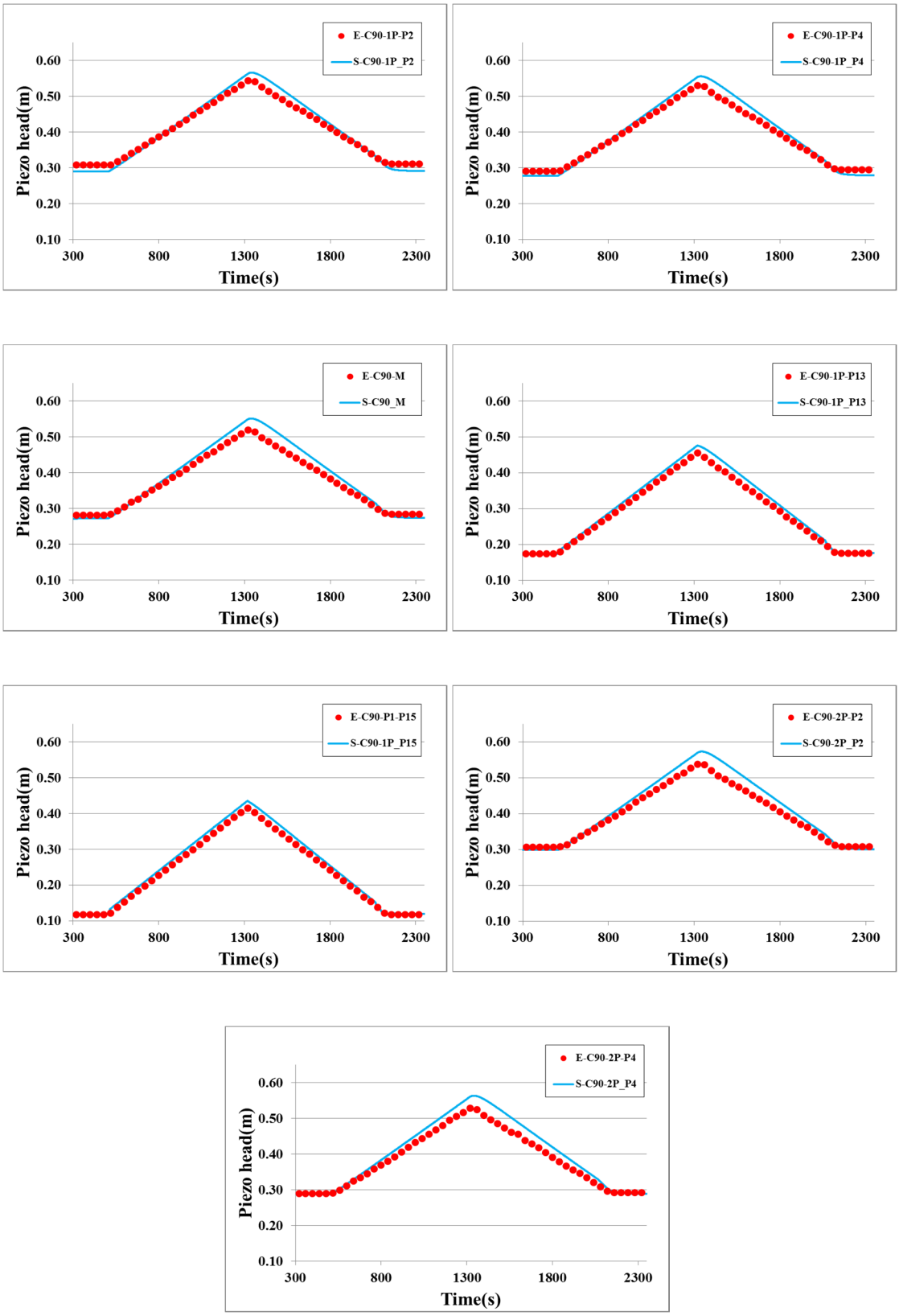

Figure 3.29 Three pipes circle cases, unsteady-state cases (90°)

Figure 3.30 Three pipes circle cases, unsteady-state cases (60°)

Figure 3.31 Three pipes circle cases, unsteady-state cases (45°)

3.8 Summary

In this chapter, two kinds of fundamental laboratory experiments are carried out under the various circumstances with no benching and no invert in order to estimate the effects of head loss depending on the different manhole shapes and pipe configurations. First, straight cases were conducted in order to evaluate the head loss depending on the manhole shape between the circular and square type, and the adjunction case experiments were conducted using different manhole shapes (same as the straight cases) and the different adjoining angle to confirm the head loss effects according to the pipe configurations, under the unsteady, as well as steady, conditions. Finally, the numerical model was developed and validated to confirm the applicability of the model using the head loss coefficients based on the experimental data from the laboratory experiments. The main findings in this chapter are described as follows:

1. In the two-pipes cases, it was clear that the pressure head losses occurred at the manhole, and the coefficients obtained are 0.259 and 0.235 for square and circular manhole types, respectively.

2. In the three-pipes cases with different manhole shapes, it was observed that the head loss of the square shape is higher than that of the circular shape, and the gap between the longitudinal coefficients (K_1) of the square and circular manhole types decreases with an increasing ratio of Q_2/Q_3 in 90° cases. In addition, the difference of the lateral coefficient (K_2) was increased along with the ratio of Q_2/Q_3 in the opposite way with the longitudinal coefficients. The analysis shows that the lateral input discharge disturbs the longitudinal flow, which causes increasing head losses at the manhole. This effect is seen stronger at the square shape manhole than at the circular shape.

3. In the three-pipes cases with different adjoining angles for the circular-type manhole, although the increasing tendency of both the longitudinal and lateral coefficients shows a similar trend with almost the same value in three different adjoining angles, they start to deviate into different patterns from $Q_2/Q_3 = 0.5$.

4. Empirical relations were developed to calculate head loss depending on manhole shapes and pipe configuration through all of the experimental cases.

5. A one-dimensional numerical model was developed for computing the hydraulic characteristics of pipe flow with the manhole. The proposed model was tested for different experimental conditions using different manhole shapes and various pipe configurations. The simulated results are in good agreement with the experimental results for not only the pressure head profile under the steady-state condition, but also the pressure head change according to time under the unsteady-state condition.

CHAPTER 4

EXCHANGE DISHCARGE BETWEEN GROUND SURFACE AND SEWER PIPE

4.1 Introduction

Urban inundation due to torrential rainfall and climate change has been one of the most common natural disasters worldwide. In Japan, the many inundation disasters that have occurred due to locally heavy rainfall during a short period of time have reinforced the need for accurate models to simulate flooding. Many researchers have developed numerical models in order to predict and prevent urban inundation caused by heavy rainfall. Hsu et al. (2000) developed a combined model for inundation simulation by coupling the SWMM model and the 2D diffusive overland flow model. However, this model could not deal with detailed information such as inundation zones and depths caused by pressurized water. Duchesne et al. (2001) demonstrated the efficiency of real-time control (RTC) to decrease storm overflows from combined sewers to receiving waters, but they did not consider exchange discharges between the ground surface and the sewer system. Akiyama et al. (2008) developed a dynamic network model for free-surface-pressurized flows, which, when combined with the Preissmann slot, simulated a closed conduit. Although this model successfully predicted areas with poor drainage and the locations of pressurized positions in the sewer pipes, it failed to simulate the exchange discharge between the ground surface and sewer pipes. Leandro et al. (2009) pointed out that sewer/surface linkages and virtual manholes were key factors for developing a more accurate combined model.

An integrated model was developed to produce more accurate results. It consisted of a 2D inundation model of the ground surface and a 1D network model of sewer pipes; a sub-model combined those two models and simulated the exchange of storm water between the ground surface and the sewer system (Kawaike and Nakagawa, 2007). This sub-model, which employed the step-down formula and the overflow formula, was found to overestimate storm water interaction discharge when compared to experimental results (Kawaike et al., 2011).

Chapter 2 focused on drainage discharge from the ground surface to the sewer system. The interaction sub-model was modified accordingly in order to suggest suitable coefficients; the formula for calculating exchange discharge is replaced in this section.

The experiments described in this chapter were carried out using an improved experimental laboratory setup that could measure a stable piezometric head in the sewer pipe as well as the inundation depth caused by insufficient sewer pipe capacity. Figure 4.1 shows a photo of the experimental setup, which will be explained later in more detail. The 1D sewer pipe model, which can reproduce changes in piezometric head based on rising and falling downstream water levels, was validated under various experimental conditions in order to develop an integrated urban inundation model. An integrated model of runoff and the sewer system, as discussed in Chapter 2, was applied to simulate variations in ground inundation depth.

4.2 Description of Experimental Set-up

Figure 4.2 shows the side view and plan view of the experimental facility, which consisted of three parts: the rainfall simulator, the ground surface, and the sewer pipe system. The experimental scale was assumed to be 1/20 based on the Froude similarity law. The rainfall simulator sprayed water onto the ground surface via 20 nozzles. The outside of the nozzle and the ground space was surrounded by a transparent curtain so that all of the sprayed water fell onto the ground surface. According to the assumed experimental scale, experimental rainfall of 30mm/hr was equivalent to rainfall of approximately 130mm/hr in the prototype scale.

The ground surface had a flat inundation basin 10m long and 2m wide, on which there was a roadway 0.5m wide, a sidewalk 0.15m wide, 10 buildings on each side, and 20 storm drains (0.05m × 0.05m) on the roadway. The storm drain was the cover of a drain box (0.05m × 0.05m × 0.05m), and the 10 drain boxes on each side of the roadway were connected by a drain channel with a 0.015m × 0.025m connection area. The length of the drain channel was 0.95m or 0.415m. One circular pipe 0.05m in diameter, 11.6m long, and with a slope of 1/971 was placed just below the flat inundation basin. This pipe could be divided into 10 segments, each of which had a piezo tube as shown in Figure 4.2 (a). Variations in inundation depth on the ground surface were measured at H1 and H2 as shown in Figure 4.2 (b). A cross section of the experimental setup is shown in Figure 4.3. The light blue line indicates connection tubes between building roofs and the sewer pipe, while the dark blue line connects a drain box and the sewer pipe. The drain channel connected all of the drainage boxes on one side of the roadway. If the piezometric head in the sewer pipe increased more than the elevation of the drainage box, the storm water flowed backward from the sewer pipe onto the ground surface through the connection tube and storm drain. The water level of the downstream tank could be adjusted by a movable weir, and the water level was assumed as the river water depth in this study. Storm

water stored in the downstream reservoir was circulated to the upstream end and added by the circulation pump as inflow discharge.

Since the upstream and downstream tanks were assumed to be rectangular manholes for the purposes of the study, special treatment was required to calculate exchange discharge among the upstream tank, downstream tank, and sewer pipe. Simulation results of this concept showed good agreement with experimental results. The concept of exit and entrance head losses between the tanks and sewer pipe differs slightly from the concept described in Chapter 3.

Seven cameras were used to record each experimental result, including water level variations of the upstream and downstream tanks, changes of piezometric head in the pipe, and inundation depth on the ground over time.

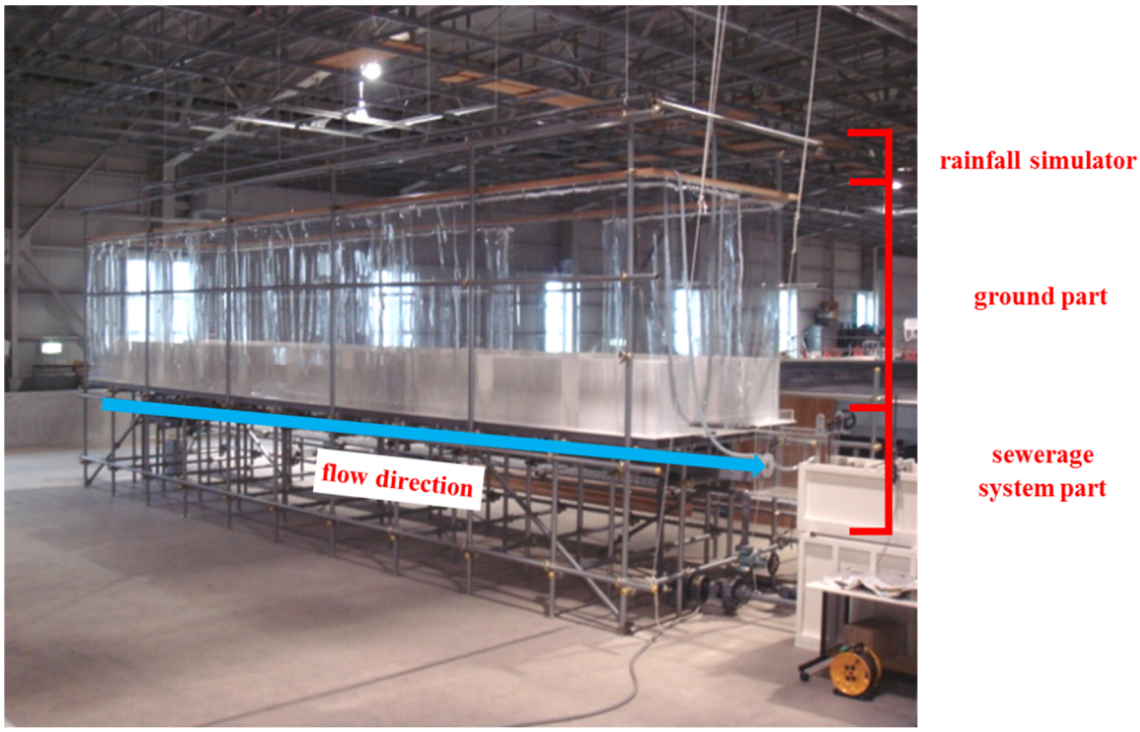

Figure 4.1 Experimental setup

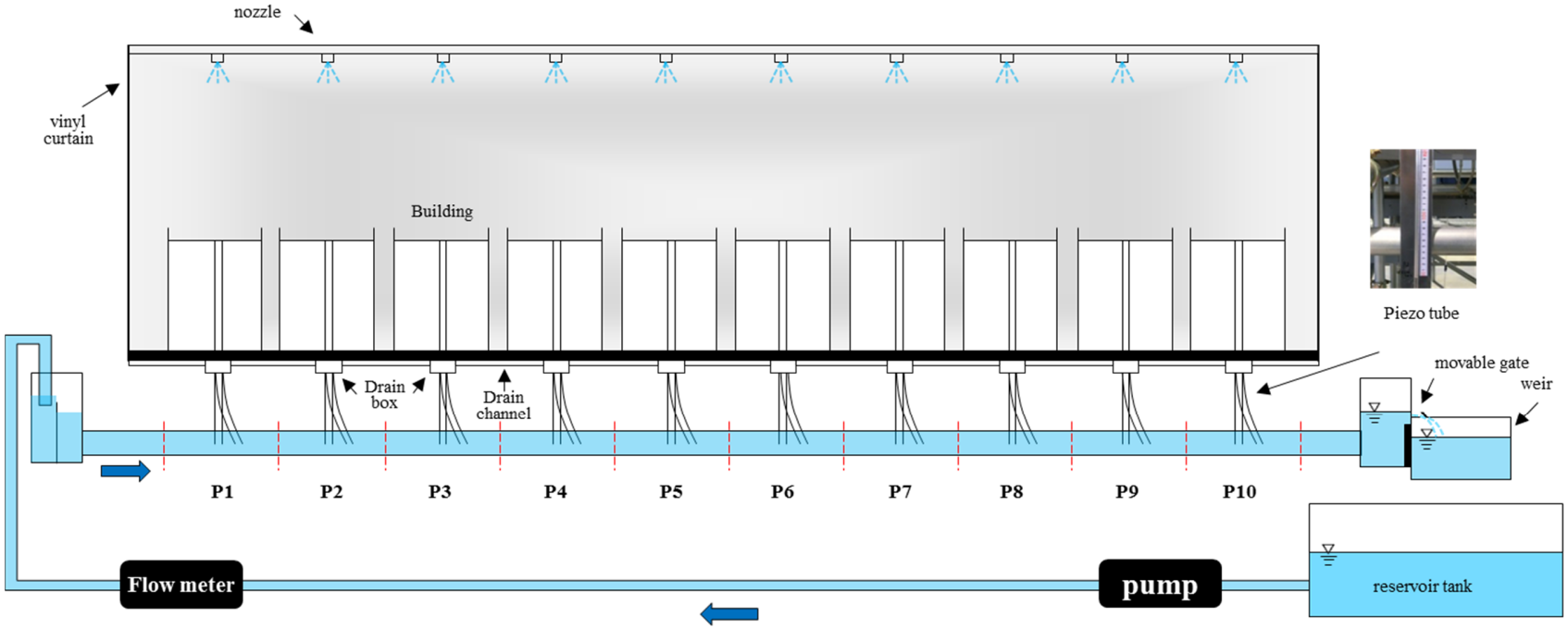

(a) side view of experimental facility

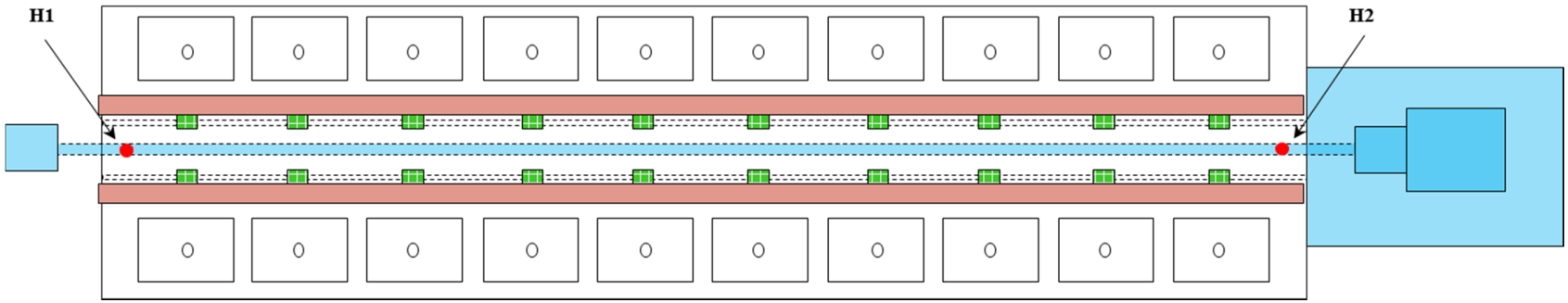

(b) Plan view of experimental facility Figure

Figure 4.2 Side view of laboratory experimental facility

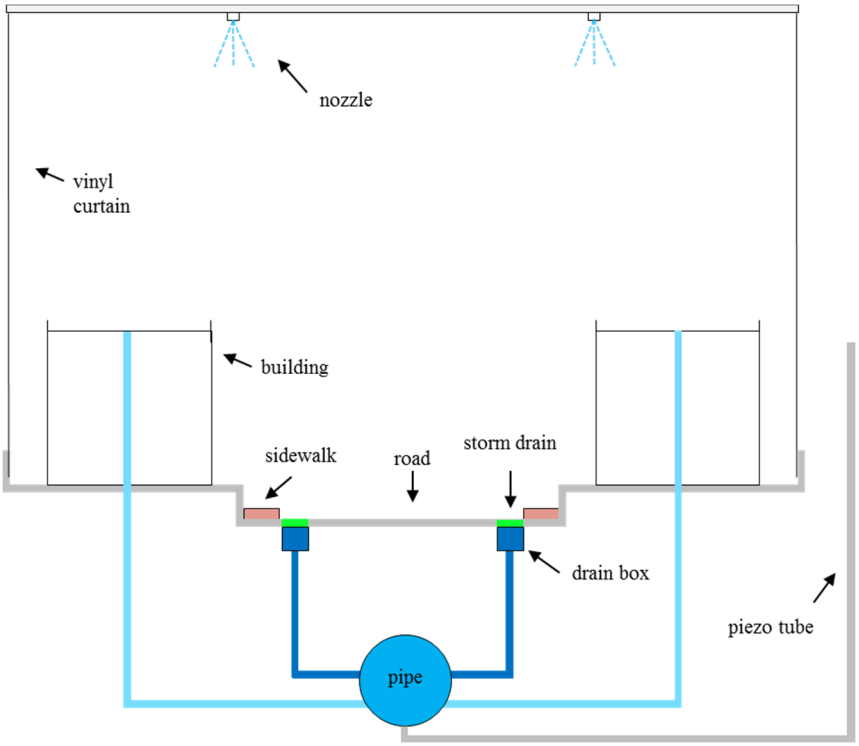

Figure 4.3 Cross section of experimental facility

4.3 Experimental Condition

Experiments were designed to assess the applicability and reproducibility of the exchange discharge between the ground surface and the sewer system, using the formulas and coefficients discussed in Chapter 2. The experiments were divided into steady-state and unsteady-state conditions. Steady-state conditions were designed for three flow patterns: open flow, partially pressurized flow, and fully pressurized flow. The experiments also evaluated more complex situations such as the coexistence of overflow from the sewer pipe to the ground surface and drainage from the ground surface to the sewer pipe under rainfall and no-rainfall conditions. The three flow patterns tested the model's applicability under all possible flow conditions. The coexistence cases of overflow and drainage were used under rainfall and no-rainfall conditions.

These eight cases can be divided into four categories of flow states within the sewer pipe: open channel flow, partially pressurized flow, fully pressurized flow, and backwards flow. In these experiments, the water surface on the ground was measured by point gauge and, depending on the category, the following parameters were measured:

- Open channel flow: water level within the sewer pipe
- Partially pressurized flow: water level within the piezometric tube
- Fully pressurized flow: water level within the piezometric tube
- Backwards flow: water level within the piezometric tube and inundation depth on the ground

The unsteady-state conditions were designed to simulate flow conditions in every possible situation: open flow, partially pressurized flow, fully pressurized flow, overflow from sewer pipe to ground surface, or vice versa. Tables 4.1 and 4.2 show the experimental conditions and measuring points under steady-state and unsteady-state conditions. In total, ten experiments were conducted to confirm and validate applicability and reproducibility.

Table 4.1 Steady-state condition experimental condition

Index	Input discharge (*l/s*)	Downstream water level (*m*)	Mean velocity (*m/s*)	Froude Number	Rainfall (*mm/h*)	Measuring point
CASE 1	0.214	0.208	0.11	0.16	0	upstream tank P1 ~ P10
CASE 2	0.301	0.216	0.15	0.22	0	
CASE 3	1.008	0.190	0.51	0.73	0	
CASE 4	0.854	0.221	0.44	0.62	0	
CASE 5	0.950	0.277	0.48	0.69	0	
CASE 6	0.950	0.317	0.48	0.69	0	
CASE 7	1.431	0.429	0.73	1.04	0	upstream tank P1 ~ P10 Inundation depth
CASE 8	1.537	0.378	0.78	1.12	27.18	

Table 4.2 Unsteady-state condition experimental condition

Index	Input discharge (*l/s*)	Change velocity of downstream water level	Measuring point
CASE I	1.335	Quickly	upstream tank P2, P5, P9 H1, H2
CASE II	1.335	Slowly	upstream tank P2, P5, P9 H1, H2

4.4 Major Apparatus for Experiments

Several pieces of equipment were used in the experiments, including a Magnetic Flowmeter to measure discharge, an RPM controller to control the inflow discharges to the upstream tank, and a point gauge to measure downstream water levels. Seven video cameras were used to record changes in inundation depth on the ground (H1 and H2 in Figure 4.2) as well as changes in piezometric head in the pipes and water levels in the two tanks (upstream and downstream) under the unsteady-state conditions.

4.5 Experimental Procedures

4.5.1 Steady-state cases

Inflow discharges was selected as a case study, and the experiment as conducted under steady-state conditions. After a waiting period of at least 30 minutes, measurements were recorded. Figure 4.4 shows a connection point between the sewer pipe and the piezo tube, while Figure 4.5 shows a piezometric panel to which the tube was attached with a scale bar. Each point (P1 ~ P10) had its own panel. All processes were repeated until each experimental case was completed as outlined above.

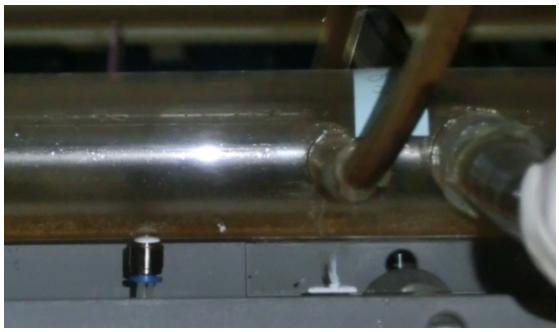

Figure 4.4 Piezometric tube connection point

Figure 4.5 The panel of piezometric tube

4.5.2 Unsteady-state cases

In the unsteady-state experiments, the inundation processes of surcharging flow, varying levels of ground inundation, backwater flow, and drainage flow happen due to gradually rising and falling downstream water levels. Two experiments were conducted to confirm the hydraulic phenomena caused by changes in the velocity (speed) of the downstream water levels. These experiments were conducted in the experimental setting shown in Figure 4.2. Two phenomena were measured in CASE I and CASE II: 1) Changes in water depth in the upstream tank and piezometric head variation of sewer pipes P2, P5 and P9, and 2) Changes in inundation depths on the ground surface at upstream (H1) and downstream (H2) locations. Video cameras recorded these parameters; Figure 4.6 shows images from these videos.

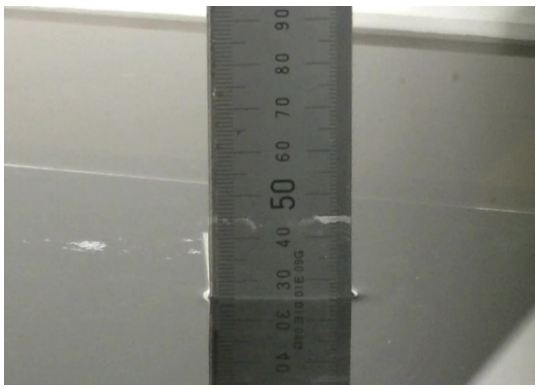

(a) Upstream of ground surface

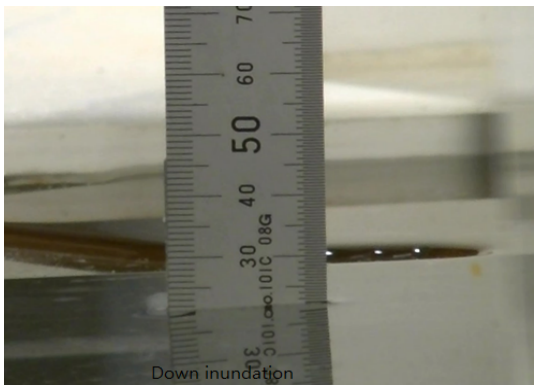

(b) Downstream of ground surface

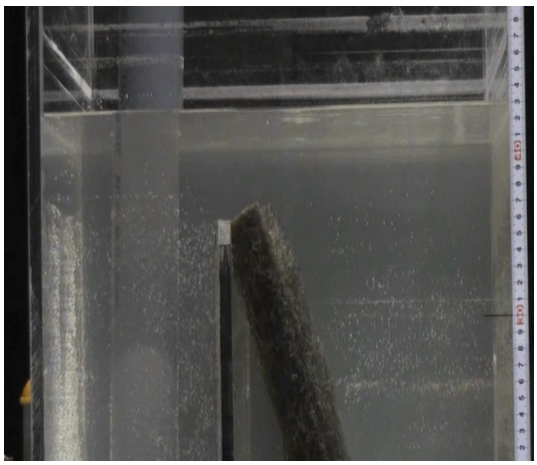

(c) Upstream tank of pipe

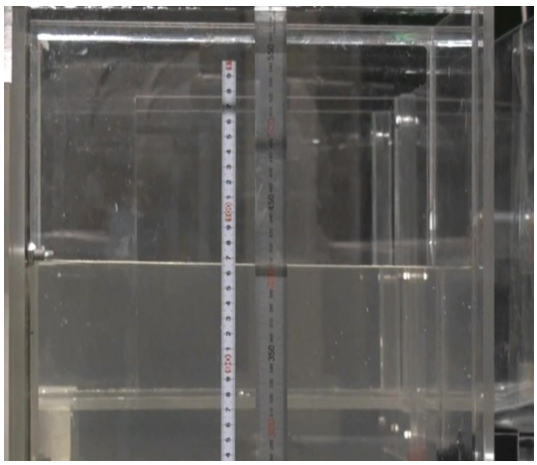

(d) Downstream tank of pipe

Figure 4.6 Inundation depth and Piezometric head caused by pressurized pipe flow

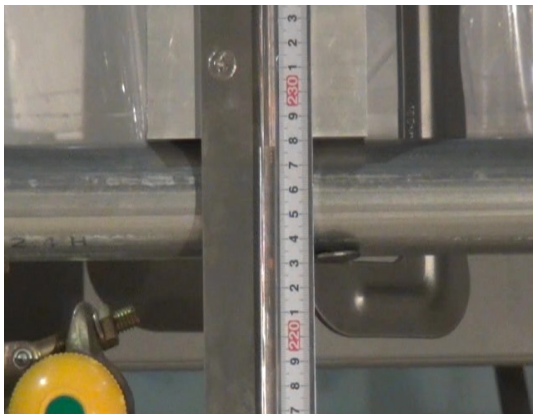

(e) Piezometric head in sewer pipe

Figure 4.6 Inundation depth and Piezometric head caused by pressurized pipe flow (continue)

4.6 Coupling Model for Ground Surface and Sewer Pipe

4.6.1 Introduction

Case studies were simulated using two types of flow models (2D ground surface flow and 1D sewer pipe flow) and two types of interaction models (discharge exchange model for ground surface/drain box/sewer pipe and discharge exchange model for upstream tank/sewer pipe/downstream tank). The flow models used in this study consisted of a horizontal 2D inundation flow model (Kawaike et al., 2011) and a 1D slot model of sewer pipe flow (Chaudhry, 1979). Interaction models consisted of the weir and orifice formulas used to calculate exchange discharge, not only between the ground surface and sewer pipe, but between the upstream tank, sewer pipe, and downstream tank. Figure 4.7 shows the schematic of the interaction process in the experimental setup. Storm water falling on building roofs drains directly into the sewer pipe through drainage tubes from holes at the center of each building roof (light blue in Figure 4.3). Storm water on the ground surface, on the other hand, flows into drainage boxes through storm drains on both sides of the roadway and is discharged from the bottom of the drainage box into the sewer pipe through the drainage tube (dark blue in Figure 4.3). Since the ground surface is acrylic, the infiltration process is not considered in this study.

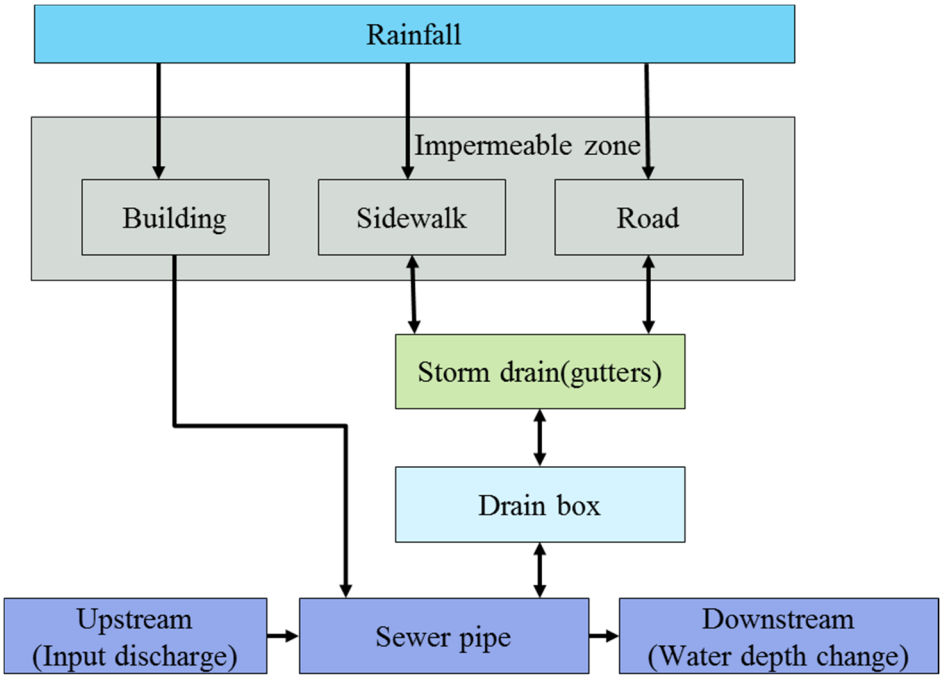

Figure 4.7 Schematic of the interaction process

4.6.2 Governing equation

4.6.2.1 2D inundation model

The governing equations used for the 2D inundation flow model are as follows:

$$\frac{\partial h}{\partial t} + \frac{\partial M}{\partial x} + \frac{\partial N}{\partial y} = r_e - q_{drain} - q_{sew-g} \tag{4.1}$$

$$\frac{\partial M}{\partial t} + \frac{\partial (uM)}{\partial x} + \frac{\partial (vM)}{\partial y} = -gh\frac{\partial H}{\partial x} - \frac{gn^2 M\sqrt{u^2+v^2}}{h^{4/3}} \tag{4.2}$$

$$\frac{\partial N}{\partial t} + \frac{\partial (uN)}{\partial x} + \frac{\partial (vN)}{\partial y} = -gh\frac{\partial H}{\partial y} - \frac{gn^2 N\sqrt{u^2+v^2}}{h^{4/3}} \tag{4.3}$$

where h is water depth, H is water level, u, v are x, y directional velocity, M (=uh), N (=vh) are x, y directional flow flux, r_e is effective rainfall, q_{drain} is drainage discharge from the ground surface to the drainage box per unit area (if its value is negative, that indicates overflow discharge from the drain box), $q_{sew\text{-}g}$ is drainage discharge from the building roofs to the sewer pipe per unit area, g is gravity acceleration, and n is Manning's roughness coefficient (n=0.012, adopted for the drain channel in this study). Computational meshes are square in shape (Δx = 5cm, Δy = 5cm), and the Finite Difference Method is adopted.

4.6.2.2 1D sewer pipe model

A 1D flow simulation with the slot model was conducted to simulate flow within a sewer pipe. The governing equations are as follows:

$$\frac{\partial A}{\partial t} + \frac{\partial Q}{\partial x} = q \tag{4.4}$$

$$\frac{\partial Q}{\partial t} + \frac{\partial (uQ)}{\partial x} = -gA\left(\frac{\partial H_p}{\partial x} + \frac{n^2|Q|Q}{R^{4/3}A^2}\right) \tag{4.5}$$

where A is the wet area of the cross section, Q is flow discharge, q is lateral inflow discharge per unit pipe length ($q_{sew\text{-}g} + q_{sew\text{-}d}$), $q_{sew\text{-}d}$ is drainage discharge from the drain box to the sewer pipe per unit area (if its value is negative, that means over flow discharge from the sewer pipe), u is velocity, R is hydraulic radius, and n is roughness coefficient. H_p is piezometric head ($H_p = Z_p + h_p$), Z_p is bottom elevation of the sewer pipe, and h_p is water depth determined as follows:

$$\mathrm{h}_p = \begin{cases} f(A) & : A \le A_p \\ D + \frac{(A - A_p)}{B_s} & : A > A_p \end{cases} \tag{4.6}$$

$$\emptyset = 2cos^{-1}\left(1 - 2\frac{\mathrm{h}_p}{d}\right) \tag{4.7}$$

$$\frac{A}{A_p} = \frac{\emptyset - sin\emptyset}{2\pi} \tag{4.8}$$

$$\frac{R}{R_p} = 1 - \frac{sin\emptyset}{\emptyset} \tag{4.9}$$

where f is a function of the relationship between water depth and the wet area of the cross section of a circular pipe, A_p is the cross sectional area of the pipe, D is pipe diameter, and B_s is slot width, which can be determined and calculated by Equation (3.8) with pressure propagation velocity a.

4.6.2.3 Drain box model: governing equation for drain box and upstream tank

A pipe / channel network is a topological set of nodes and links (Djordjević et al., 2004). From this perspective, the drain box and upstream tank act as nodes. The governing equation for the drain box is as follows:

$$F_d \frac{dZ}{dt} = q_{drain} - q_{sew-d} \tag{4.10}$$

where F_d is a horizontal area of the drain box, Z is water level at the drain box, and $q_{sew\text{-}d}$ is

drainage discharge from the drain box to the sewer pipe (if its value is negative, that means over flow discharge from the sewer pipe). The flow in the drain channel that connects the drain boxes is neglected because its discharge is too small to be significant.

The governing equation for the upstream tank is as follows:

$$F_t \frac{dZ}{dt} = q_p \tag{4.11}$$

where F_t is a horizontal area of the upstream tank, Z is the water level at the upstream tank, and q_p is outlet discharge from the upstream tank to the sewer pipe (if its value is negative, that means input discharge to the upstream tank from the pipe). The relationship between the flow variables, nodes, and link endpoints will be described later.

4.6.2.4 Interaction model between the ground surface and drainage box

Storm water on the ground surface computational mesh with storm drain mesh is drained through the drain box. Drainage discharge is calculated by the weir and orifice formulas:

Weir formula:

$$\mathrm{Q} = \frac{2}{3} C_{dw} L_1 \sqrt{2g} (h_m - h_d)^{3/2} : (h_m - h_d) \leq B_{01}/2 \tag{4.12}$$

Orifice formula:

$$\mathrm{Q} = C_{do} A_d \sqrt{2g(h_m - h_d)} : (h_m - h_d) > B_{01}/2 \tag{4.13}$$

where Q is drainage discharge from the ground surface into the drain channel, h_m is water level on the ground surface, h_d is the piezometric head of the drainage box, and A_d is a vertical area of storm drain. C_{dw} and C_{do} are the coefficients of the weir and orifice formulas taken as 0.48 and 0.57, respectively, as suggested in Chapter 2. B_{01} is the smallest width of the storm drain, and L_1 is the perimeter length of the storm drain. Storm water is assumed to be drained immediately into the drainage box.

When the piezometric head exceeds the water level on the ground surface, inundation on the ground begins to occur from the storm drain. Overflow discharge is calculated by the following overflow formulas:

Weir formula:

$$Q = -\frac{2}{3} C_{dw} L_1 \sqrt{2g} (h_d - h_m)^{3/2} : (h_d - h_m) \leq B_{01}/2 \quad (4.14)$$

Orifice formula:

$$Q = -C_{do} A_d \sqrt{2g(h_d - h_m)} : (h_d - h_m) > B_{01}/2 \quad (4.15)$$

The negative sign on the right side denotes surcharge flow onto the ground surface.

4.6.2.5 Interaction model between the drainage box and sewer pipe

Storm water on the drain box computational mesh with sewer pipe segment is drained through the drainage tube (dark blue line in Figure 4.3). Drainage discharge is calculated by the weir and orifice formulas:

Weir formula:

$$Q = \frac{2}{3} C_{dw} L_2 \sqrt{2g} (h_d - h_p)^{3/2} : (h_d - h_p) \leq B_{02}/2 \quad (4.16)$$

Orifice formula:

$$Q = C_{do} A_u \sqrt{2g(h_d - h_p)} : (h_d - h_p) > B_{02}/2 \quad (4.17)$$

where B_{02} is the smallest width of the drainage tube and L_2 is the perimeter length of the drainage tube. Storm water is assumed to be drained immediately into the sewer pipe.

When the piezometric head in the sewer pipe exceeds the water level in drain box, pressurized storm water begins to flow from the sewer pipe. Surcharge flow discharge is calculated by the following overflow formula:

Weir formula:

$$Q = -\frac{2}{3} C_{dw} L_2 \sqrt{2g} (h_p - h_d)^{3/2} : (h_p - h_d) \leq B_{02}/2 \quad (4.18)$$

Orifice formula:

$$Q = -C_{do} A_u \sqrt{2g(h_p - h_d)} : (h_p - h_d) > B_{02}/2 \quad (4.19)$$

The negative sign on the right side denotes surcharge flow into the drain box.

Storm water that falls into drainage box, onto a roof, or onto the ground surface is treated separately. In this study, there is a small area of computational mesh for the drainage box and building roof, and storm water is drained or overflowed according to Equations (4.12) ~ (4.19). Storm water that falls onto the drainage box or the roof of a building drains immediately into the sewer pipe, and overflow from the sewer pipe flows into the drain box immediately. Figure 4.8 describes these interaction-models.

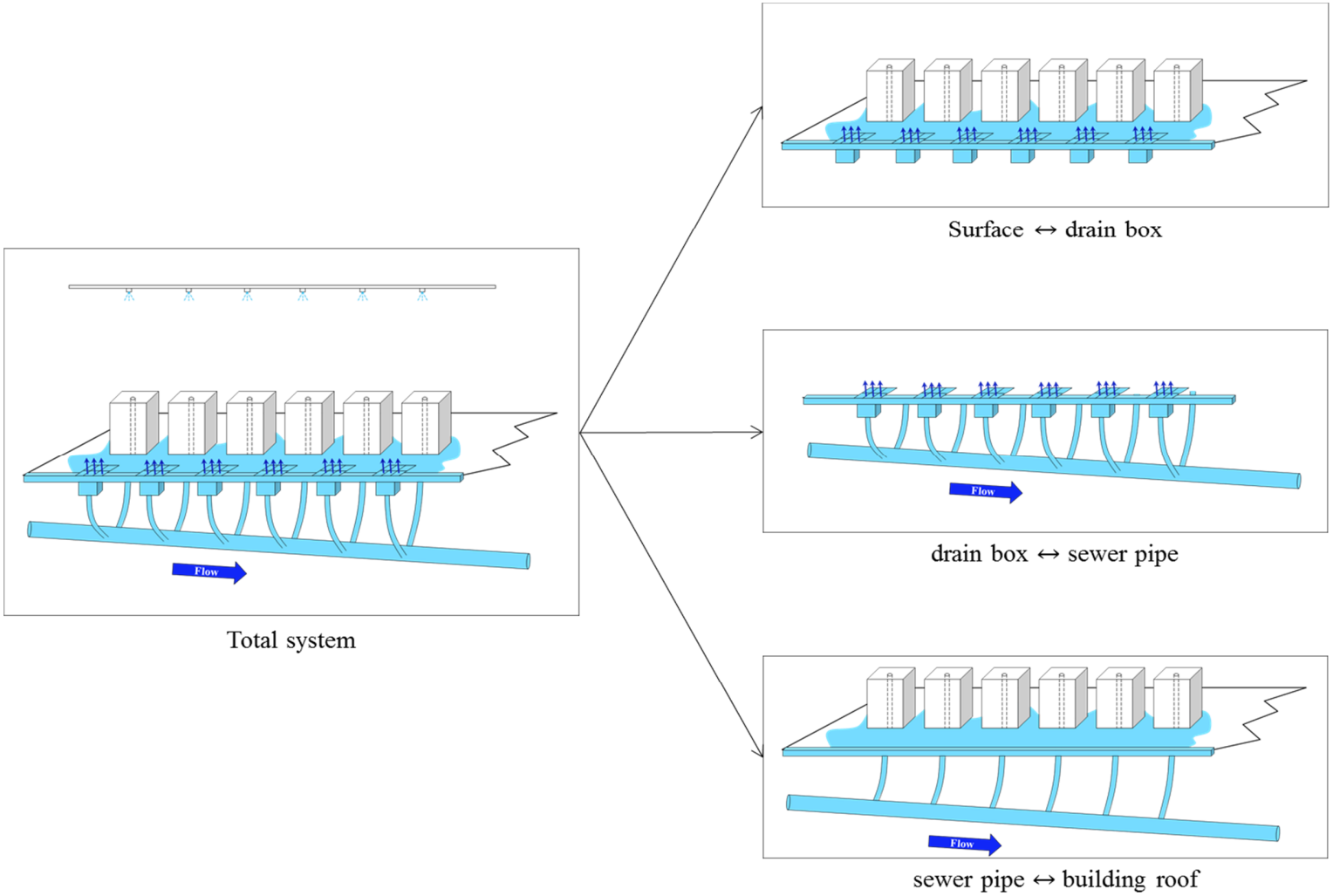

Figure 4.8 Interaction modeling concept between ground surface, drain box and sewer pipe

4.6.2.6 Exchange discharge between the upstream tank and sewer pipe

Although Equation (4.11) is used to calculate the water depth of the upstream tank, the exchange discharge between the upstream tank and the sewer pipe requires special treatment because the upstream tank is assumed to be a manhole in this study. If the hydraulic head in the tank is higher than the next sewer pipe's head, then the storm water on the tank mesh is discharged into the sewer pipe. The the outlet discharge is then calculated with the following orifice formulas:

In the case of $h_p/h_t \leq 2/3$

$$\mathrm{Q} = C_1 A_t \sqrt{2gh_t} \tag{4.20}$$

In the case of and $h_p/h_t > 2/3$

$$\mathrm{Q} = C_2 A_p \sqrt{2g(h_t - h_p)} \tag{4.21}$$

Q is this positive direction outlet discharge, A_t is the wet area of the virtual pipe cross section of the upstream tank (this calculation method will be explained later), h_t is water depth of the tank from the bottom of the next sewer pipe, A_p is the wet area of the pipe cross section, h_p is hydraulic head in the next sewer pipe, and c_1 and c_2 are the coefficients 0.35 and 0.91, respectively.

If, on the other hand, the pressure head of the next sewer pipe connected to the downstream tank is higher than the tank pressure head, then storm water flows into the downstream tank. This is calculated using the following formulas:

In the case of $h_t/h_p \leq 2/3$

$$\mathrm{Q} = C_3 A_p \sqrt{2gh_p} \tag{4.22}$$

In the case of $h_t/h_p > 2/3$

$$\mathrm{Q} = C_4 A_t \sqrt{2g(h_p - h_t)} \tag{4.23}$$

In order to calculate exchange discharge between the sewer pipe and the upstream tank, it is necessary to obtain the A_t value which can be called as the virtual pipe cross section of upstream tank. Figure 4.9 shows that A_t can be calculated using the hydraulic characteristic curves of the circular sewer pipe.

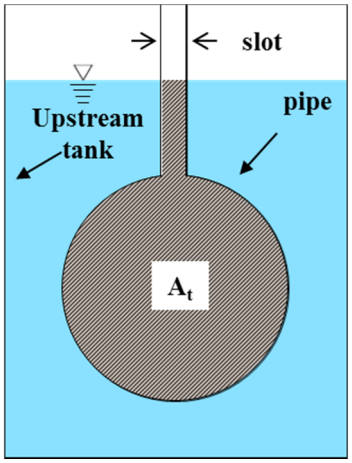

Figure 4.9 Calculation concept of virtual pipe cross section of upstream

- The shape of the first segment of pipe is projected onto the upstream tank
- Upstream tank is assumed to be a pipe
- A_t is calculated using water elevation in the upstream tank

The downstream A_t can be calculated using this method.

4.7 Results and Analysis

Numerical simulations and experiments were performed to investigate the applicability of this model to four kinds of flow regimes and pressurized processes in the sewer pipe. An exchange discharge interaction between the surface and sewer system, which was based on ascending and descending downstream water levels was also confirmed. Changes in piezometric head in the pipe and variations in inundation depth on the ground surface over time were illustrated in Figures 4.11 through 4.15. To simulate the urban inundation process with the sewer system, a distributed 2D runoff flow model for the ground surface and a 1D Preissmann slot model for the sewer pipe were integrated with coupling models. This combination of models simulated the exchange drainage and overflow discharge between a runoff flow model and the sewer pipe model; the simulation included special treatments of the interactions among the upstream tank, the downstream tank, and the sewer pipe.

4.7.1 Steady-state conditions

Figure 4.10 (g) shows the experimental and simulated results under fully pressurized conditions. In these conditions, water on the ground surface was drained to the sewer pipe through drainage boxes downstream, with coexistence of overflow upstream under no-rainfall

conditions. Simulation results of sewer pipe piezometric head and inundation depth agreed well with the experimental results. It was easy to understand that the water in the sewer pipe was overflowing to the ground surface when the piezometric head was higher than the ground surface elevation. On the other hand, although piezometric head in the sewer pipe was higher than ground surface elevation, the water on the ground drained to the sewer pipe through the drain box because water elevation on the ground was higher than the piezometric head 8m upstream. It is important to note that the hydraulic grade line was not a straight line because the amount of exchange discharge at every connection within the drain box in the sewer pipe differed according to each piezometric head in the pipe and water level in drain box. This phenomenon is caused by complex interaction effects.

Figures 4.10 (a) through (g) compare the experimental and simulation results of the model. These cases were designed to confirm the model's applicability to three kinds of flow regimes: open flow, partially pressurized flow, and fully pressurized flow. The simulation results are in good agreement with experimental results. Figure 4.10 (h) shows simulated and experimental results with rainfall conditions. In this case inflow discharge was 1.537*l/s* and the downstream water level was 0.378m. It is worth noting that the inflow discharge of CASE-8 is greater than for CASE-7. However, the inundation depth on ground surface, as well as piezometric head in the pipe were lower than for CASE-7 because of lower downstream water levels than in CASE-8. These experimental results suggest that the capacity of the sewer system is flexible depending on downstream water levels. Therefore downstream water levels and interaction effects should be considered in order to design a sewer system with the maximum capacity.

4.7.2 Unsteady-state conditions

Figure 4.11 shows variations in the sewer pipe's piezometric head and water levels in the upstream water tank. Figure 4.12 shows simulated results of inundation water depth distribution over time. Figure 4.11 (a) shows water level variations in the upstream water tank based on changes in downstream water level. The downstream water level changed with a nearly straight slope, while variations in the upstream water tank showed curved lines with two inflection points for each ascending time and descending time. These phenomena were directly related to the inundation timing on the ground surface. For instance, the two inflection points were found at 920 seconds and 1090 seconds on an ascending curve. At the same times, inundation occurred on the ground surface as shown in Figure 4.11 (e). Similarly, inflection points on the descending curve at 1600 seconds and 1690 seconds reflected the endings of the drainage processes. The drain box explained the occurrence of different slopes with these inflection points at the center.

The occurrence of inundation on the ground indicates that a storm drain is full of water overflowing from the sewer pipe. If there is no connection with the ground surface, the overflow discharge from the upstream tank is completely determined by downstream water level. Therefore, the water level of the upstream tank may increase linearly before inundation occurs because there is no other exit. This has already been confirmed by the experimental results in described in Chapter 3. On the other hand, the increasing gradient of the upstream water level starts to decrease after ground surface inundation begins to occur; this is because outlet discharge can inundate the ground surface. The opposite phenomena will occur after passing the maximum inundation depth. For example, the decreasing slope of the upstream water level is very mild at around 1600 seconds, and the slope begins to drop drastically.

These phenomena are also strongly related to be drainage process of inundated water on the ground surface. Maximum inundation depth is recorded at 1270 seconds and then the drainage process concludes at approximately 1600 seconds, at which point the drained discharge abates the decrease of the piezometric head in the sewer pipe. However, the outlet capacity of the sewer pipe increases depending on decreases in the downstream water level; the water level in the upstream tank is drastically lowered as soon as the drainage process on the ground surface ends. These effects are observed in Figure 4.11 (a) ~ (d) and the effects are reduced according to the distance between the downstream tank and their own position.

Inundation overflow starts upstream and gradually extends downstream. This model reproduced not only the maximum inundation depth on the ground, but also different inundation start times upstream and downstream as shown in Figure 4.12.

Experimental CASE-II was designed to identify the effect of duration time using the same maximum downstream water levels as in CASE-I. Figure 4.13 shows the experimental and simulated data. Figure 4.13 (a) shows water level variations in the upstream water tank according to the downstream water level changes. Two inflection points for each ascending and descending time periods are identified in Figure 4.13 (a). The difference between the two inflection points is relatively mild; they can be found at 1,580 seconds and 2,220 seconds on an ascending curve. At the same time, inundation occurred on the ground surface as shown in Figure 4.13 (e). Variations in the upstream water tank and in each piezometric head show curve lines similar to CASE-I as shown in Figure 4.15.

As seen in CASE-I, inflection points on the descending curve at 3,700 seconds and 3,900 seconds reflect the end of the drainage process. Maximum inundation depth is recorded at 2,750 seconds and the drainage process ends at around 3,900 seconds. At this point drained discharge is used to abate the decrease of piezometric head in the sewer pipe. Generally, variations in the

piezometric head of P2, P5, P9 reflect trend similar to CASE-I, as shown in Figure 4.13 (b) ~ (d). In addition, the duration time is directly proportional to the maximum upstream tank water level, inundation depth on the ground surface, and piezometric head. The duration time of CASE-II (3,270 seconds) is about 3.7 times longer than CASE-I (880 seconds), and the maximum inundation depth of CASE-II (4.7cm) is higher than CASE-I (2.5 cm).

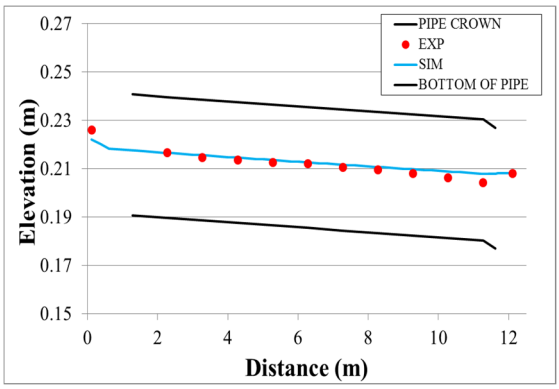

(a) CASE-1

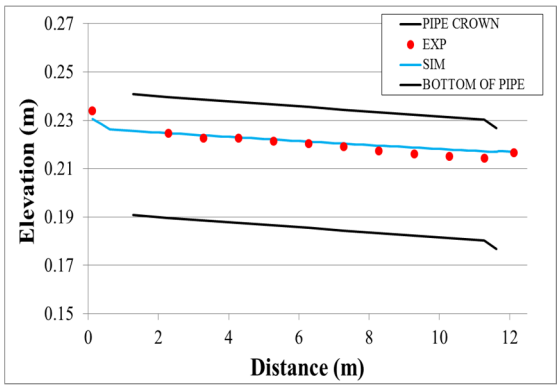

(b) CASE-2

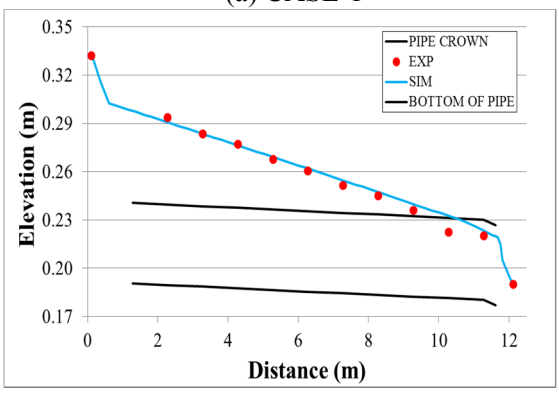

(c) CASE-3

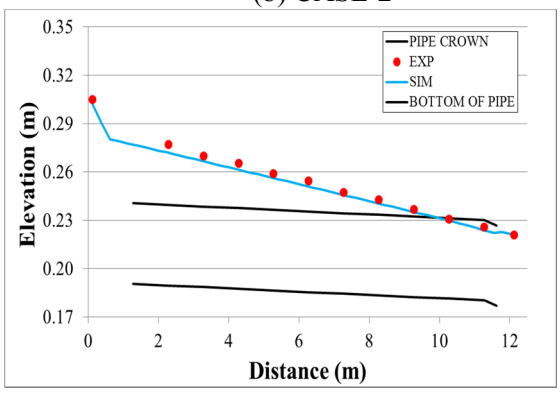

(d) CASE-4

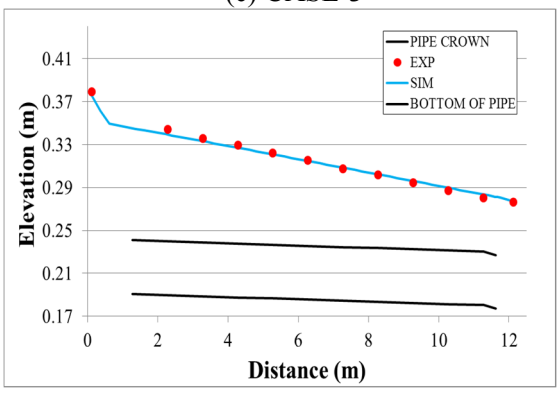

(e) CASE-5

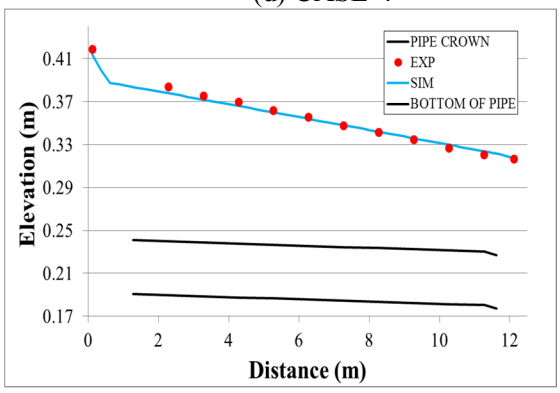

(f) CASE-6

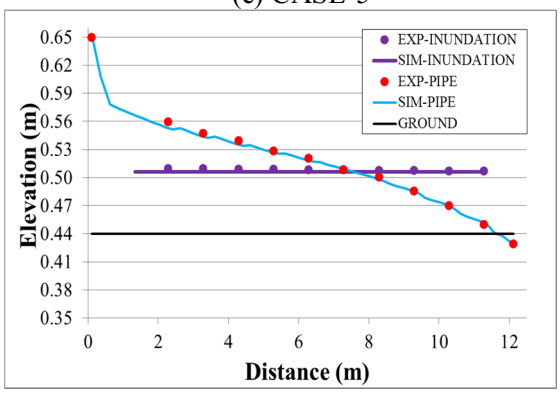

(g) CASE-7

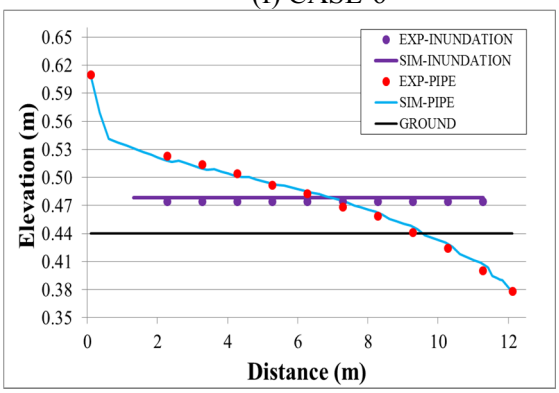

(h) CASE-8

Figure 4.10 Comparison of piezometric head and inundation depth under steady-state condition

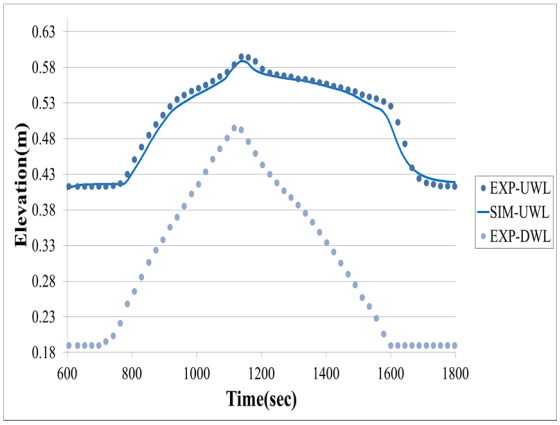

(a) Upstream tank water level change

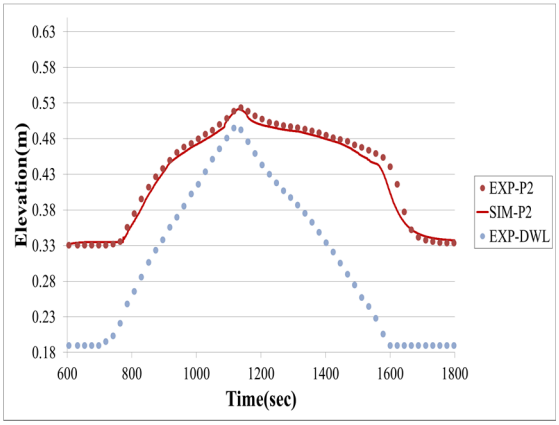

(b) Piezometric head change of P2

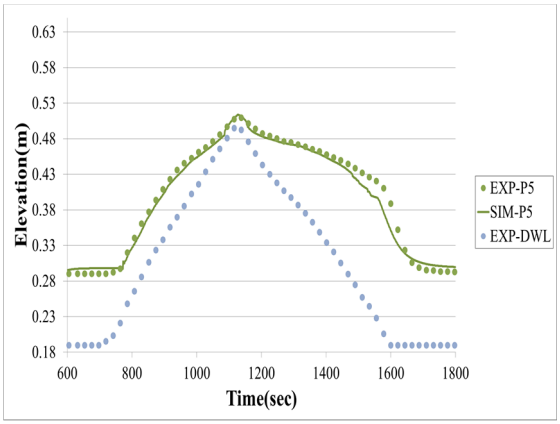

(c) Piezometric head change of P5

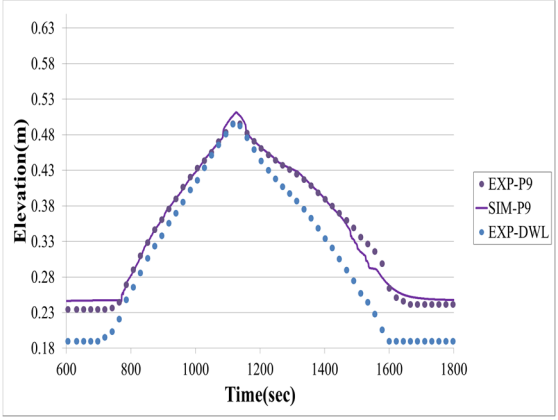

(d) Piezometric head change of P9

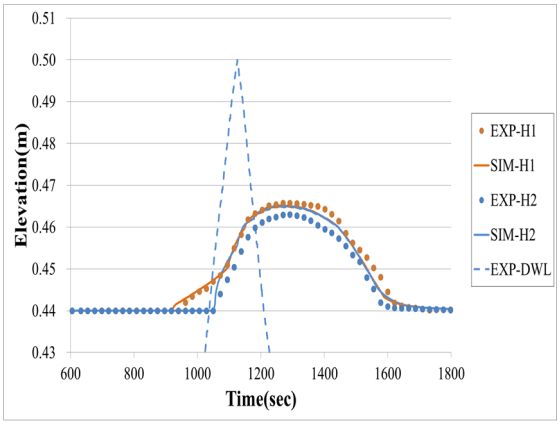

(e) Inundation depth change

Figure 4.11 Comparison of experimental and simulated results of (CASE-I)

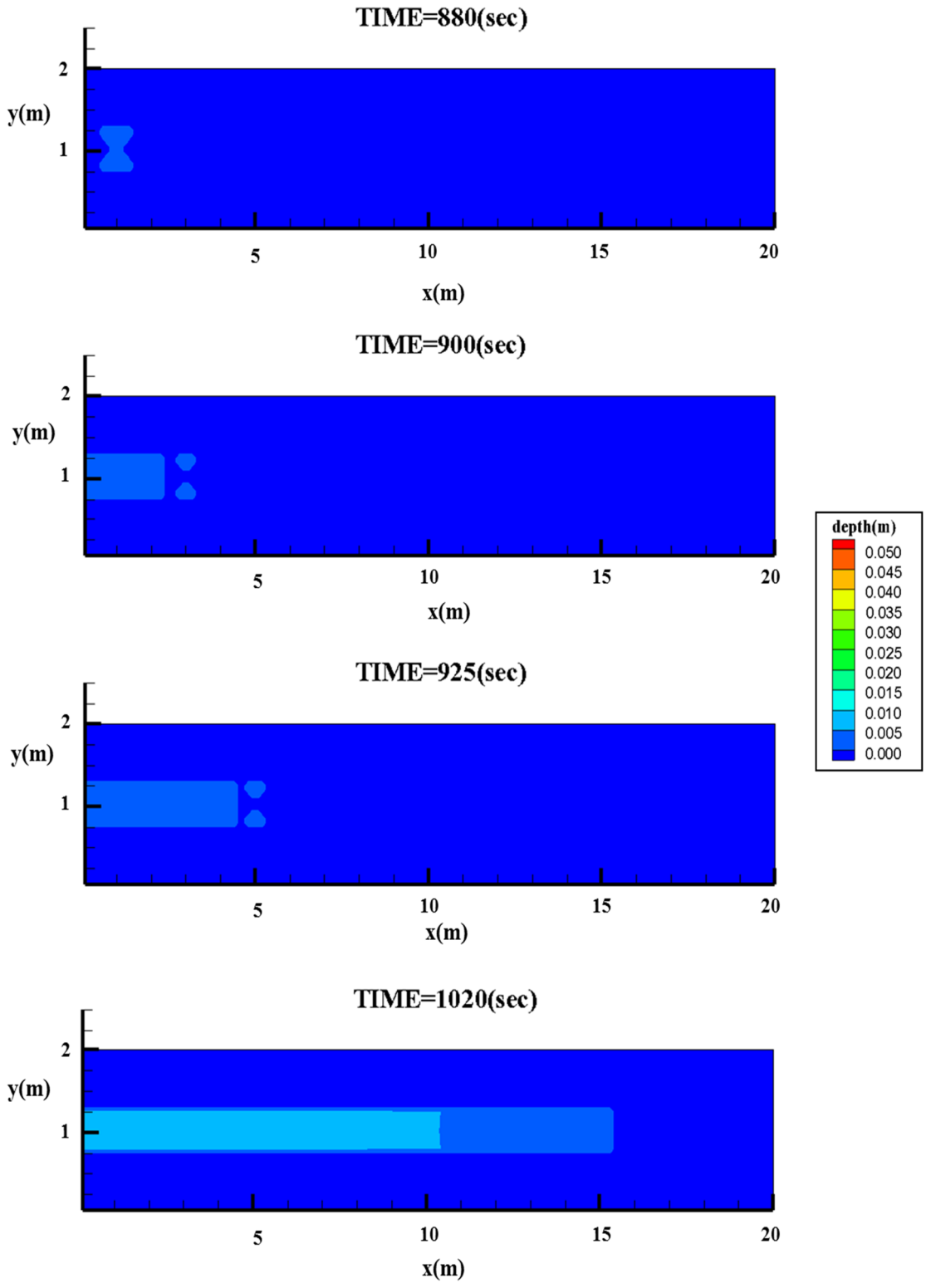

Figure 4.12 Variation of inundation depth on ground surface (CASE-I)

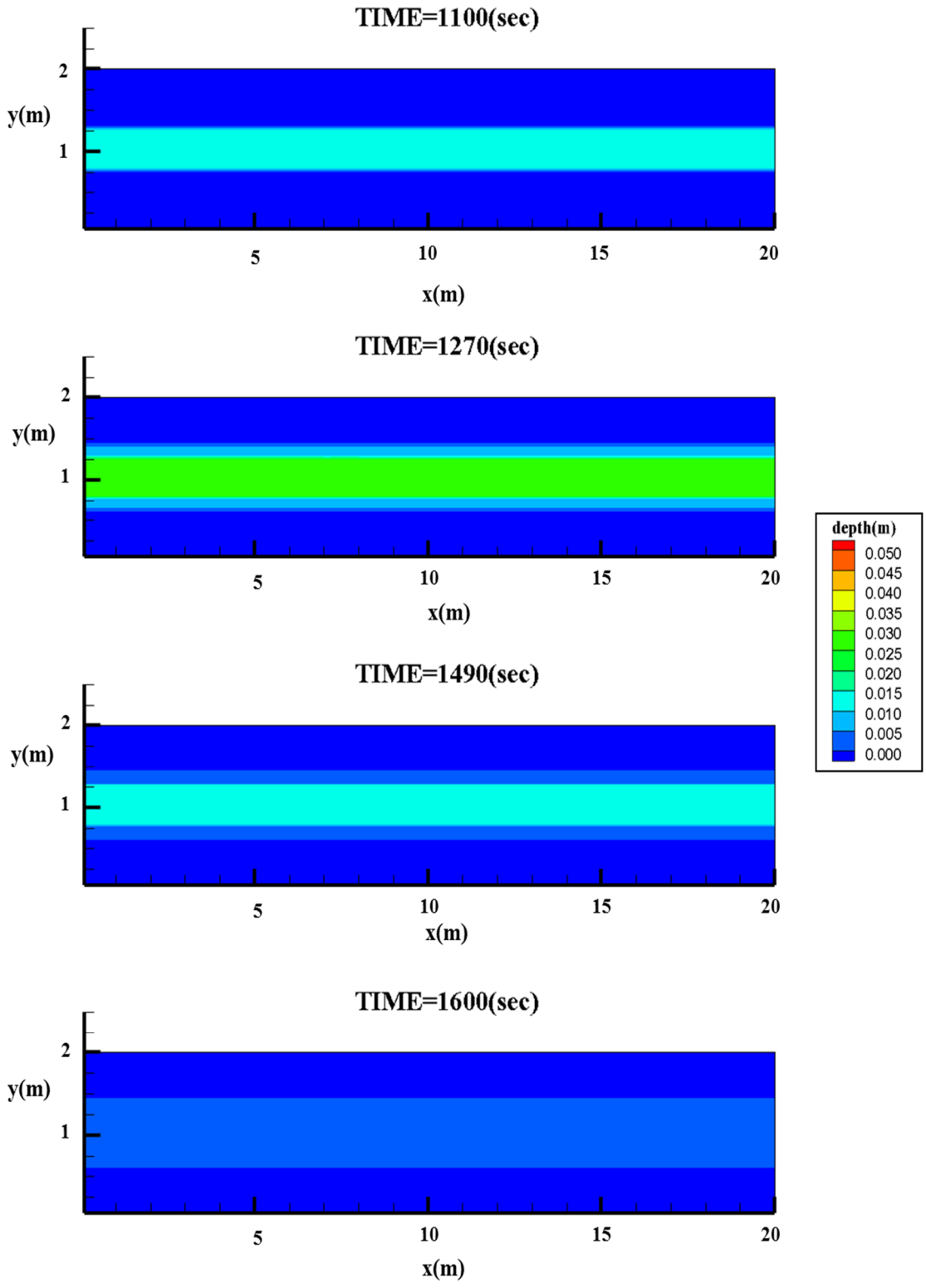

Figure 4.12 Variation of inundation depth on ground surface (CASE-I) (continue)

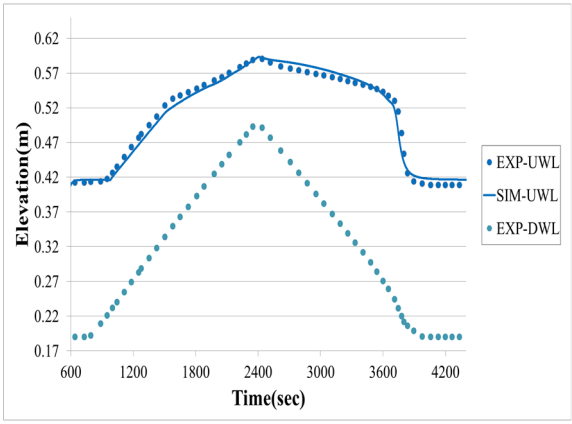

(a) Upstream tank water level change

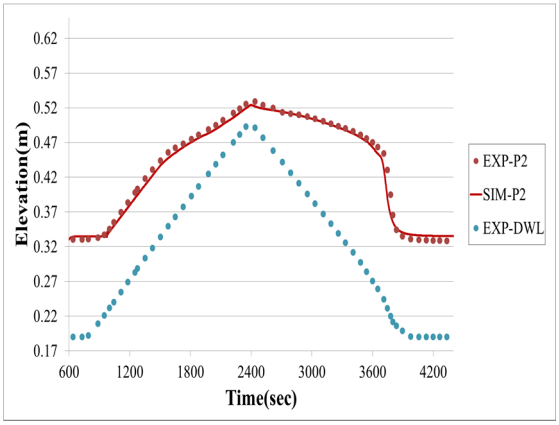

(b) Piezometric head change of P2

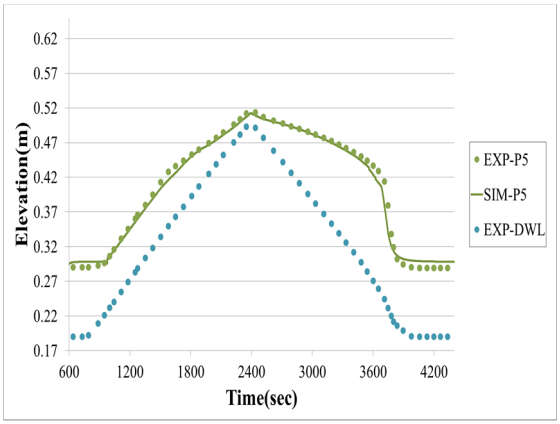

(c) Piezometric head change of P5

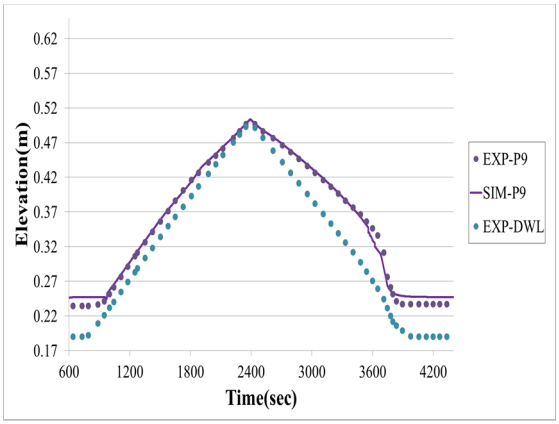

(d) Piezometric head change of P9

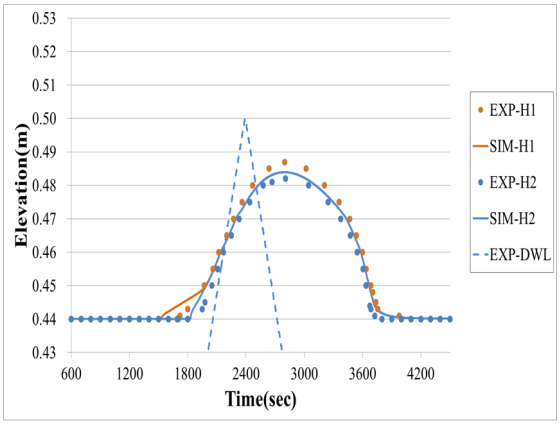

(e) Inundation depth change

Figure 4.13 Comparison of experimental and simulated results of (CASE-II)

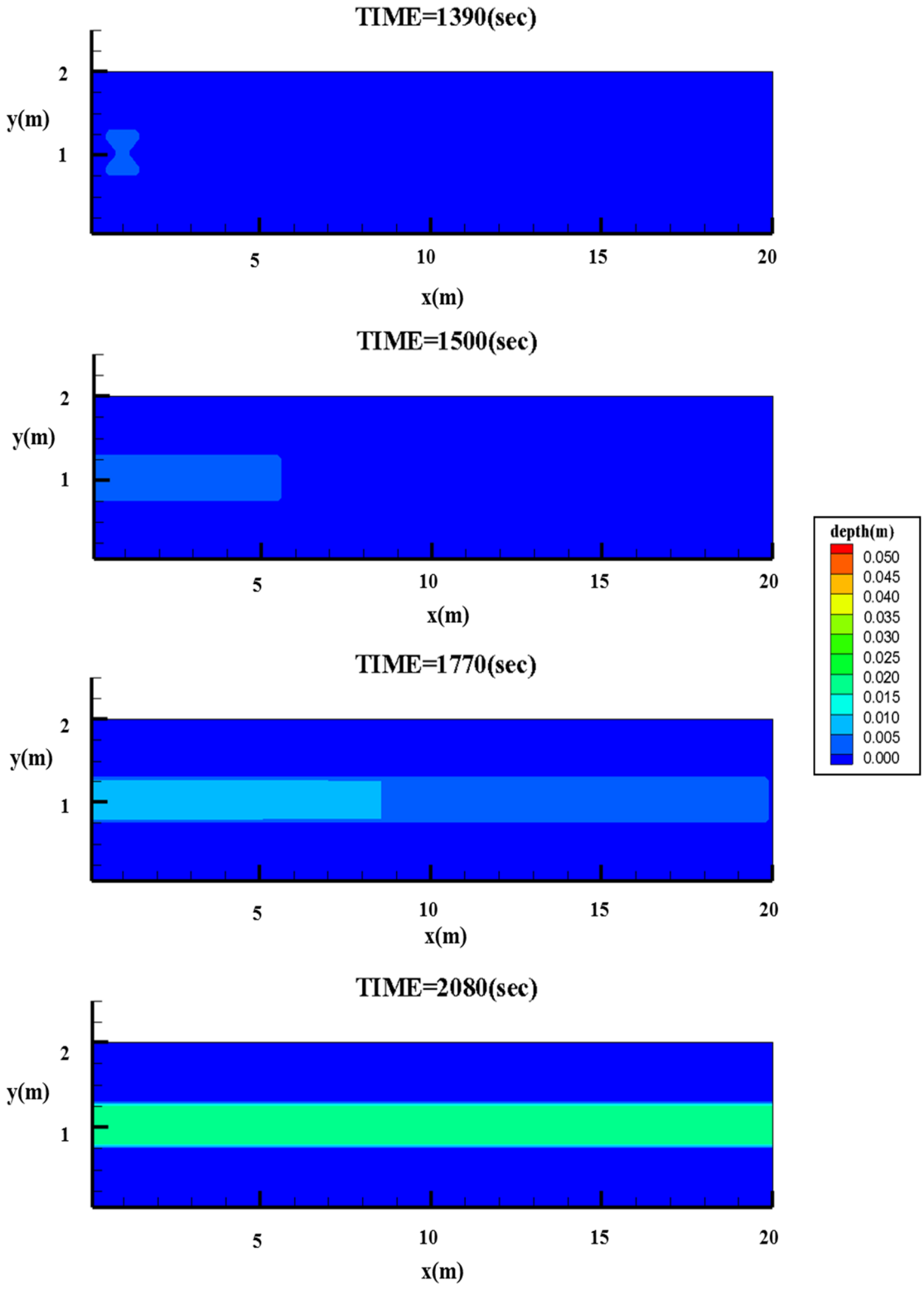

Figure 4.14 Variation of inundation depth on ground surface (CASE-II)

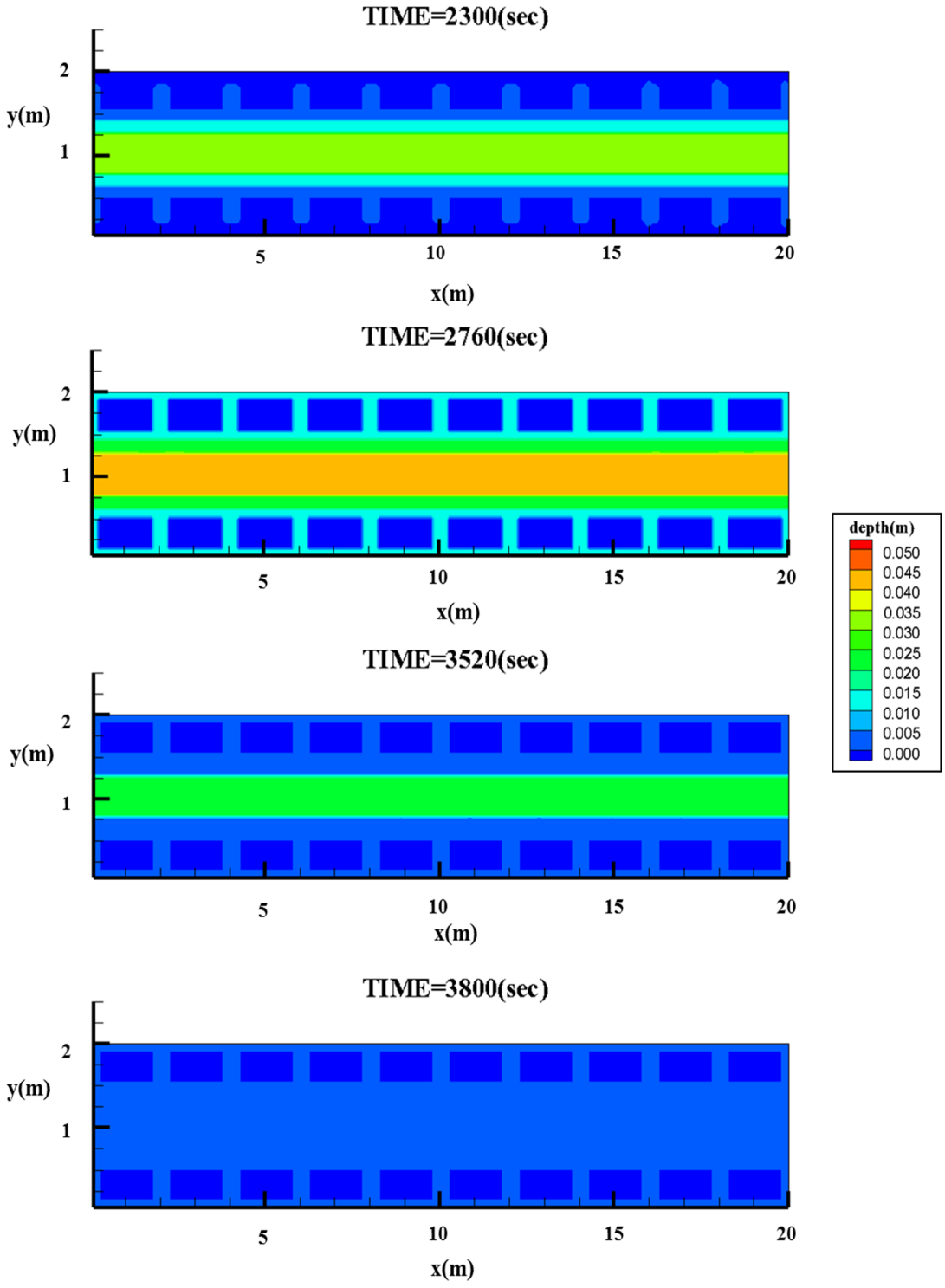

Figure 4.14 Variation of inundation depth on ground surface (CASE-II) (continue)

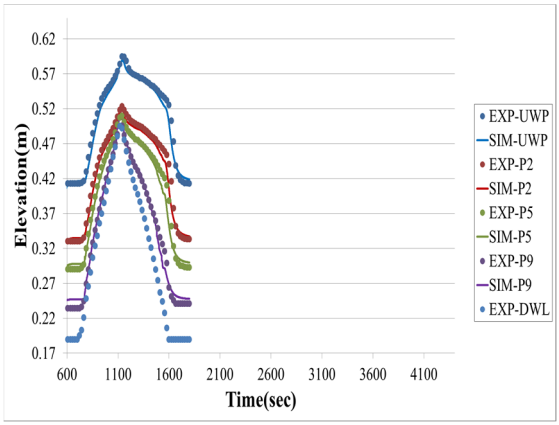

(a) Piezometric head change of CASE-I

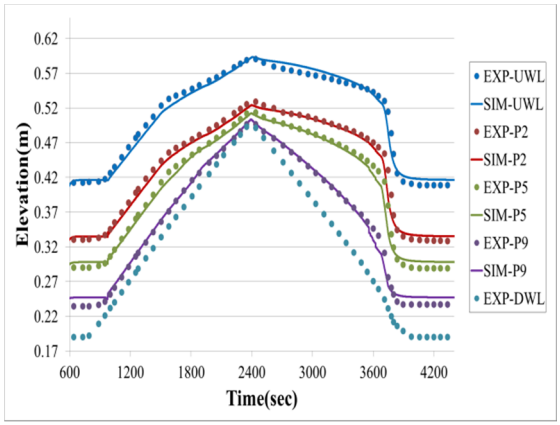

(b) Piezometric head change of CASE-I

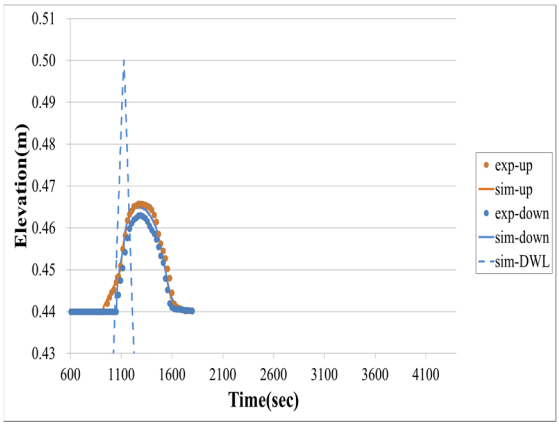

(c) Inundaton depth variation of CASE-II

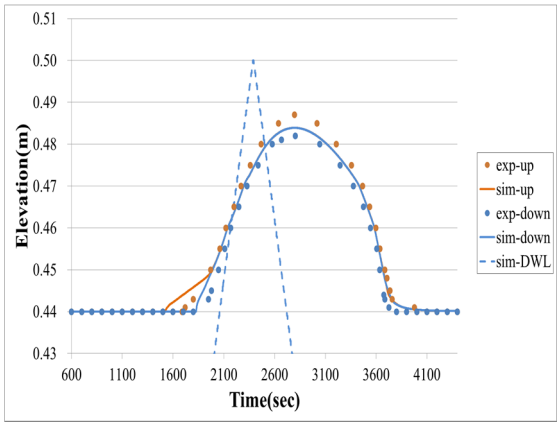

(d) Inundaton depth variation of CASE-II

Figure 4.15 Comparison of CASE-I and CASE-II with same time range

Figure 4.14 shows variations in inundation depth on the ground surface in CASE-II, reproducing a propagation trend not only from upstream to downstream, but also between buildings.

The experimental and simulated results showed very good agreement for steady-state cases and unsteady-state cases. In the steady-state cases, simulation results reproduced experimental inundation depths on the ground surface as well as piezometric head in the sewer pipe. In the unsteady-state cases, the results reproduced not only maximum inundation depth on the ground, but also increasing and decreasing timing. Moreover, various hydraulic interaction phenomena were identified and analyzed. It can be stated, therefore, that the interaction models for the surface, drain box, and sewer pipe are applicable to steady-state and unsteady-state conditions. This model can be used extensively to predict severe urban inundation occurrence, which will assist in the development of action plans.

4.8 Summary

Numerical analyses and experimental studies were carried out to investigate interactions between the sewer system and the ground surface under steady-state and unsteady-state conditions. A two-dimensional runoff model and a one-dimensional Preissmann slot model were adapted for urban inundation analysis in order to simulate discharge exchange between the sewer system and ground surface under a variety of flow conditions. Under steady-state conditions with or without rainfall, calculation results for inundation depth on the ground surface and piezometric head in the sewer pipe agreed with experimental results. In addition, simulation results of steady-state conditions reproduced the coexistence of overflow and drain phenomena with stable inundation depths on the ground surface.

Experimental results for unsteady-state cases confirmed many hydraulically interesting phenomena. First upstream water level and piezometric head are affected not only by downstream water level, but also ground inundation circumstances. Second, the drain box is an important factor in urban inundation simulation because it changes the inflection point of the slope. This means that if there is no connection with the ground surface, the overflow discharge from the upstream tank is completely determined by downstream water level; the water level of the upstream tank may be increased linearly before inundation occurs due to the lack of an exit. Third, duration time and high downstream water levels could contribute to inundation depth, as indicated by the experimental results of CASE-I and CASE-II. Finally, in unsteady-state cases, the experimental results reproduced not only the maximum inundation depth on the ground, but also the increasing and decreasing timing. Every interaction model and special treatment effectively reproduced experimental results in the integrated model. therefore, this model can be used extensively to predict severe urban inundation and help develop action plans.

CHAPTER 5

CONCLUSIONS AND RECOMMENDATIONS

In this study, laboratory experiments of inlet discharge through storm drain, interaction effects of storm water between the manhole and pipes, and bidirectional interaction between ground surface and sewer system, were carried out for developing an integrated urban inundation model. In the first experiments, the inlet flow from ground surface to sewer system can be divided by the relation between flow depth and smallest width of storm drain cover as weir flow and orifice flow. $H_t / b_0 = 0.5$ could be criterion to decide flow pattern. In the second experiments, interaction effects of storm water at the manhole were investigated according to different manhole shapes and pipe configuration. In addition to that, a one-dimensional numerical model was developed incorporating the momentum equation and dynamic equation based on the rigid column theory. Finally, the inundation mechanism and the applicability of the inlet discharge calculation method were validated through the integrated experimental facility that consists of a rainfall simulator, ground surface with building, storm drain box, and sewer pipe. The conclusions based on the studied cases are to be interpreted within this chapter. These conclusions are summarized in the following section. The final section gives some recommendations for developing a more reasonable integrated urban inundation model.

5.1 Conclusions

Since the results of the present study have been investigated and analyzed in the previous chapters, the most important conclusions are summarized as follows.

5.1.1 Inlet discharge through the storm drain

In order to investigate the storm water interaction between the ground surface and lower-layer part, and to suggest new coefficients to calculate inlet discharge, laboratory experiments were carried out with the square and gird type storm drain cover under the steady-state flow condition. The flow showed two kinds of patterns: free surface flow and non-free surface flow in the storm drain, depending on the relation between the smallest width of storm drain cover and water depth. The flow patterns were categorized by the relations. Weir and orifice formulas

were adapted to represent the flow patterns, and various experiments were conducted to evaluate their coefficients.

The weir discharge coefficient was obtained through experimental data was initially 0.381, and the orifice coefficient was 0.51. Although the relation suggested by Chanson et al. (2002) showed an acceptable trend line, the simulation result was approximately 1.5 ~ 14% smaller than the experimental data when the initial values that were obtained by experimental data were used. Therefore each coefficient was revised and changed by trial and error method which considers velocity head. Finally they were decided as C_{dw} = 0.48 and C_{do} = 0.57. The modified coefficients show acceptable results, and the reason why each coefficient should be changed was judged from the fact that the water depth was used instead of total head in the simulation. This means that the flow water depth has higher energy than static water, so that the small value of the velocity head was used when both coefficients were analyzed.

An interesting factor to note here is that there is no significant difference between the square type and grid type coefficients. Generally, different shapes have different coefficients when discharge is calculated by the weir or the orifice formula. The reason why they have the same value of the coefficients could be explained by the fact that the grid space is too wide to represent its shape property so that there is no significant difference between grid and square storm drain cover areas. Two cover shapes were designed only to distinguish the general form of the storm drain cover shape but not the physical values such as cross-sectional area, perimeter of storm drain, etc.

Simulations were carried out to estimate the applicability of the suggested formulas, coefficients, and criteria. The simulation results of the inlet discharge depending on the change of water depth are in good agreement with the experimental results.

5.1.2 Interaction effect of storm water between the manhole and pipes

To investigate the effects of head losses at the manhole depending on different manhole shapes and pipe configurations, laboratory experiments were carried out under the various experimental conditions using the straight and adjunction pipe with no benching and no invert.

First, straight cases were conducted in order to evaluate the head loss according to manhole shape (circular and square type) under the unsteady-state as well as the steady-state condition. The head loss coefficient shows constant values regarding the manhole shapes, and each coefficient is obtained as 0.259 and 0.235 for the circular and square type manhole shapes, respectively.

Second, three pipe case experiments were carried out to investigate the effects of the head

loss caused by pipe configurations under steady-state and unsteady-state conditions. In three pipes cases with different manhole shapes, it was observed that the head loss of the square shape is higher than the circular shape, and the gap between the longitudinal coefficients (K_1) of square and circular manhole types decreases with an increasing ratio of Q_2/Q_3 in 90° cases. In addition, the difference of the lateral coefficient (K_2) was increased along with the ratio of Q_2/Q_3 in the opposite way with longitudinal coefficients. The analysis shows that the lateral input discharge disturbs the longitudinal flow and causes increasing head losses at the manhole. This effect is seen to be stronger at the square shape manhole than at the circular shape.

In addition, although the increasing tendency of both longitudinal and lateral coefficients shows a similar trend with almost the same value in three different adjoining angles, they start to deviate into different patterns from $Q_2/Q_3 = 0.5$. Empirical relations were developed to calculate head loss depending on manhole shapes and pipe configuration through all the experimental cases.

A one-dimensional numerical model was developed for computing the hydraulic characteristics of the pipe flow with the manhole. The proposed model was tested for different experimental conditions using different manhole shapes and various pipe configurations. The simulated results are in good agreement with the experimental results for not only the pressure head profile under the steady-state condition, but also the pressure head change according to time under the unsteady-state condition.

5.1.3 Exchange discharge between ground surface and sewer pipe

The mechanisms of discharge exchange between overland flow and sewer system differ according to relations among the pressure head in pipe, the pressure head in the storm drain box, and the water depth on the ground surface. To confirm these complex mechanisms, numerical analysis and experimental studies were carried out under steady-state and unsteady-steady conditions.

Experimental results of unsteady-state cases confirmed many hydraulically interesting phenomena. Generally, pipe flow patterns are affected by downstream water depth, already confirmed in Chapter 3. However, upstream tank water level and piezometric head were affected by not only downstream water level, but also ground inundation circumstance. For instance, if the pressure in the pipe cannot reach the ground elevation, the water only flows along the pipe. It is an even, pressurized flow condition in the sewer pipe because there is no additional outlet for the flowing water. However, the pressure can reach the ground surface elevation. The water may have an additional flow direction instead of only flowing along the

pipe, and this phenomena was revealed at different inflection points in the piezometric head change curve under unsteady-state condition. In addition, it was proved that the drain box was not a negligible factor in the urban inundation because the occurrence of a different slope with the inflection point can be explained by the existence of the drain box. There are two governing cross-sections, the storm drain cover and the connection tube, from the ground surface to the sewer pipe. Although the pressure head in the sewer pipe has higher value than the storm drain the exchange discharge is governed by the storm drain box because the overflow discharge should pass both the connection tube and the storm drain cover at once. In this case, a small value governs the exchange discharge.

CASE-I and CASE-II were designed to estimate the difference of the inundation depth depending on the duration time. Both experimental results showed that a longer duration time may cause severe inundation damage.

A two-dimensional runoff flow model and a one-dimensional Preissmann slot model were incorporated for urban inundation analysis involving three kinds of subroutine for computing the exchange discharge. Simulated results of the steady condition could reproduce a coexistence of overflow and drain phenomena with stable inundation depth on the ground surface. The model successfully represented the discharge exchange between the sewer system and the ground surface, as well as all flow conditions such as open flow, partially-pressurized flow, and fully-pressurized flow under the unsteady-state condition. In addition, the simulated results of the inundation depth on the ground surface and piezometric head in the sewer pipe of the steady cases, without rainfall and with rainfall, are in good agreement with the experimental results. Finally, not only the maximum inundation depth on the ground, but also ascending and decreasing timing could reproduce the experimental results very well in the unsteady-state cases.

5.2 Recommendations for Future Researches

This study has led to a better understanding of several important things related to the estimation of inlet discharge through a storm drain, assessment of head losses effects regarding manhole shapes and pipe configurations, and the detailed interaction between surface flow and sewer pipe flow involving storm drain boxes caused by the variation of downstream water level. It has also verified the development of a numerical model to serve as a tool to predict the inlet and overflow through the storm drain, to simulate the head loss effect depending on manhole shapes and pipe configurations, as well as the discharge exchange between the ground surface

and the sewer pipe considering storm drain boxes. All simulation results showed good agreement with experimental results, however the application of the model to real basin and laboratory scale experiments under various conditions are still remained as a task to be performed. Below are some suggested issues for future investigations in order to improve the performance of the model and understand more deeply the unban inundation mechanism:

(a) In this study, a deterministic method was used to decide the inflow and overflow discharge coefficients. It might be thought that using the fixed values is very convenient for simulations, however it may cause numerical instability when one value is changed to another value. Therefore, in future work, it is necessary to investigate a linear relation for determining the inflow and overflow discharges.

(b) The least square method was applied to represent head losses at the manhole according to different shapes and various pipe configurations. Generally, the least square method cannot represent general phenomena conditions. Thus, it is recommended to establish an empirical formula.

(c) In Chapter 2 and 3, channel slope and pipe slope were zero. Bed and channel slope can change hydraulic conditions, and it can also create different effects to measure head losses at the manhole and inflow/overflow discharge through the storm drain. Therefore it is necessary to carry out another experiment under a different slope.

(d) Inundation processes can be affected by overland flow and the arrangement of buildings on the ground surface. However, in this research, only an interaction mechanism was considered to investigate the inundation and drainage process through considering exchange discharge between ground surface and sewer pipe. Therefore, it is recommended to evaluate the effect of runoff as well as the arrangement of structures on the ground surface in future work.

(e) In Chapter 3 and 4, the independent variable was only the change in the downstream water level. Urban inundation can be caused by various unexpected phenomena such as torrential rainfall, failure of pumping station, storm drain cover clogging due to debris, etc. Therefore, it is necessary to perform more diverse experiments under various conditions.

(f) Although many experiments were conducted to investigate the urban inundation mechanism and process, a laboratory-scale experiment which can represent only one part and not a whole system was designed and carried out. Therefore it is recommended to carry out a total systemic experiment using a scaled-down model for an integrated urban inundation process and mechanism.

(g) In this study, an integrated urban inundation model was developed with a two-dimensional overland flow and a one-dimensional sewer pipe model. The model was verified

only by using laboratory experimental results. In order to improve the model, it is necessary to verify the model with actual field cases.

Reference

Akiyama, J., Shige-eda, M. and Tanabe, T.: Dynamic Network Model for Free-Surface-Pressurized Flows and Its Applicability to Sewer Network in the Urban Area., Advances in River Engineering, Vol. 14, JSCE, pp. 241-246, 2008 (in Japanese).

Amaguchi, H., Kawamura, A., Olsson, J. and Takasaki, T.: Development and Testing of a Distributed Urban Storm Runoff Event Model with a Vector-based Catchment Delineation, Journal of Hydrology, Vol. 420-421, pp. 205-215, 2012.

Aronica, G.T. and Lanza, L.G.: Drainage Efficiency in Urban Areas: a Case Study, Hydrological Processes, Vol. 19, pp.1105–1119, 2005.

Barnard, T. E., Kuch, A. W., Thompson, G. R., Mudaliar, S and Philips B. C.: Evolution of an Integrated 1D/2D Modeling Package for Urban Drainage. In: Contemporary Modeling of Urban Water Systems, Edited by: James, W., Irvine, K., McBean, E., Pitt, R. and Wright, P. Hamilton, ON: CHI Publications. Monograph, 2007.

Burnella, S., Hager, W. H. and Minor, H. E.: Hydraulic of Bottom Rack Intake, Journal of Hydraulic Engineering, ASCE, Vol. 129, No. 1, pp. 2-10, 2003.

Campana, N.A. and Tucci, C.E.M.: Predicting Floods from Urban Development Scenarios: Case study of the Diluvio Basin, Porto Alegre, Brazil, Urban Water, Vol. 3, No. 1-2, pp. 113-124, 2001.

Cantone, J. and Schmidt, A.: Improved understanding and prediction of the hydrologic response of highly urbanized catchments through development of the Illinois Urban Hydrologic Model, Water Resources Research, Vol. 47, pp. W08538.

Cea, L., Garrido, M. and Puetas, J.: Experimental Validation of Two-dimensional Depth-averaged Models for Forecasting Rainfall-runoff from Precipitation Data in Urban Areas, Journal of Hydrology, Vol.382, No. 1-4, pp. 88-102, 2010.

Chanson, H., Aoki, S., and Maruyama, M.: Unsteady Two-Dimensional Orifice Flow: a Large-Size Experimental Investigation, Journal of Hydraulic Research, Vol. 40, No. 1, pp. 63-71, 2002.

Chaudhry, M. H.: Applied Hydraulic Transients, Van Nostrand Reinhold, 1979.

Cunge, J. A., and Mazaudou, B.: Mathematical Modelling of Complex Surcharge Systems: Difficulties in Computation and Simulation of Physical Situations, in P. Balmer, P. A. Malmqvist, and A. Sjöberg, eds., Proc. 3rd International Conference Urban Storm Drainage, 1:363–373, Chalmers University of Technology, Göteborg, Sweden, 1984.

Cunge, J. A., and Wegner, M.: Numerical integration of Barré de Saint-Venant's flow equations by means of an implicit scheme of finite differences, La Houille Blance, No. 1, pp. 33-39, 1964.

Del Giudice , G. and Hager, W. H. : Supercritical flow in 45degree Junction Manhole, Journal of irrigation and Drainage Engineering, Vol. 127, No. 2, pp. 100-108, 2001.

Djordjević, S., Prodanović, D. and Maksimović , Č.: An Approach to Simulation of Dual Drainage. Water Science and Technology, Vol. 39, No. 9, pp.95-103, 1998.

Djordjević, S., Prodanović, D., and Maksimović, C.: An Approach to Stimulation of Dual Drainage, Water Science and Technology, Vol. 39, No. 9, pp. 95-103, 1999.

Duchesne, S., Mailhot, A., Dequidt, E. and Villeneuve, J. P.: Mathematical Modeling of Sewers under Surcharge for Real Time Control of Combined Sewer Overflows, Urban water, Vol. 3, No. 4, pp. 241-252, 2001.

Ferreri, G. B., Freni, G and Tomaselli P.: Ability of pressman slot scheme to simulate smooth pressurization transient in sewers, Water Science & Technology, Vol. 62, No. 8, pp. 1848-1858, 2010.

Fewtrell, T., Bates, P.D., Horritt, M. and Hunter, N.: Evaluating the Effect of Scale in Flood Inundation Modelling in Urban Environments, Hydrological Processes, Vol. 22, No. 26, pp. 5107–5118, 2008.

Funk & Wagnall's Standard Dictionary (International Edition) New York, pp. 1152, 1960.

Gisonni, C. and Hager, W. H. : Supercritical flow in the 90° junction, Urban water, Vol. 4, No. 4, pp. 363-372, 2002.

Hilary, K. M. and James, B.: Reduced Complexity Strategies for Modelling Urban Floodplain Inundation, Geomorphology, Vol. 90, pp. 226-243, 2007.

Hsu, M. H., Chen, S. H. and Chang, T. J.: Inundation Simulation for Urban Drainage Basin

with Storm Sewer System, Journal of Hydrology, Vol. 234, No. 1-2, pp. 21-37, 2000.

Hsu, M. H, Chen, S, H. and Chang, T. J.: Dynamic Inundation Simulation of Storm Water Interaction between Sewer System and Overland Flows, Journal of the Chinese Institute of Engineers, Vol. 25, No. 2, pp. 171-177, 2002.

Hunter, N. M., Bates, P. D., Horritt, M. S. and Wilson, M. D.: Simple Spatially Distributed Models for Predicting Flood Inundation: A Review, Geomorphology, Vol. 90, pp. 208–225, 2007.

Hunter, N.M., Bates, P.D., Neelz, S., Pender, G., Villanueva, I., Wright, N.G., Liang, D., Falconer, R.A., Lin, B., Waller, S., Crossley, A.J., Mason, D.C.: Benchmarking 2D Hydraulic Models for Urban Flooding, Proceedings of the Institution of Civil Engineers-Water Management Vol. 161, No. 1, pp.13–30, 2008.

Inoue, K.: Study on Its Application to Water Engineering and Numerical Analysis of Open Channel Unsteady Flow, Kyoto University, pp. 189-197, 1986.

James, W. L., Steven, J. W., Mark, P and James, S.: Bottom Slot Discharge Outlet for Combined Sewer Diversion Structure, Journal of Hydraulic Engineering, Vol. 137, pp. 248-253, 2011.

Johnson, M. C.: Discharge Coefficient Analysis for Flat-topped and Sharp-crested Weirs, Irrigation Science, Vol. 19, pp. 133-137, 2000.

Johnston, A. J. and Volker, E. R.: Head Losses at Junction Boxes, Journal of Hydraulic Engineering, Vol. 116, No. 3, pp. 326-341, 1990.

Juan, S., Nataly, B and Diva, P. R.: Hydraulic behavior of Junction manholes under supercritical flow conditions, Journal of Hydraulic Research, Vol. 50, No. 6, pp. 631-636, 2012.

Jun, B. H., and Yen, B. C.: Dynamic Wave Simulation of Unsteady Open Channel and Surcharge Flows in Sewer Network, Civil Engineering Studies Hydraulic Engineering Series No. 40, University of Illinois at Urbana-Champaign, Urban, IL, 1985.

Kawaike, K. and Nakagawa, H.: Flood Disaster in July 2006 in the Matsue City Area and its Numerical Modeling, XXXII IAHR Congress Proceedings, 2007.

Kawaike, K., Nakagawa, H., Baba, Y. and Shimizu, A.: Experimental Study on Validation of

Stormwater Interaction Model between the Ground Surface and Sewerage System, 34th IAHR World Congress Proceedings, pp.1889-1896, 2011.

Kawaike, K., Shimizu, A., Baba, Y., Nakagawa, H., Takeda, M.: Verification of Numerical Model for Urban Inundation due to Torrential Rainfall using Physical Experimental Flume with a Sewer Pipe, Ann. J. of Hyd. Eng., JSCE, Vol.55, pp.985-990, 2011.

König, A., Sægrov, S., and Schilling, W.: Damage Assessment for Urban Flooding, Ninth International Conference on Urban Drainage, Portland, Oregon, USA, 2002.

Leandro, J., Chen, A. S, Djordjević, S and Savić, D. A.: Comparison of 1D/1D and 1D/2D Coupled (Sewer/Surface) Hydraulic Models for Urban Flood Simulation, Journal of Hydraulic Engineering, Vol.135, No. 6, pp. 495-504, 2009.

Li, W. F, Chen, Q. W. and Mao, J. Q.: Development of 1D and 2D Coupled Model to Simulate Urban Inundation: An Application to Beijing Olympic Village, Chinese Science Bulletin, Vol. 54, No. 9, pp. 1613-1621, 2009.

Maciej, M.: Head loss at two-way circular manholes in drainage systems under surcharge conditions, Environment Protection Engineering, Vol. 33, No. 2, pp.183-191. 2007.

Mark, O., Weesakul, S., Apirumanekul, C., Aroonnet, S. B and Djordjević, S.: Potential and limitations of 1D Modeling of Urban Flooding, Journal of Hydrology, Vol. 299, pp. 284-299, 2004.

Marsalek, J.: Head Losses at Sewer Junction Manholes, Journal of Hydraulic Engineering, Vol.110, No. 8, pp.1150-1154, 1984.

Merlein, J.: Flow in Submerged Sewers with Manholes, Journal of Urban Water, Vol. 2. No. 3, pp. 251-255, 2000.

Mignot, E., Paquier, A. and Haider, S.: Modeling Floods in Dense Urban Areas using 2D Shallow Water Equations, Journal of Hydrology, Vol. 327, pp. 186–199, 2006.

Mrowiec, M.: Head Loss at Two-way Circular Manholes in Drainage Systems under Surcharge Conditions, Environment Protection Engineering, Vol. 33, No. 2, pp.183-191, 2007.

Nasello, C., and Tucciarelli, T.: Dual Multilevel Urban Drainage Model, Journal of Hydraulic Engineering, Vol. 131, No. 9, No. 748-754, 2005.

Neal, J. C., Bates, P. D., Fewtrell, T. J., Hunter, N. M., Wilson, M. D., and Horritt, M. S.: Distributed whole city water level measurements from the Carlisle 2005 urban flood event and comparison with hydraulic model simulations, Journal of Hydrology, Vol. 368, pp. 42–55, 2009.

Pedersen, F. B. and Mark, O. : Head Losses in Storm Sewer Manholes: Submerged Jet Theory, Journal of Hydraulic Engineering, Vol. 116, No. 16, pp. 1317-1328, 1990.

Pederwen, F. B. and Mark, O.: Head Losses in Storm Sewer Manholes : Submerged Jet Theory, Journal of Hydraulic Engineering, Vol. 116, No. 11, pp. 1317-1328, 1990.

Saldarriaga, J., Bermúdez, N. and Rubio, D.P.: Hydraulic Behaviour of Junction Manholes under Supercritical Flow Conditions, Journal of Hydraulic Research, Vol. 50, No. 6, pp.631-636, 2012.

Sangster, W.M., Wood, H.W., Smerden, E.T. and Bossy, H.G.: Pressure Changes at Storm Drain Junction, Bulletin. No. 41, Engineering Experiment Station, University of Missouri, Columbia, 1958.

Schmitt, T. G., Thomas, M. and Ettrich, N.: Analysis and Modeling of Flooding in Urban Drainage Systems, Journal of Hydrology, Vol. 299, pp. 300-311, 2004.

Smith, M. B.: A Gis-based Distributed Parameter Hydrologic Model for Urban Areas, Hydrological Processes, Vol. 7, No. 1, pp. 46-61, 1993.

Sandra, S. F., Julien, L., Vincent, G. and Yves, Z .: Two-dimensional Shallow-water Model with Porosity for Urban Food Modeling, Journal of Hydraulic Research, Vol. 46, No. 1, pp. 45–64, 2008.

Wang, K. H., Cleveland, T. G., Towsley, C. and Umrigar, D.: Head Loss at Manholes in Pressurized Sewer Systems, J. American Water Resources Association, Vol. 34, No. 6, pp.1391-1400, 1998.

Wasantha Lal, A.M.: Performance Comparison of Overland Flow Algorithms, Journal of Hydraulic Engineering, ASCE, Vol. 124, No. 4, pp. 342–349, 1998.

Yu, D. and Lane, S. N.: Urban Fluvial Flood Modelling using a Two-dimensional Diffusion-wave Treatment, part 1: Mesh Resolution Effects, Hydrological Processes, Vol. 20, pp. 1541–1565, 2006a.

Yu, D. and Lane, S. N.: Urban Fluvial Flood Modelling using a Two-Dimensional Diffusion-wave Treatment, part 2: Development of a Sub-grid-scale Treatment, Hydrological Processes, Vol. 20, pp. 1567–1583, 2006b.

Zhao, C. H., Zhu, D. Z. and Rajaratnam, N. : Supercritical sewer flows at a combining junction: A Model Study of Edworthy Trunk Junction, Calgary, Alberta, Journal of Environmental Engineering and Science, Vol. 3, No. 5, pp. 343-353, 2004.

Zhao, C., Zhu, D. Z. and Rajaratnam, N.: Experimental Study of Pressurized Flow at Combining Sewer Junctions, Journal of Hydraulic Engineering, Vol. 132, No. 12, pp. 1259-1271, 2006.

List of Figures

List of Tables

Curriculum Vitae

Name: Seungsoo LEE

Citizenship: Republic of Korea

Birth: December 29, 1981 In ChungNam, Republic of Korea

Ph.D. Student (2010 ~ 1013)
Department of Civil and Earth Resources Engineering
Kyoto University, Kyoto, Japan

M. Sc. in Hydraulic Engineering (2008~2010)
Department of Hydraulic and Environmental Engineering, Faculty Engineering
Chungnam National University, Daejeon, Republic of Korea

B.E. in Civil Engineering (2000~2008)
Department of Civil Engineering, Faculty Engineering
Chungnam National University, Daejeon, Republic of Korea

Papers based on the Thesis

Lee. S., Nakagawa, H., Kawaike, K. and Zhang, H. : Experimental Validation of inlet discharge coefficient through the storm drains for urban inundation analysis, *The IHP Symposium on Extreme Events Meteorological, Hydrological and Tsunami Disasters: Social Adaptation and Future"(EXTREME 2011) and Regional steering Committee for Southeast Asia and the Pacific, UNESCO International Hydrological Program*, pp.80-86, October, 2011.

Lee. S., Nakagawa, H., Kawaike, K. and Zhang, H. : Study on Inlet Discharge Coefficient through the different shapes of Storm Drains for Urban Inundation Analysis, *Annual Journal of Hydraulic Engineering, JSCE,* Vol.56, pp.I-31-I-36, February, 2012. (CD-ROM)

Lee, S. S., NAKAGAWA, H., KAWAIKE, K. and ZHANG, H. : Experimental study on Validation of Combined Model for Urban Inundation Analysis, *Annuals of Disaster Prevention Research Institute*, Kyoto University, No. 55B, pp.483-491, June, 2012.

Lee, S. S., NAKAGAWA, H., KAWAIKE, K. and ZHANG, H. : Experimental study on validation of discharge coefficient between the Ground Surface and Sewerage system, *The 18th Congress of the Asia and Pacific Division of the International Association for Hydro-Environment Research and Engineering IAHR-APD*, August, 2012. (USB-Memory)

Lee, S. S., NAKAGAWA, H., KAWAIKE, K. and ZHANG, H. : Experimental Validation of Interaction Model at Storm Drain for Development of Integrated Urban Inundation Model, Annual Journal of Hydraulic Engineering, JSCE, Vol.57, pp.II-1-I-109, February, 2013, (CD-ROM).

Lee, S. S., NAKAGAWA, H., KAWAIKE, K. and ZHANG, H.: Experimental Study on Development of Integrated Urban Inundation Model, *Journal of Disaster Research*, Vol.8 No.1, pp. 129-130, February, 2013.

Lee, S. S., NAKAGAWA, H., KAWAIKE, K. and ZHANG, H.: Experimental Study on Head Losses in the Sewer Pipe due to Manhole Shapes, *Annuals of Disaster Prevention Research Institute*, Kyoto University, No. 56B, June, 2013. (in printing)

Lee, S. S., NAKAGAWA, H., KAWAIKE, K. and ZHANG, H.: Study on Experimental Validation of Interaction Model among Sewer Pipe, Manhole and Ground Surface for Development of Integrated Urban Inundation Model, *35th IAHR World Congress*, September, 2013. (in Printing)